

UNCLASSIFIED

AD 658 995

FINAL ENGINEERING REPORT ON WIND TUNNEL TEST STUDY

Collins Radio Company  
Cedar Rapids, Iowa

June 1958

*Processed for . . .*

DEFENSE DOCUMENTATION CENTER  
DEFENSE SUPPLY AGENCY



U. S. DEPARTMENT OF COMMERCE / NATIONAL BUREAU OF STANDARDS / INSTITUTE FOR APPLIED TECHNOLOGY

UNCLASSIFIED

LIBRARY COPY

~~CONFIDENTIAL~~  
**UNCLASSIFIED**

PROPERTY  
COLLINS RADIO CO.

Report No. CER-826  
Part I  
Copy No. 17



PART I

FINAL ENGINEERING REPORT

ON

WIND TUNNEL TEST STUDY (u)

1 June 1958

DA-44-177-TC-448

P. O. DEE-10017

Covering Period from 25 January to 1 April 1958

AD658995



DECLASSIFIED

AUTHORITY *Collins Aeron. Res. Lab. 26 Sept. 67*  
DECLASSIFICATION DATE *21 Jan. 1979*  
SIGNED BY *W. G. Buckner*  
RECORDED BY *W. L. Hamer, Register*  
(COLLINS EMPLOYEE - DOTE)  
*26 Sept. 1967*

NOTICE: This document contains information affecting the national defense of the United States, within the meaning of the Espionage Laws, Title 18, U.S.C., Sections 793 and 794, the transmission or revelation of which in any manner to an unauthorized person is prohibited by law.

COLLINS RADIO CO.

10 JAN 1960

8118

CEDAR RAPIDS, IOWA

GROUP IV  
DOWNGRADED AT 3 YEAR INTER-  
VALS; DECLASSIFIED AFTER  
12 YEARS.  
DOD DIR 5200.10

Reproduced by the  
CLEARINGHOUSE  
for Federal Scientific & Technical  
Information Springfield Va. 22151

COLLINS AERONAUTICAL RESEARCH LABORATORY

A. M. Lippisch, Director  
Cedar Rapids, Iowa

This document has been approved  
for public release and sale; its  
distribution is unlimited.

OCT 4 1967  
E 84

~~CONFIDENTIAL~~  
**UNCLASSIFIED**

~~CONFIDENTIAL~~

~~UNCLASSIFIED~~

A PUBLICATION OF  
THE AERONAUTICAL RESEARCH LABORATORY

COLLINS RADIO COMPANY

Cedar Rapids, Iowa

Printed in the United States of America

~~CONFIDENTIAL~~

~~UNCLASSIFIED~~

FINAL ENGINEERING REPORT  
ON  
WIND TUNNEL TEST STUDY

1. INTRODUCTION.

This is the first part of the final report, which includes information pertaining to the construction and testing of the CARV\*. This wind tunnel test model was constructed and tested according to the specifications set forth by the Chrysler Corporation (Chrysler PO DEE-100017 under prime contract DA-44-177-TC-448).

The initial program for testing the CARV\* called for: (1) modification of existing wind tunnel facilities to allow testing of the 1/10 scale model, (2) testing the model to determine its aerodynamic characteristics in pitch to 30°, in yaw to 90°, and in roll to 30°; these tests to be performed with forward speeds between 0 and 50 miles per hour, and (3) testing the model to determine the control vane effectiveness.

As is the case in testing most unorthodox configurations, the scope of the program was altered considerably during the testing as the results began to indicate fields of more specialized interest.

Modification of the existing wind tunnel facilities was undertaken to allow for six component measurements in pitch and in roll attitudes.

The first part of the test program as performed up until March 31, 1958 covered the following investigations:

- (a) Vane effectiveness in hovering.
- (b) Forward flight conditions for tandem configuration.
- (c) Forward flight conditions for abreast configuration.
- (d) Finding a method to reduce the positive pitching moment.
- (e) Miscellaneous.

\*Chrysler Aerial Research Vehicle

The following professional and technical personnel worked on this project during the period covered by this report.

Dr. A. M. Lippisch	Director of the Collins Aeronautical Research Laboratory
Mr. E. A. Sielaff	Senior Engineer
Mr. J. C. Brown	Senior Assistant Engineer
Mr. R. N. Pugh	Senior Assistant Engineer
Mr. R. F. Colton	Junior Assistant Engineer
Mr. L. H. Connover	Aeronautical Engineering Assistant
Mr. L. L. Miner	Laboratory Assistant
Mr. W. C. Green	Laboratory Assistant
Mr. A. G. Johnson	Laboratory Assistant
Mr. M. V. Hoppenworth	Laboratory Assistant
Mr. J. A. Felthous	Draftsman
Mr. E. A. Sieh	Draftsman

**2. IDENTIFICATION OF SYMBOLS.**

The symbols used in this report may be identified by referring to the following list. Figures 1 and 2 will also aid in identifying the symbols.

<u>Symbol</u>	<u>Dimensions</u>	<u>Definition</u>
C	lb	Side force
$C_C = \frac{C}{\rho u^2 S}$		Side force coefficient in hovering
$C_D = \frac{D}{\rho u^2 S}$		Drag coefficient in hovering
$C_L = \frac{L}{\rho u^2 S}$		Lift coefficient in hovering
$C_1 = \frac{L'}{\rho u^2 S d}$		Rolling moment coefficient in hovering

<u>Symbol</u>	<u>Dimensions</u>	<u>Definition</u>
$C_m = \frac{M'}{\rho u^2 S d}$		Pitching moment coefficient in hovering
$C_n = \frac{N'}{u^2 S d}$		Yawing moment coefficient in hovering
D	lb	Drag
$K_D = \frac{D}{q_0 S}$		Drag coefficient for forward flight
$K_L = \frac{L}{q_0 S}$		Lift coefficient for forward flight
$K_N = \frac{N}{q_0 S}$		Normal force coefficient for forward flight
$K_1 = \frac{L'}{q_0 S}$		Rolling moment coefficient for forward flight
$K_m = \frac{M'}{q_0 S}$		Pitching moment coefficient for forward flight
L	lb	Lift
L'	lb ft	Rolling moment
M'	lb ft	Pitching moment
N	lb	Normal force
N'	lb ft	Yawing moment
S	ft <sup>2</sup>	Area of the two shrouds combined measured in the plane of the propellers
d	ft	Diameter of the shrouds measured in the plane of the propeller
e	ft	Distance of the normal force from the C. G. (+ forward)
n	RPM	Revolutions per minute of the propellers
q <sub>0</sub>	lb/ft <sup>2</sup> and kg/m <sup>2</sup>	Dynamic pressure of the air from wind tunnel (measured)

<u>Symbol</u>	<u>Dimensions</u>	<u>Definition</u>
$q_1$	lb/ft <sup>2</sup> and kg/m <sup>2</sup>	Dynamic pressure of the slip stream of the propeller
$r$	ft	Radial distance from propeller axis to blade section
$u$	ft/s	Propeller tip speed
$v_o$	ft/s	Tunnel speed reduced to stand- ard sea level condition
$v_a$	ft/s	Axial air speed through propeller
$v_T$	ft/s	Tangential velocity of blade section of propeller
$\theta$	degrees	Angle of pitch of the model
$\bar{\alpha}$	degrees	Effective angle of attack of a section of the propeller
$\delta$	degrees	Deflection angle of the vanes
$\delta$	degrees	Angle between the chord of the propeller blade section and the plane of rotation
$\delta_o$	degrees	Angle of blade setting of the propeller at the hub
$\rho$	lb s <sup>2</sup> /ft <sup>4</sup>	Air density during the test
$\phi$	degrees	Effective pitch angle of the propeller
$\omega$	radians/s	Angular velocity of the propeller

**Subscripts:**

A, B, C, D in connection with  $\delta$  indicate pitch vanes.

1, 2, 3, 4 in connection with  $\delta$  indicate roll vanes.

**3. TEST APPARATUS.**

Some construction was necessary in order to adapt the existing wind tunned facilities to the testing program outlined for the model. A general description of the testing system and the construction phase of the test model can be found in IDR-449-1 dated February 15, 1958.

The following information is in addition to the information supplied in the previous report.

### 3.1 WIND TUNNEL DESCRIPTION.

The wind tunnel utilized for testing the model is an open throat, open circuit tunnel which has a throat diameter of 36 inches. The range of wind velocities available for testing purposes is 1.5 feet/second to 40 feet/second. The maximum error encountered in measuring the wind velocities was  $\pm 1\%$ . The test model was supported so that its center of gravity was located on the center line of the tunnel and 32 inches from the plane of the mouth of the tunnel. The model was suspended 60 inches from the floor.

### 3.2 MODEL MODIFICATIONS.

In addition to the facilities described in IDR-499-1 for adjusting the vanes to various angles, more recent modifications made it possible to vary the position of the vanes in a vertical direction (see figure 3). The vanes can either be set at the original position, (position 1), at the intermediate position (position 2) which places the leading edge of the vane in the plane of the shroud exit, or at the lower position (position 3), which places the leading edge of the vane one chord length below the shroud exit (see figure 4). The vane chord lengths were increased by one chord length for certain phases of the testing program.

### 3.3 SCALE SYSTEM.

Figures 5 and 6 show the scale arrangement that was used to obtain the force and moment data. The scales are harvard trip balance, double beam types and have a capacity of two kilograms. The rated sensitivity of the scales is 0.1 of a gram and the error in measuring accuracy does not exceed 0.1%. For the tests performed, stops were added to the scales in order to limit their range of travel. The locations of each scale and their respective functions are shown in figure 7.

A special frame was used to adjust the pitch angle of the model. This frame was mounted on the scale platform (see figure 8).



### 3.4 MEASURING APPARATUS.

The equipment used to monitor the operating voltage and current for the model motors, the motor rpm rates, and the wind velocities below the shrouds and in the wind tunnel are shown in figures 9 and 10. Magnetic pickup devices were installed on one motor shaft to facilitate the recording of the rpm rate. The outputs from these devices were fed to a spectrum analyzer which is capable of displaying information between the range of 2000 rpm and 110,000 rpm. The accuracy of the equipment was within 0.2%.

A regulated, variable power supply unit furnished the necessary operating voltages for the two DC motors used in the test model. A vernier control was also employed to aid in regulating the voltage output of the power source. Power was measured with a voltmeter and ammeter, which provided accurate power data to within  $\pm 0.5\%$ .

Pressure surveys for the areas directly below the model shrouds were accomplished with the rake attachment shown in figure 11, which was attached to the shroud during the test runs. The rake assembly was designed so that each tube represents an equal area of flow from the shroud. The tubes of the rake were attached to the multiple manometer shown in figure 11. The accuracy of the readings obtained was within  $\pm 0.25$  millimeters of  $H_2O$ .

A Prandtl tube, used in conjunction with a Betz manometer, provided a means of checking the wind velocities in the tunnel. The manometer has a range of 0 to 800 millimeters of  $H_2O$ . The minimum accuracy obtained was within  $\pm 0.1\%$ .

### 4. TEST PROCEDURE.

The following is a description of the procedure used to obtain data during a performance test. These data were used to plot the curves of dimensionless coefficients. Although a particular test run is considered here for purposes of illustration, the methods described apply generally to the entire testing program.

The first part of the procedure outlined below (steps 1 through 8) was necessary to establish a performance point. The second part of the procedure was required to establish the

stability derivatives  $\left( \frac{\partial K_L}{\partial \theta}, \frac{\partial K_D}{\partial \theta}, \frac{\partial K_m}{\partial \theta} \right)$  around this point.

UNCLASSIFIED  
CONFIDENTIAL

Step 1. With the wind tunnel turned off the lift scales were checked for zero values for the range of pitch angles to be covered during the test. These values were measured and recorded so that the proper weights could be added to the scales during the test runs. This procedure ensured that the measured lift values were net readings.

Step 2. The model was then set at the  $-20^\circ$  pitch angle with the proper zero weights on the lift scales.

Step 3. The DC generator for the tunnel motor was started, warmed up, and switched to the tunnel blower motor.

Step 4. The approximate propeller speed was determined (computations based on previous work) which would deliver the required 1600 gms. lift. The model motors were then energized.

At this point it might be well to consider the reasoning involved in setting up the forward flight performance test program. It was felt that the only point of practical significance was the condition of steady horizontal flight. This condition is obtained when the drag on the model is equalized by the thrust produced by the propellers and inlets. This condition can be stated as follows:  $\text{Drag} - \text{Thrust} = \text{Drag measured} = 0$ . In addition to this, the lift was maintained at a constant value (1600 gms.) for each of the performance data points. This magnitude of lift was selected so that it would be as large as possible and still not exceed the range of available power in the model motor for all conditions of forward and hovering flight. The remaining steps are required to produce the conditions outlined above.

Step 5. After completing step 4 the two drag scales were unblocked and the tunnel wind speed was gradually increased until both drag scales were balanced simultaneously. If a slight amount of yawing moment existed, the weights on the drag scales were adjusted so that the force added on one scale was subtracted from the other scale.

Step 6. When the exact wind velocity was determined at the condition  $D = 0$ , the drag scales were blocked and the four remaining scales were read in order. While these scales were being read, the wind velocity and prop rpm rate were held constant. Also, at this time, the wind velocity and the power input to the motors was recorded.

UNCLASSIFIED  
CONFIDENTIAL

Step 7. After the lift and side force measurements were made, the power to the model motors was turned off and the exact amount of lift was computed. The direction and approximate magnitude of the change required to bring the lift to 1600 gm was then determined.

Step 8. By an iteration process of this kind, it was usually possible to attain the required lift ( $\pm 0.5\%$ ) after no more than four tries.

Step 9. Once the tunnel wind speed and the prop speed for the steady horizontal flight condition at this angle was determined the six components were measured for  $2.5^\circ$  and  $5^\circ$  angle increments above and below the original  $-20^\circ$  pitch angle. The two parameters mentioned above (rpm, tunnel speed) were held constant for these additional readings.

Step 10. The raw data obtained from the tests were recorded on standard data sheets. These data were analyzed, interpreted and finally plotted on graph paper.

## 5. TEST RESULTS

The material in this section summarizes the tests performed up to March 31, 1958.

These tests covered investigations in the following areas:

- (a) Vane effectiveness in hovering for pitch, roll and yaw.
- (b) Forward flight conditions for tandem configurations which involved:
  - (1) Determining the zero drag conditions, and the change in lift, drag and pitching moments due to varying the angle of attack and the forward speed.
  - (2) Vane effectiveness in pitch.
- (c) Forward flight conditions for abreast configurations involving:
  - (1) Determining the zero drag conditions and the change in lift, drag and pitching moments due to varying the angle of attack and the forward speed.
  - (2) Vane effectiveness in pitch.
- (d) Finding a method to reduce the positive pitching moment.
- (e) Miscellaneous.

Each of the areas of investigation listed above are discussed in detail in the following material. Section 6 of this report includes graphs which were drawn from the data obtained from the various test runs.

## 5.1 DISCUSSION OF TEST RESULTS.

(a) Vane effectiveness in hovering for pitch, roll, and yaw. The model configuration for these test runs was as specified for the original design and included four roll vanes and two pitch vanes in each shroud. The propeller setting was  $\alpha_0 = 30^\circ$ . The model was suspended in the hovering position and the tests were performed at prop speeds of 4000, 5500, and 7000 rpm. The tunnel wind speed was zero.

## (1) Yaw effectiveness.

Figures 16 and 17 show the lift and yawing moment coefficients for 4000, 5500, and 7000 rpm as a function of the vane deflection. Vanes 1 and 2 in the front shroud and 3 and 4 in the rear shroud were deflected by equal angles in opposite directions. The pitch vanes A, B, C, and D were in the neutral positions.

## (2) Roll effectiveness.

Figures 18, 19, and 20 show the lift, side force and rolling moment coefficients for 4000, 5500, and 7000 rpm as a function of the vane deflection. All roll vanes (1, 2, 3, and 4) were deflected by the same angle and in the same direction. The vanes A, B, C, and D were in the neutral positions. The effect of deflecting the roll vanes on one side only is shown in figure 21. The sets 1 and 3 were deflected, and all other vanes were in neutral positions. These test runs were performed at prop speeds of 7000 rpm only and for positive deflections.

## (3) Pitch effectiveness.

Figures 22, 23, and 24 represent the lift, drag and pitching moment coefficients for 4000, 5500, and 7000 rpm. The pitch vanes A, B, C, and D are deflected by the same angle and in the same direction. All roll vanes are in a neutral position. Since the pitching moment coefficients show considerable scattering and indicate no vane effectiveness for negative deflections, more tests were performed at prop speeds of 7000 rpm only to see if any improvement could be achieved. Figures 25 and 26 show the coefficient curves which resulted from deflecting the pitch vanes in the rear shroud in opposite directions. All other vanes are in

neutral positions. Blocking of the rear shroud by deflecting all vanes in the shroud inward resulted in a pitching moment coefficient curve as shown in figure 27. The graphs in figures 28 and 29 represent some of the significant coefficients obtained by deflecting the pitch vanes in the rear or front shroud only. Finally the vanes in the rear shroud were lowered to position 3 (see figure 4) and the double pitch vanes were installed (see figure 12). The measurements for this configuration were taken several times and the pitching moment coefficients obtained are plotted in figure 30. The curves which should be identical scatter widely and show no consistency.

- (4) General investigations concerning vane effectiveness in hovering. There were a large number of runs which were not included in the data point numbering system simply because these runs were either pressure measurements or spot checks of various configurations designed to provide one particular result.

In the initial phases of this work it was felt that the control vanes were ineffective because the mass flow in the region of the vanes was too small. Consequently, the effort in the first phase was directed toward increasing the velocity near the wall relative to the central part of the stream. This velocity increase can be accomplished in at least two ways. One method is to make suitable inlet modifications. Another is to redistribute the pitch of the prop blades to provide for more work at the tips.

The inlet modifications were tried first. A summary of the configurations tested is shown in figures 31 and 32 and the curves corresponding to the dynamic pressure distributions for those configurations for which data were recorded are shown in figures 33, 34, and 35. A detail drawing of the total head rake used to obtain this pressure information appears in figure 35A. The second method of accomplishing the desired velocity distribution is to redistribute the pitch along the prop blades. This "prop twisting" was done after an optimum inlet configuration had been decided upon, with one exception, that being that the prop in the

rear shroud had been "straightened out" according to the pitch distribution no. 1 (see figure 36) previous to the inlet tests and was used during all of these runs. All of the rest of the prop distribution work was done with the final ring form (see figure 32) above the inlet.

The prop pitch analysis was done as described in the following text. In all of the work the induced angle of attack increment was neglected. Figure 15 along with the following definitions will serve to identify the terms in the equations used in the ensuing discussion.

$\mathcal{J}$  = angle between plane of rotation and chord line of the blade section.

$\bar{\alpha}$  = effective angle of attack of this blade section.

$\phi$  = angle between plane of rotation and relative wind at prop blade section (effective pitch angle).

$$v_T = \omega r = \frac{2\pi nr}{60}$$

$$v_a = \sqrt{2/\rho} \sqrt{q_1}$$

$$\tan \phi = v_a / v_T = \frac{\sqrt{2/\rho} \sqrt{q_1} 60}{2\pi nr}$$

Since all of the test runs were performed at a constant prop speed ( $n = 7000$  rpm) the above expression can be simplified to the form:

$$\tan \phi = K \frac{\sqrt{q_1}}{r}$$

By measuring  $q_1$  with the total head rake at various stations it is then only a matter of using the above equation to determine the angle of the relative wind at that station.

Assuming that it is desired to obtain a uniform velocity distribution with the same thrust that is provided with the actual distribution, a curve can be drawn which represents the  $\phi$  distribution for uniform flow.

Having established the desired  $\phi$  curve, and also curves for the measured values of  $\mathcal{J}$  and  $\phi$ , the following procedure can be used to determine the required  $\mathcal{J}$  distribution.

At any station

$$\bar{\alpha}_{\text{actual}} = \mathcal{J}_{\text{meas}} - \phi_{\text{meas}}$$

This expression allows us to determine the actual angle of attack. With this information  $\mathcal{J}_{\text{desired}}$  is determined from the equation.

$$\mathcal{J}_{\text{desired}} = \phi_{\text{desired}} + \bar{\alpha}_{\text{actual}}$$

This value of  $\mathcal{J}$  is the angle at which the prop pitch must assume at that particular station in order that the desired velocity distribution may be approached. This process of iteration is continued until the desired velocity distribution is obtained. Normally this process allows the particular velocity distribution to be approached quite rapidly (see figures 36, 37, and 38).

The graph in figure 36 shows the curves that were obtained from the initial condition. The graph in figure 37 represents the distribution after the first twisting procedure and the graph shown in figure 38 represents the final distributions.

This prop configuration was used for both props for all tests from no. 170 on. Figure 39 is a plot of the  $C_m$  versus  $\delta$  curve after the modifications mentioned above had been performed. The graph illustrates how  $\mathcal{J}_0$  for the front prop was changed to provide for  $C_m \approx 0$  at  $\delta = 0$ .

(b) Forward flight conditions for tandem configurations,

(1) Determining the zero drag conditions.

The zero drag conditions were determined for the original shroud and vane configurations with all of the vanes in the neutral position. Figure 40 shows the lift and pitching moment coefficient as a function of the pitch angle, the drag component being zero. Figures 41 and 42 show these same functions with the rpm of the props held constant (4000 and 7000). The graph in figure 43 represents the tunnel velocity (reduced to standard sea level conditions) as a function of the pitch angle with the rpm rate of the props at 4000 and 7000 and with the drag equal to zero.

The travel of the center of pressure for the different steady horizontal flight conditions at various pitch angles is shown in the graph of figure 44.

The change of the lift, drag and pitching moment coefficients with variations of the pitch angle and forward speed was determined in the following manner:

Keeping the lift component constant (1.600 kg.), the zero drag conditions were determined for four different angles of pitch ( $\theta = -10^\circ, -20^\circ, -30^\circ$  and  $-37.5^\circ$ ), for which the corresponding tunnel velocities were  $v_0 = 10.6, 17.4, 23.8$  and  $28.4$  ft/s. Then the angle of pitch was varied  $\pm 5^\circ$  in  $2.5^\circ$  increments from the original angle, with the tunnel wind velocity and the prop rpm rate being held constant.

The results of these tests are shown in figure 45. Additional test runs were made holding the angle of pitch and the prop rpm rate constant and varying the tunnel speed by two increments above and below the zero drag velocity. The results of these tests are shown in figures 46 and 47. The vanes were placed in position 2 (see figure 4).

(2) Vane effectiveness in pitch.

The effect of deflecting the pitch vanes in the rear shroud only is shown in figure

The vanes were in position 3 (see figure 4) and double pitch vanes had been called. It can be seen that deflecting the vanes in this case did not produce any positive results as far as effectiveness was concerned. Measurements were also taken with only the pitch vanes in the front shroud deflected. The double pitch vanes remained in position 3. In this case the measurements were taken only with the vanes deflected in the negative direction. Figure 49 shows that no satisfactory results were obtained.

A series of tests were performed with all the double pitch vanes deflected. No change in effectiveness was apparent during these tests (see figure 50). Vertical fins were added to the inner vanes of sets A and D, but did not have any substantial effect (see figures 51 and 13). The curve of figure 52 show the coefficients



with all of the vanes in position 2 (see figure 4) and deflected by equal angles in the same direction.

In order to investigate the effect of the size of the vanes on vane effectiveness, the chord lengths of vanes C and D were doubled (see figure 14). The data shown in figure 53 were obtained with the vanes placed in position 2. The corresponding curves for vanes of normal chord length are also shown. The effect of doubling the chord length of all of the vanes is shown in figure 54.

(c) Forward flight conditions for abreast configuration.

- (1) Determining the zero drag conditions, change in lift, drag and pitching moments due to varying the angle of attack and the forward speed.

The zero drag conditions for the tests performed in this phase of the work were determined using the original shroud configuration. The double pitch vanes were installed and all vanes were placed in position 2 (see figure 4) and had zero deflection. Figure 55 shows the lift and pitching moment coefficient as a function of the pitch angle, the drag being zero. Figure 56 represents the forward speed, reduced to standard sea level conditions, as a function of the pitch angle at constant lift. Figure 57 shows  $e/d$  as a function of the pitch angle at zero drag.

The change in the lift, drag and pitching moment coefficients for small variations in the pitch angle and forward speed was determined in the same way that these coefficients were found for the tandem arrangement. The results of the tests are shown in figures 58, 59, and 60.

- (2) Vane effectiveness in pitch.

The vane effectiveness in pitch was determined by first deflecting the vane sets 1, 2, 3, and 4 (see figure 2), which act in the abreast arrangement as pitch vanes, by the same angle and in the same direction. The pitch angle used was  $-20^\circ$ . The results of these tests are shown in figure 61.

For additional testing, the results of which are shown in figure 62, the vanes were initially deflected outward by  $10^\circ$ , i. e., the undeflected condition was

$\delta_1 = \delta_3 = +10^\circ$  and  $\delta_2 = \delta_4 = -10^\circ$ . From this position the vanes were deflected by equal amounts in the same direction. No improvement was obtained.

- (d) Finding a method to reduce the positive pitching moment.

In order to eliminate the nose up pitching moment the blade setting of the front prop was varied from  $33.25^\circ$  to  $25.25^\circ$  at the hub in increments of  $2^\circ$ . The results obtained with the prop set at these various angles are shown in figure 63. The pitching moment was reduced to zero by reducing the prop angle  $4.6^\circ$ . Figure 63 also shows the corresponding increase in the rolling moment for the reductions in the pitch angle.

The second phase of this work was directed toward finding the cause of the large nose up pitching moment and determining what could be added in the way of lift reducers to diminish this tendency. The configurations tested are shown in figure 64 and the results of the tests are shown in figure 65. All of the tests from 1 through 13 were performed with a prop speed of 7000 rpm and a pitch angle of  $-25^\circ$ . The series of tests for configuration 14 were performed with a prop speed of 5710 rpm and a pitch angle of  $-20^\circ$ . The shrouds were in the abreast position for these tests.

The rest of the time spent in the pitching moment investigations was devoted to taking pressure measurements at the shroud inlets to see if the pressure existing at the lips was sufficient to account for the strong nose up pitching moment in forward flight.

The pressure distributions obtained from these tests are shown in figures 66, 67, and 68. Table 5-1 lists the significant data obtained.

TABLE 5-1. PITCHING MOMENT PRESSURE DATA

Test No.	Shroud Arrangement	Pitch Angle	Prop rpm	Tunnel $q_0$	$\frac{N_{shroud}}{N_{total}}$	$\frac{(e/d)_{shroud}}{(e/d)_{total}}$
1	tandem	0	5712	0	.30	
2	tandem	-20°	5712	$1.55 \frac{kg}{M^2}$		.75
3	abreast	0	5900	0	.34	
4	abreast	-20°	3900	$1.55 \frac{kg}{M^2}$	.18	.70

(e) Miscellaneous.

- (1) The results of the power measurement tests are plotted in figure 69. During these tests, the lift was maintained at a constant value of 1600 gms. and the drag component was held at a value of zero. The upper curve in figure 69 represents the data obtained with the tandem configuration. Each angle on the curve represents a different angle of pitch.
- (2) In order to determine the effect of upward speeds on the lift characteristics in hovering, the model was suspended with the inlets of the shroud facing the tunnel mouth. The force parallel to the axis of the shrouds (lift) was measured for different wind speeds. Figure 70 shows the lift as a function of the upward speed.
- (3) Another series of tests was run in order to check whether the position of the tunnel axis had any effect on the measurements. Data were taken for the same vane deflections, prop speed, tunnel speed and pitch angle. However, the model was adjusted 3, 6, and 9 inches above and below the tunnel axis for vane deflections of 0° and 30° (see figure 71). It can be seen that the slope of the curves is practically zero for the central position of the model, which indicates that this position yields the correct test data.

6. ILLUSTRATIONS.

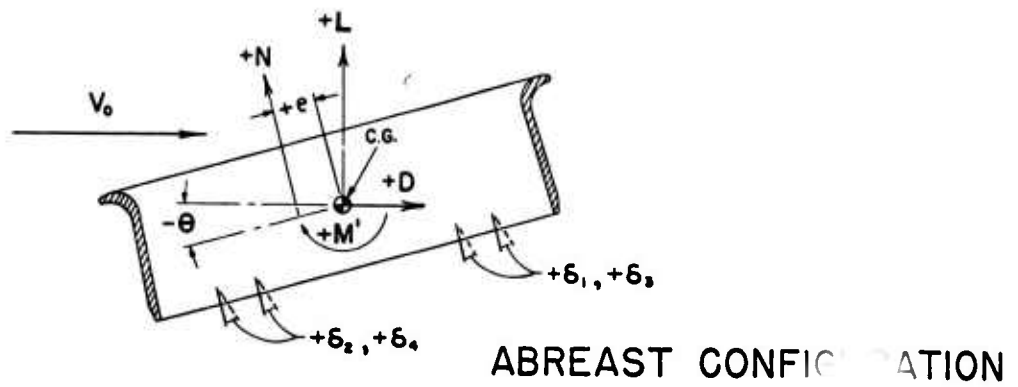
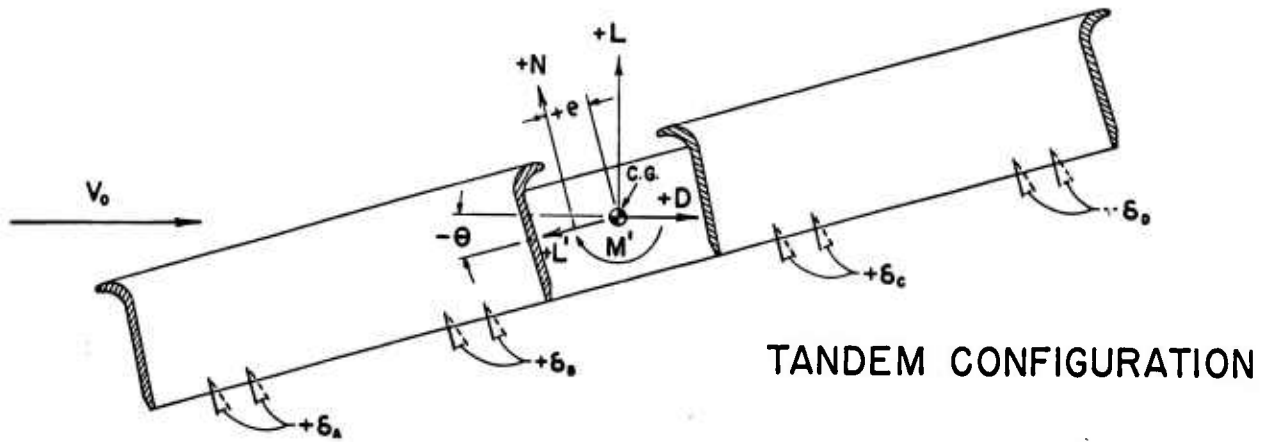


Figure 1. Symbol Identification (Forward Flight Condition)

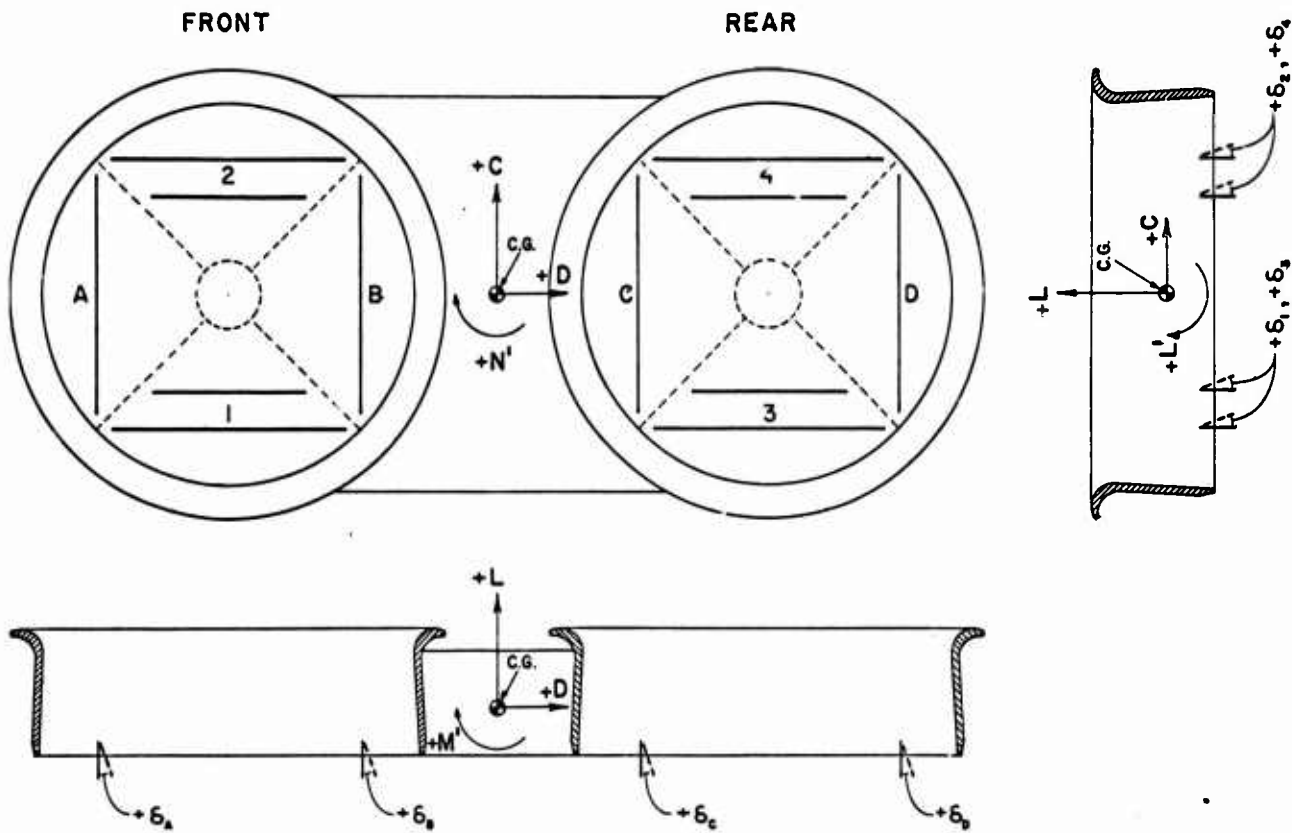
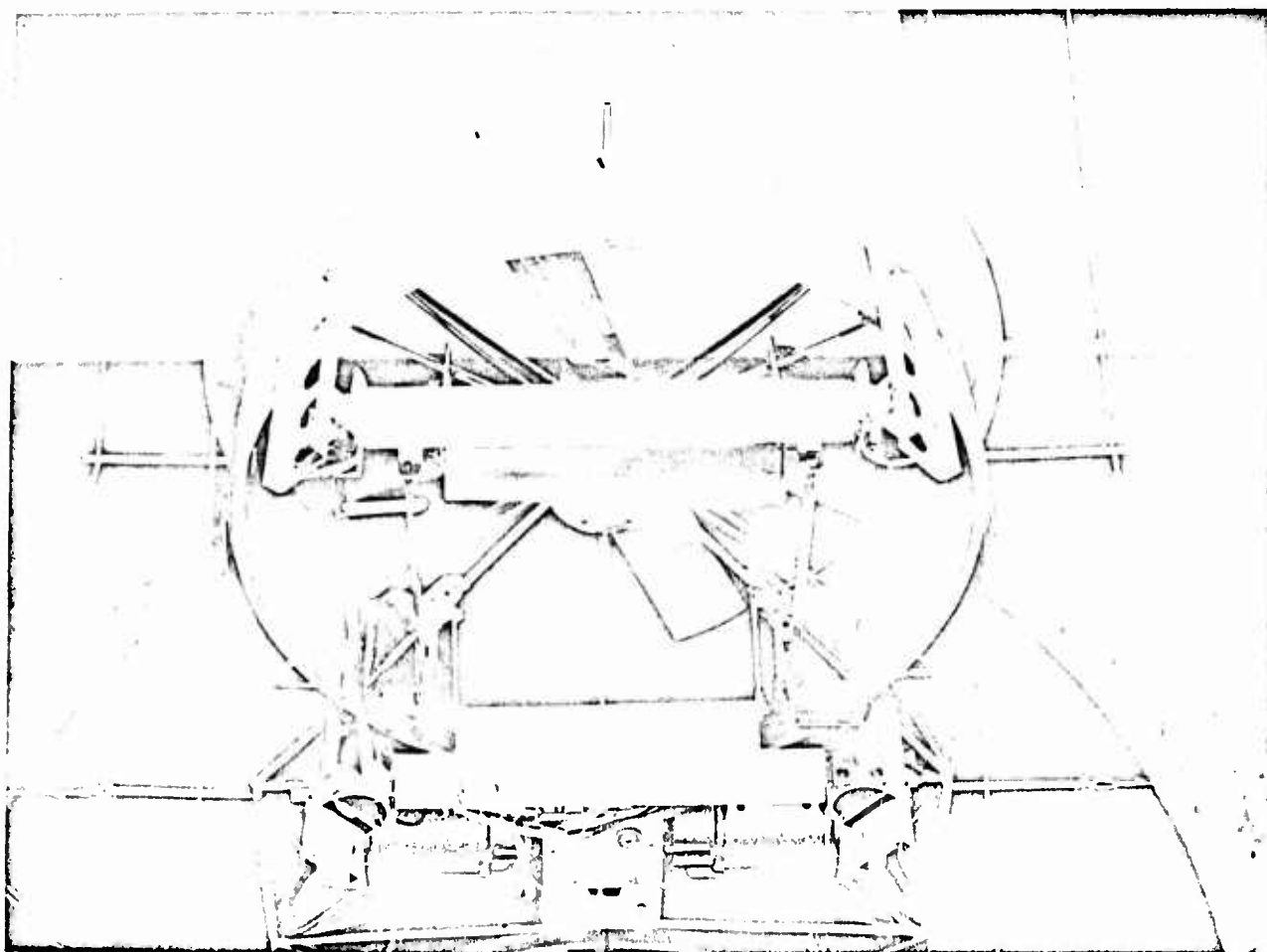


Figure 2. Symbol Identification (Hovering Flight Characteristics)



**Figure 3. Closeup View of Model Shroud Showing Attachments  
for Adjusting Vanes in Vertical Direction  
(Vanes in Position #3)**

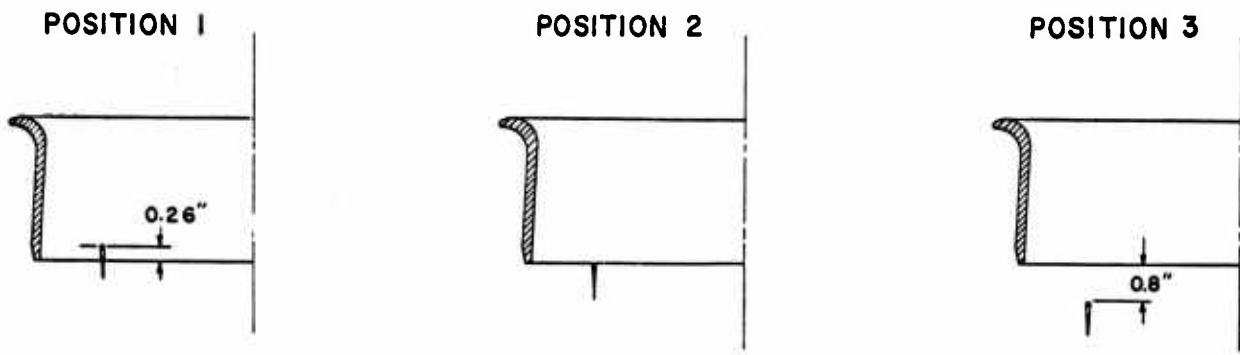


Figure 4. Vane Positions

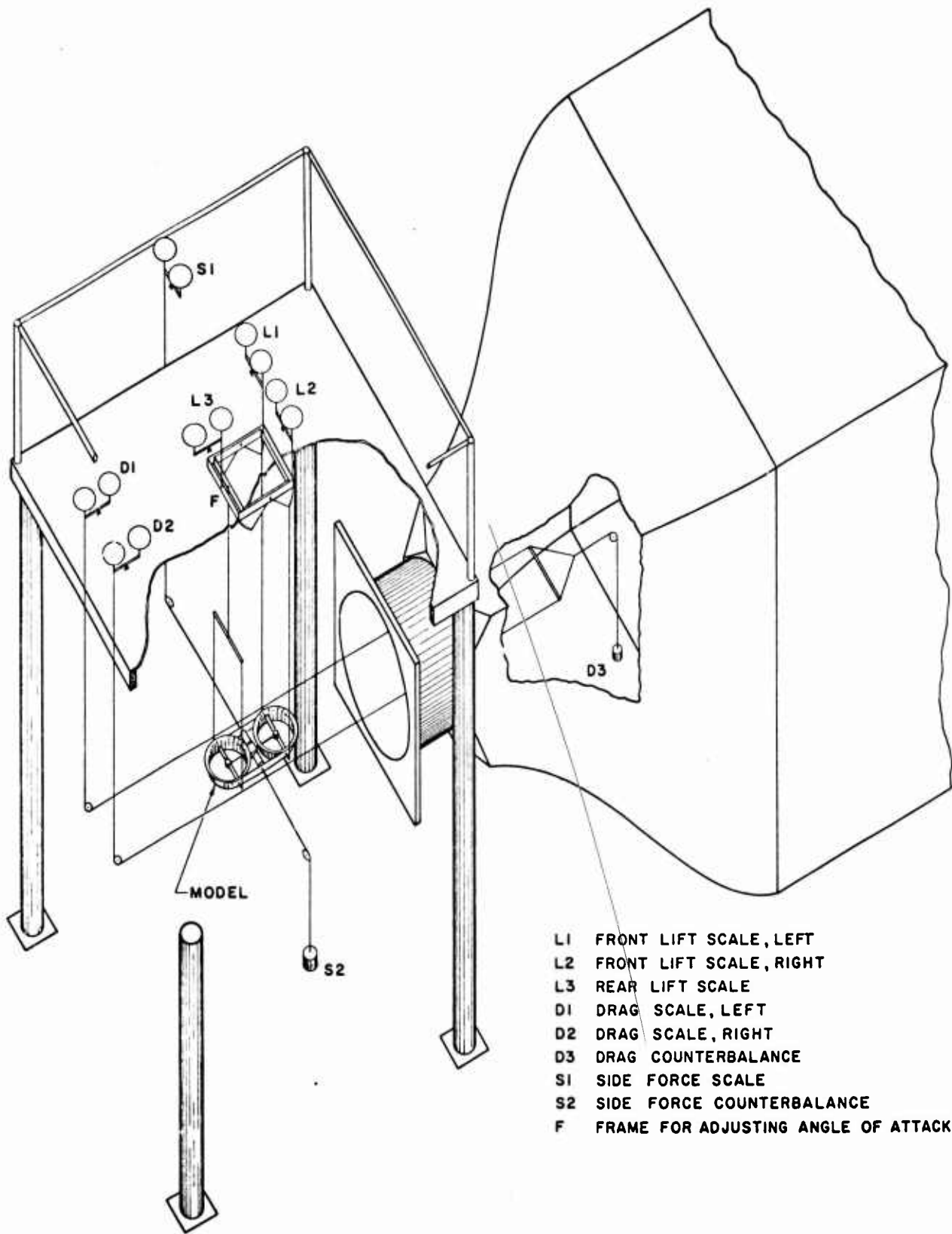


Figure 5. Wind Tunnel Scale System (Looking to Rear)



Figure 6. Wind Tunnel Scale System (Looking Forward)





- L1 FRONT LIFT SCALE, LEFT
- L2 FRONT LIFT SCALE, RIGHT
- L3 REAR LIFT SCALE
- D1 DRAG SCALE, LEFT
- D2 DRAG SCALE, RIGHT
- D3 DRAG COUNTERBALANCE
- S1 SIDE FORCE SCALE
- S2 SIDE FORCE COUNTERBALANCE
- F FRAME FOR ADJUSTING ANGLE OF ATTACK

Figure 7. Wind Tunnel Scale System

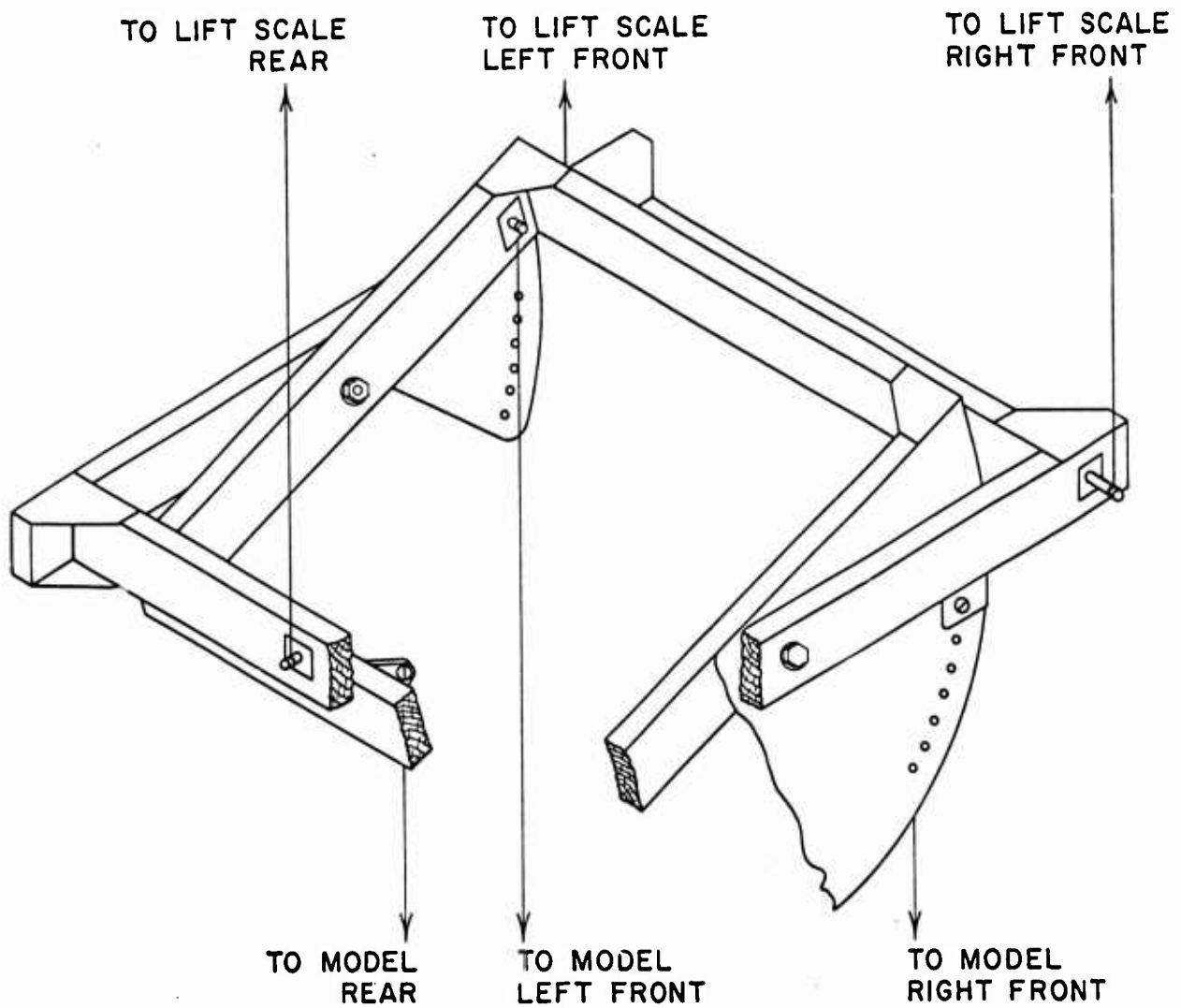


Figure 8. Pitch Adjustment

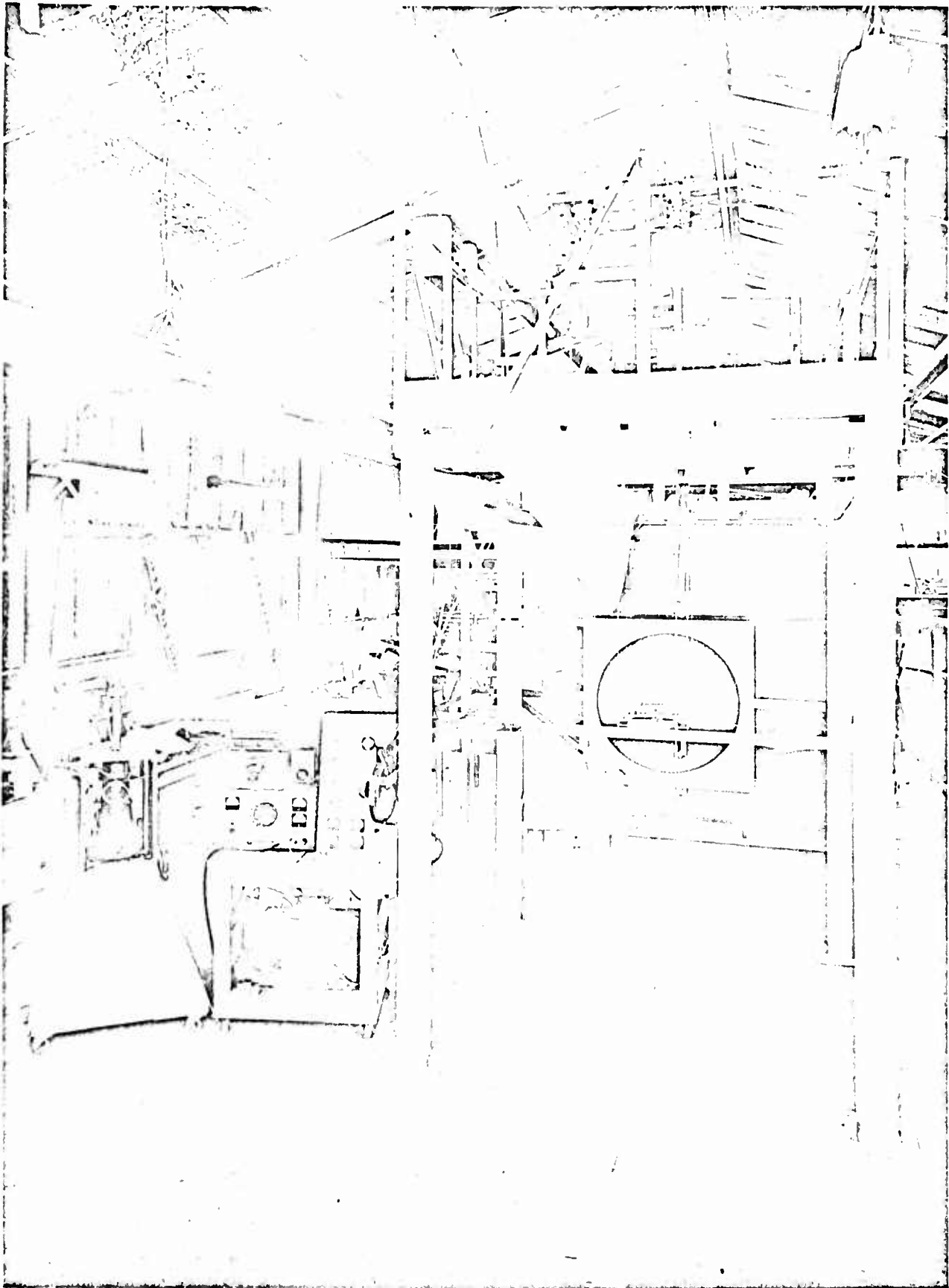


Figure 9. Wind Tunnel Testing Facilities

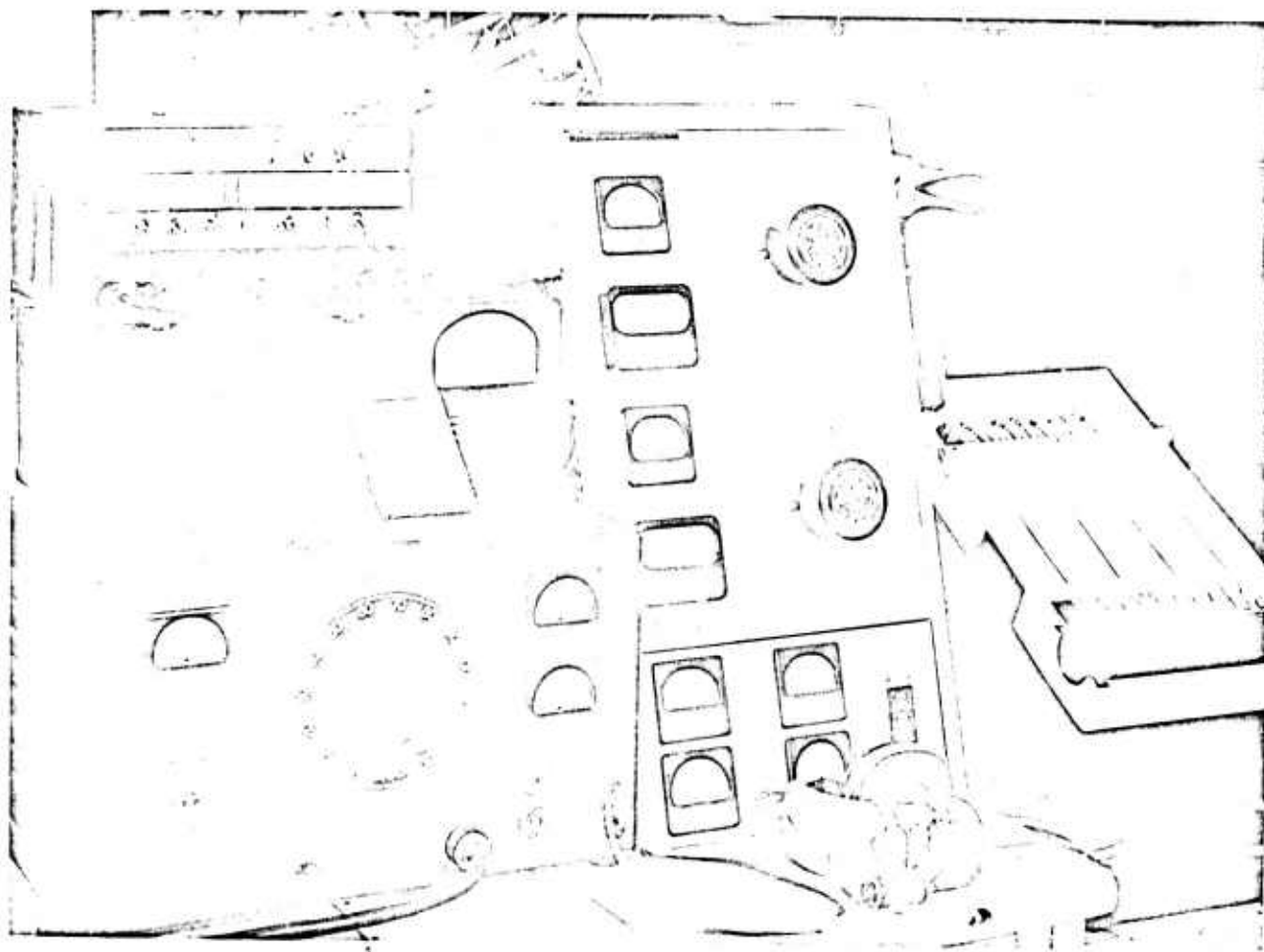


Figure 10. Measuring Equipment

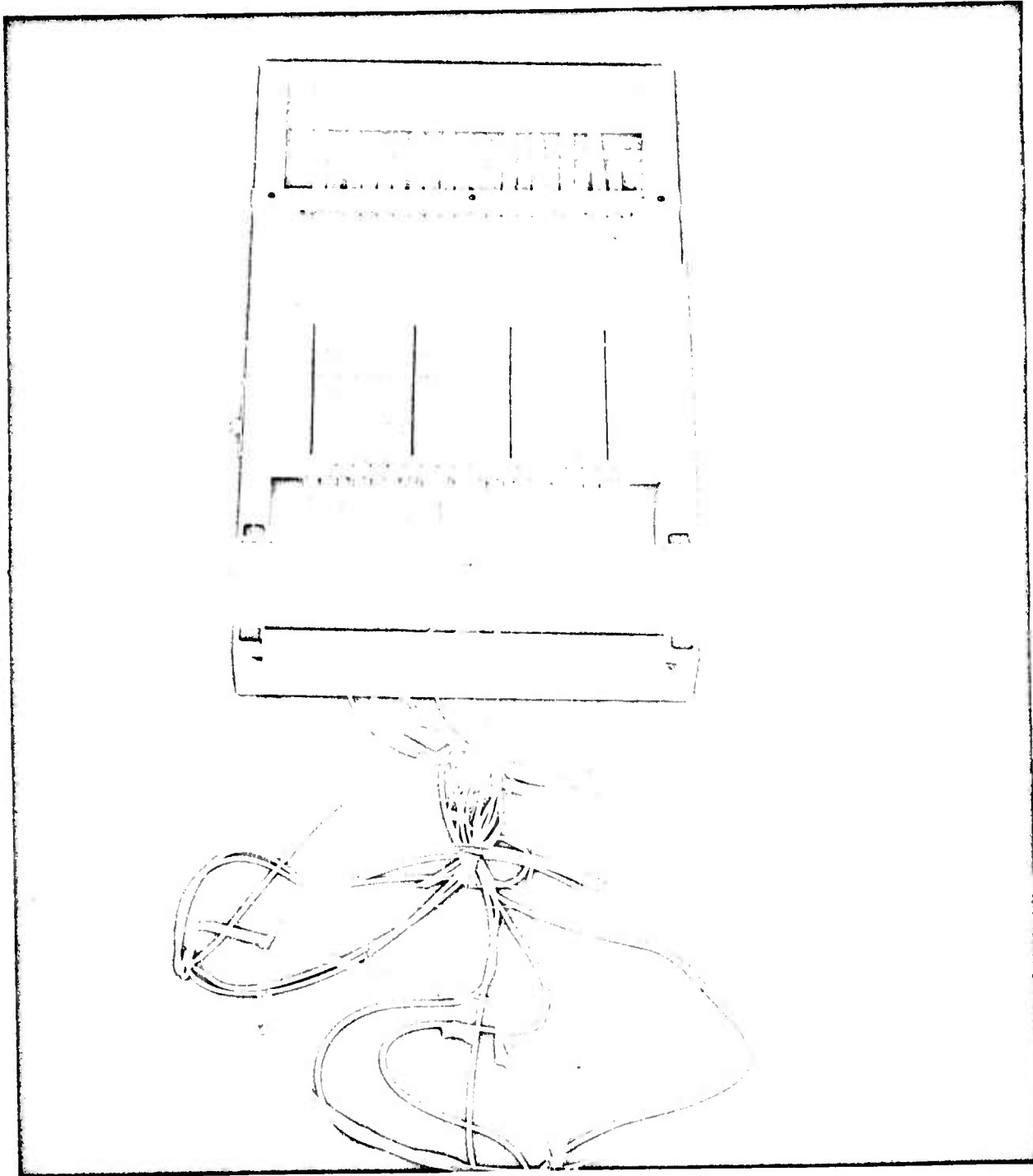


Figure 11. Total Head Rake and Multiple Manometer

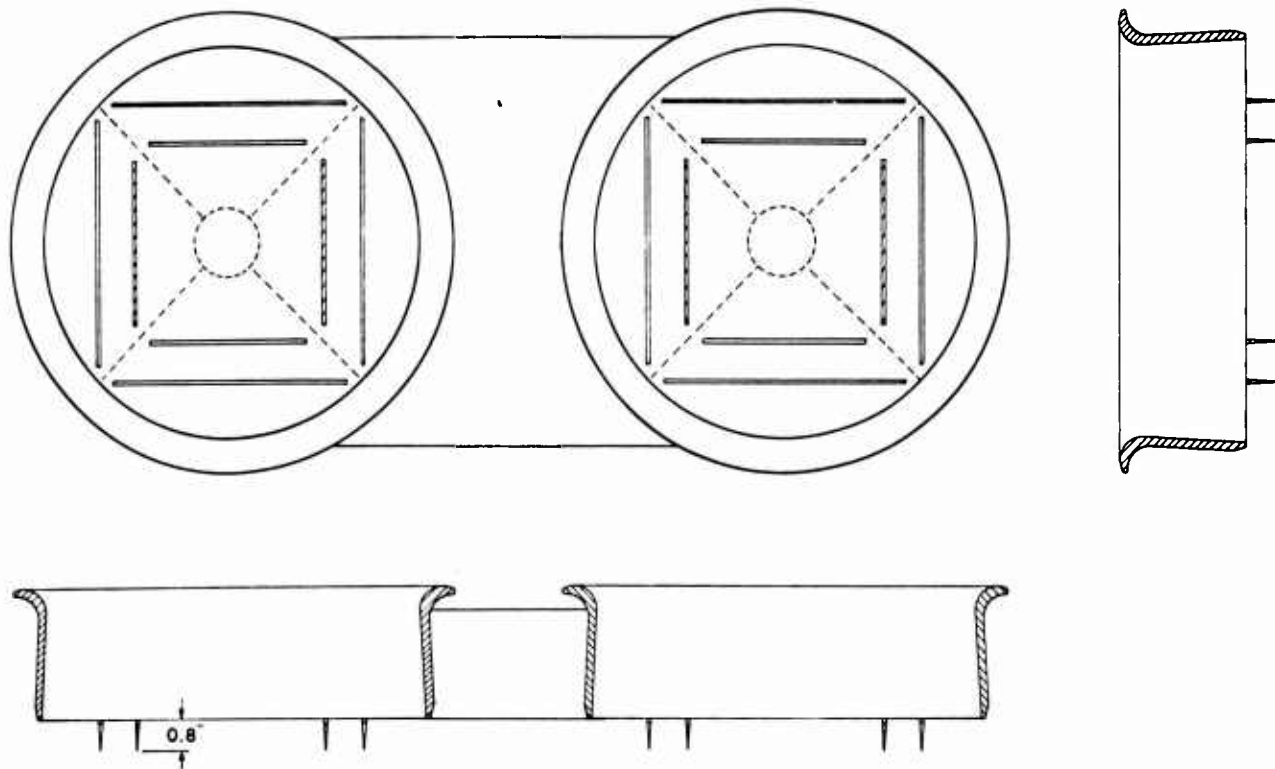


Figure 12. Double Pitch Vanes

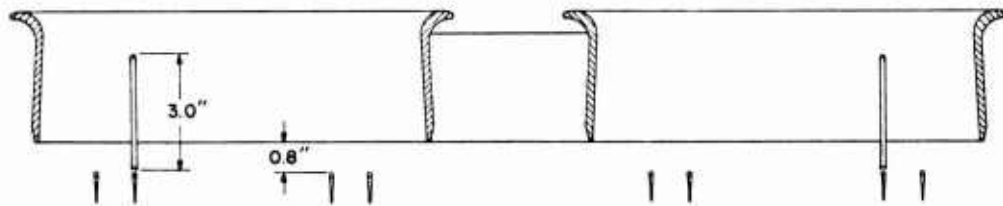


Figure 13. Fins Above Inner Vanes of Set A and D

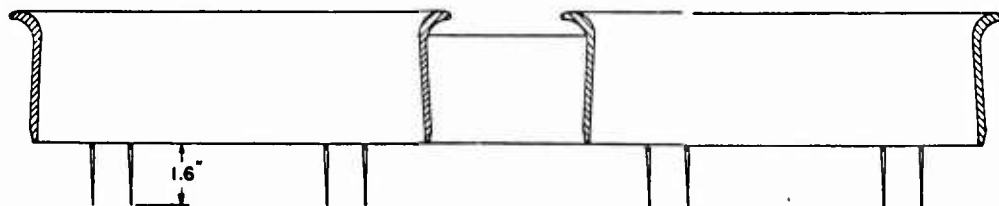


Figure 14. Vanes with Double Chord Length

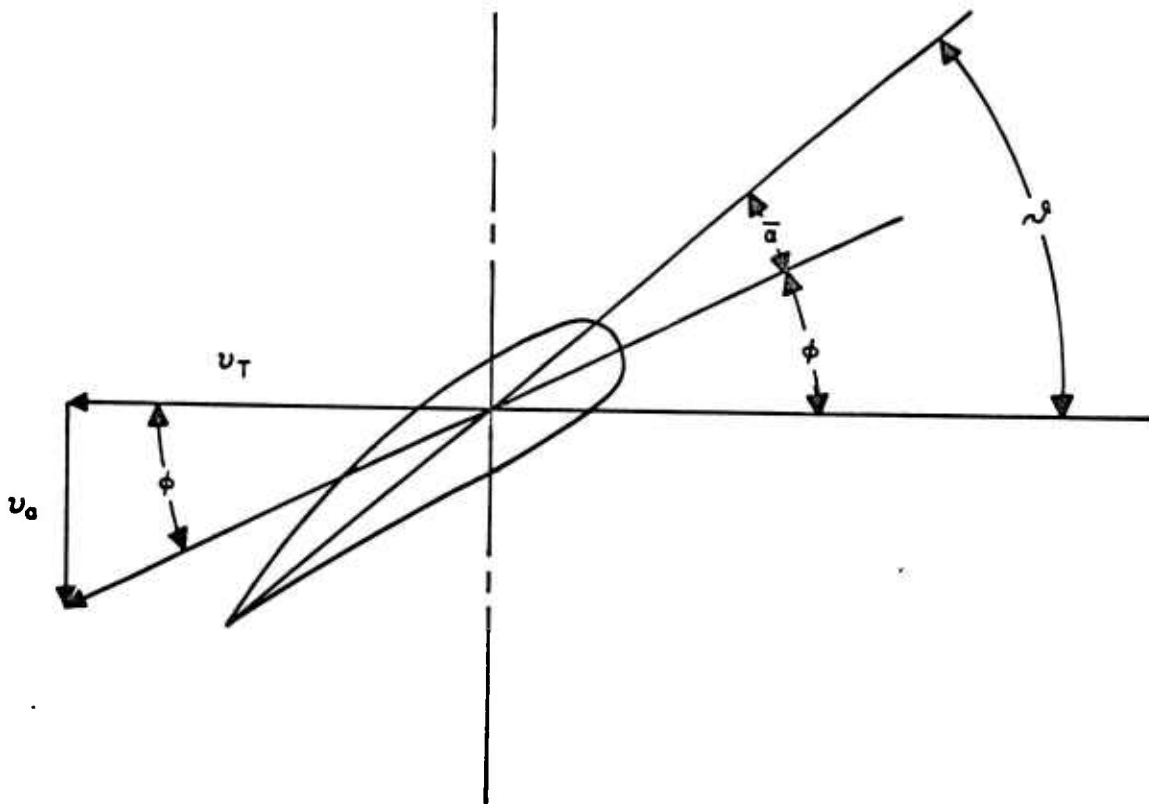


Figure 15. Prop Section with Symbols used in Related Calculations

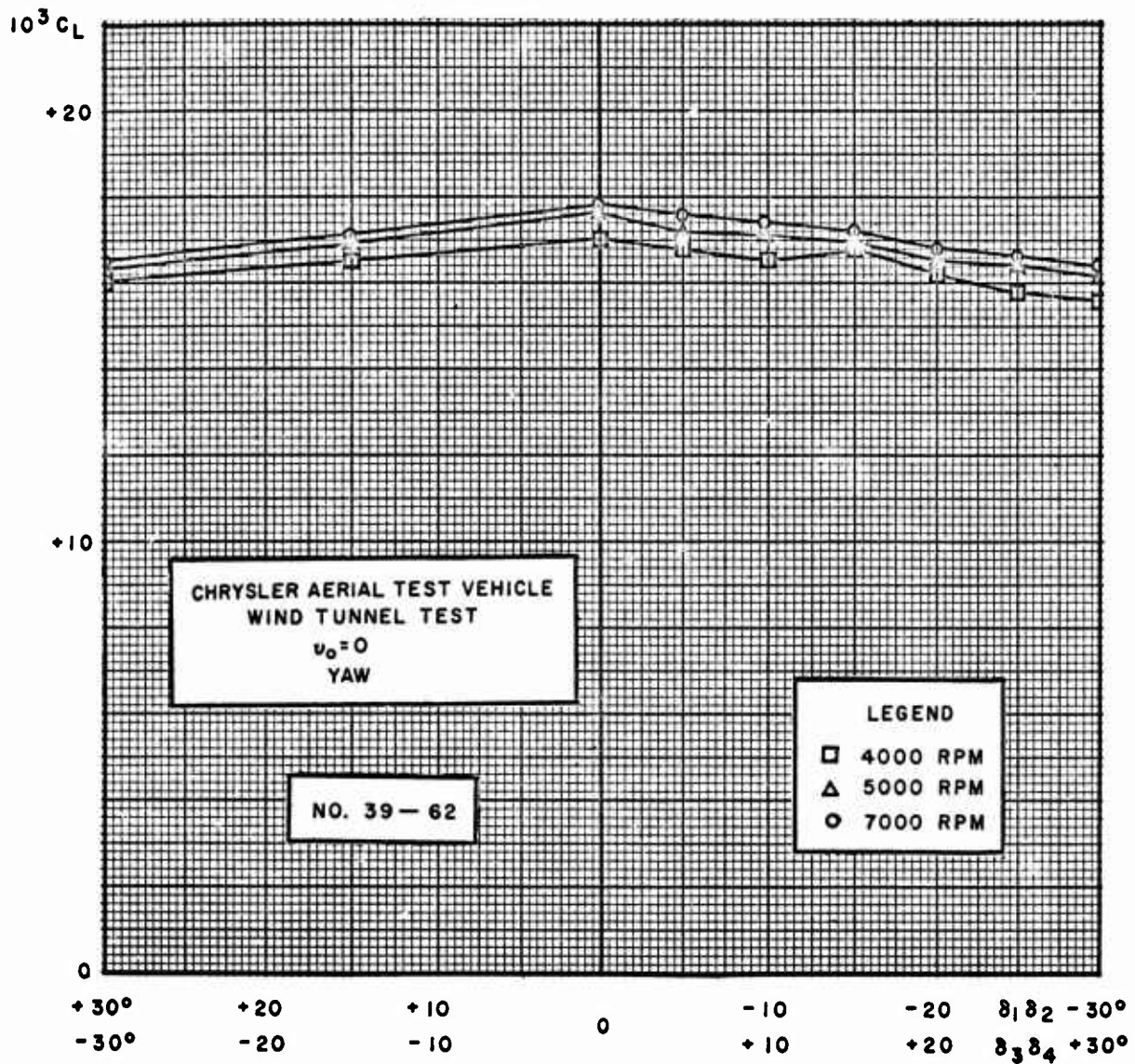


Figure 16.  $C_L$  vs Vane Deflection for Yaw in Hovering



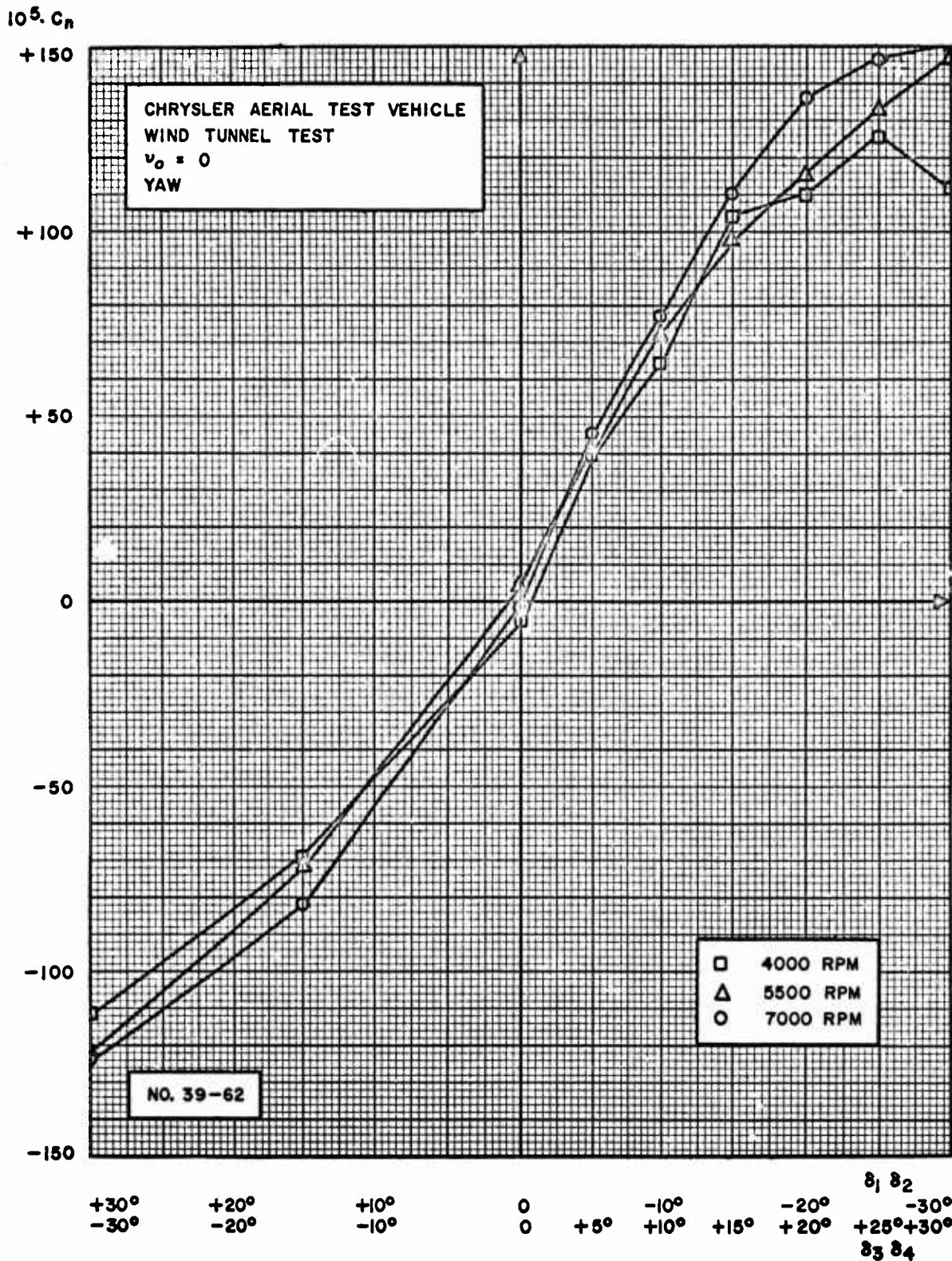


Figure 17.  $C_n$  vs Vane Deflection for Yaw in Hovering

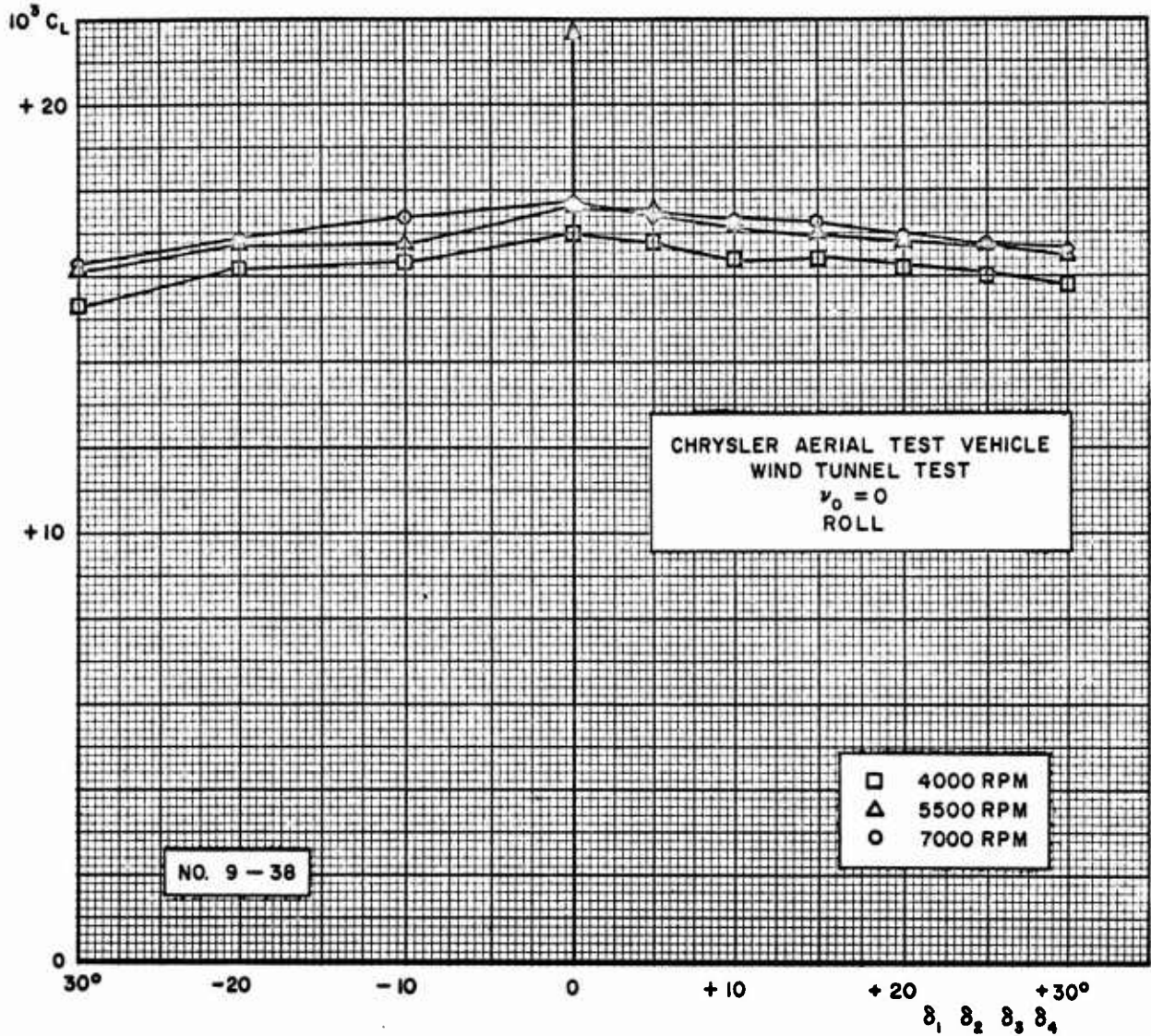


Figure 18.  $C_L$  vs Vane Deflection for Roll in Hovering

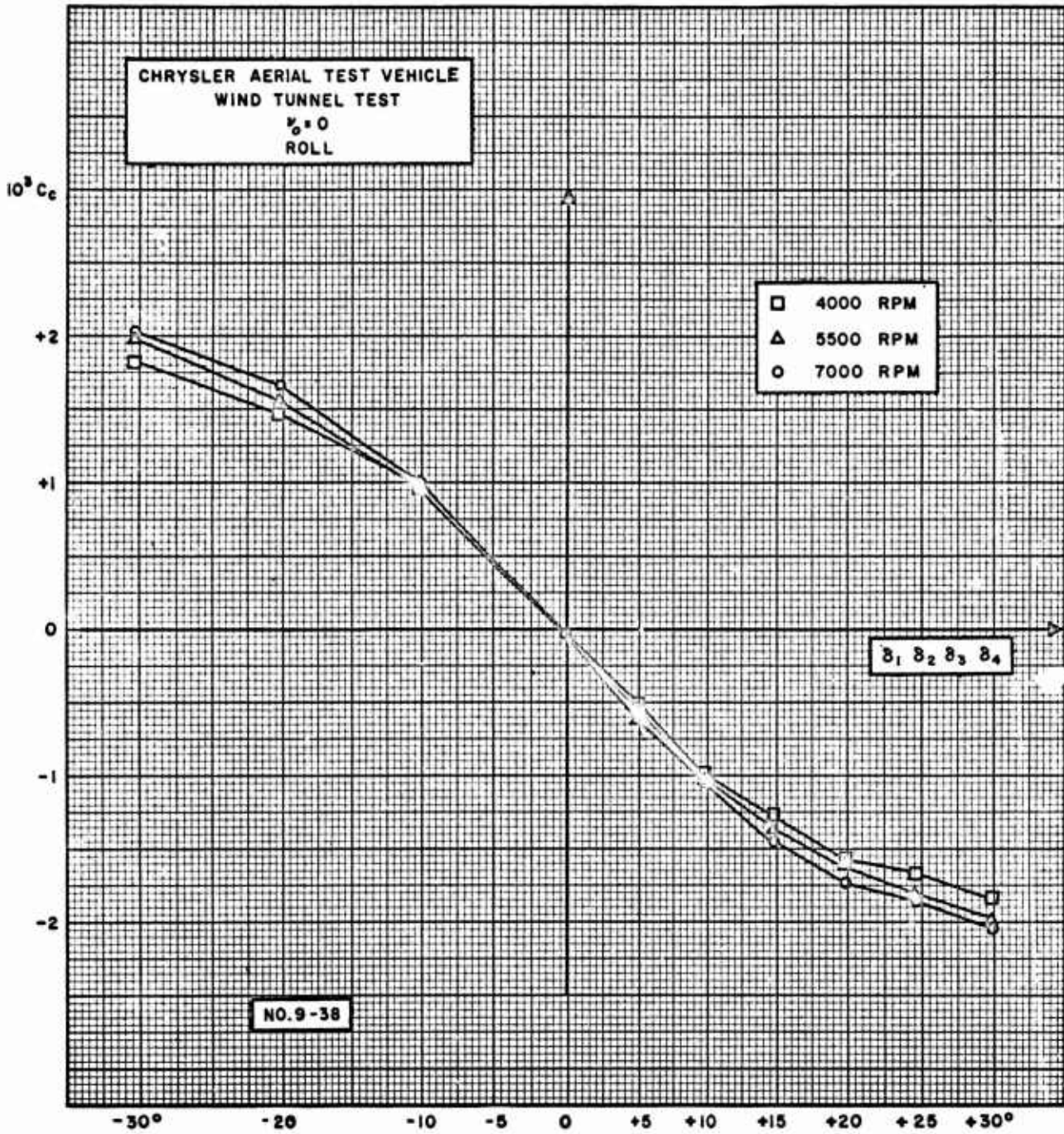


Figure 19.  $C_c$  vs Vane Deflection for Roll in Hovering

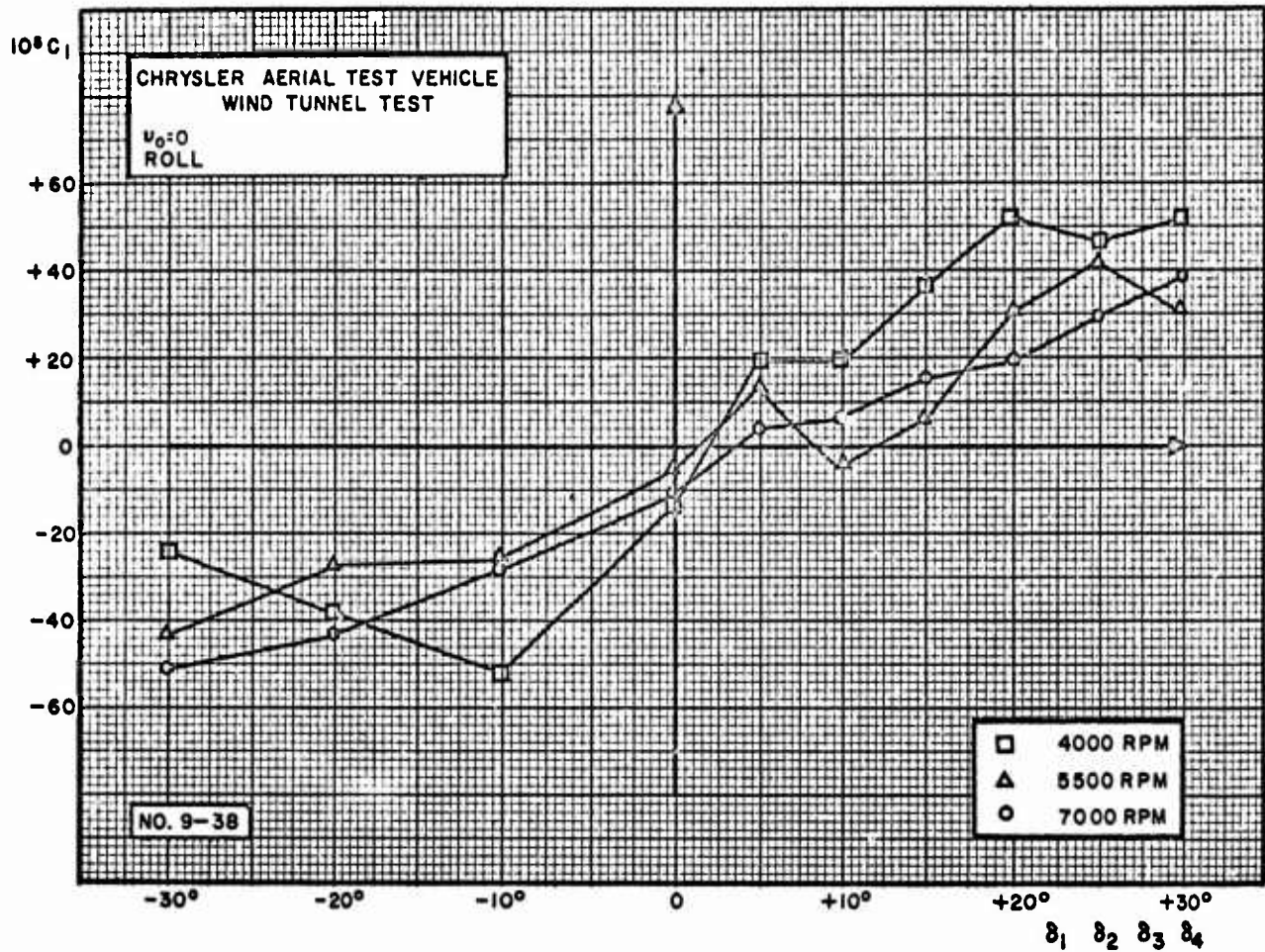


Figure 20.  $C_1$  vs Vane Deflection for Roll in Hovering

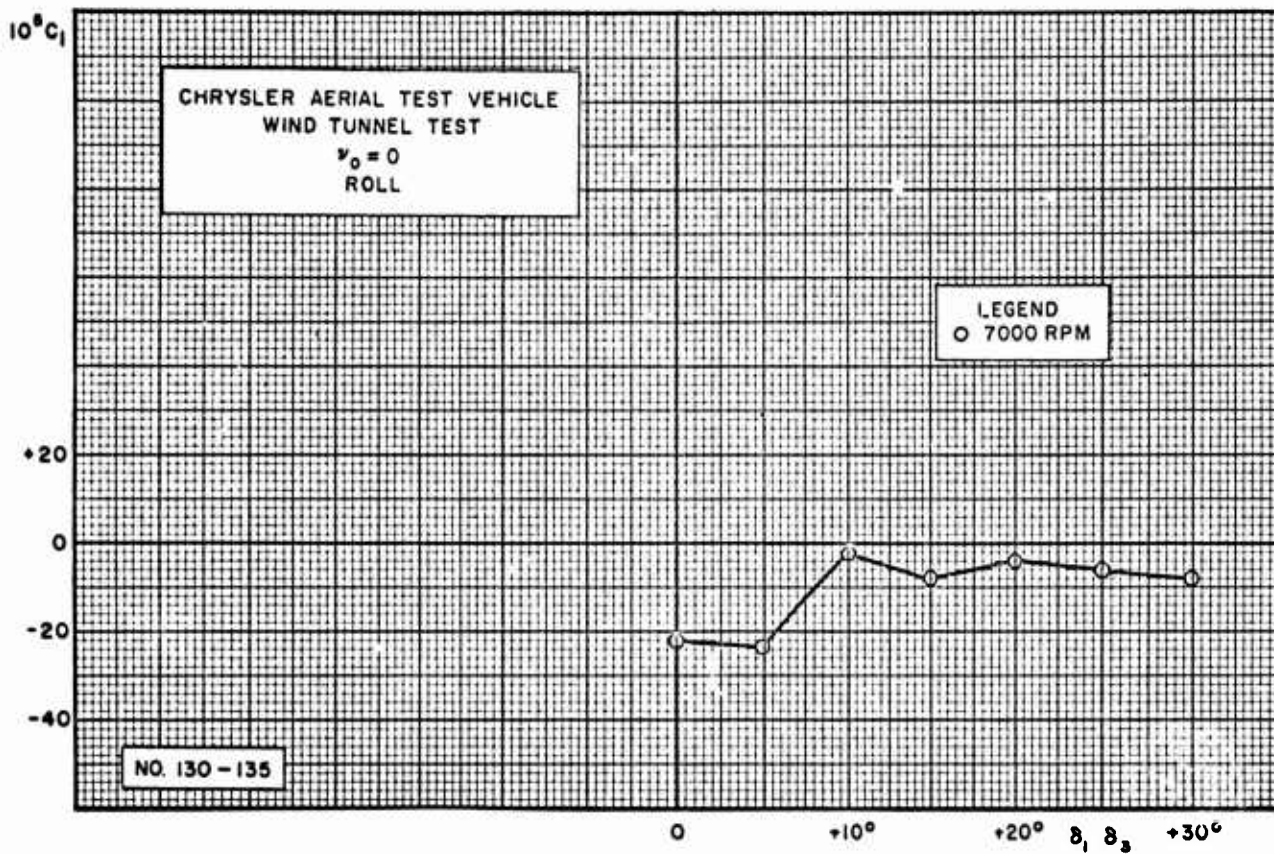


Figure 21.  $C_1$  vs Vane Deflection for Roll in Hovering.  
Roll Vanes Deflection on One Side Only

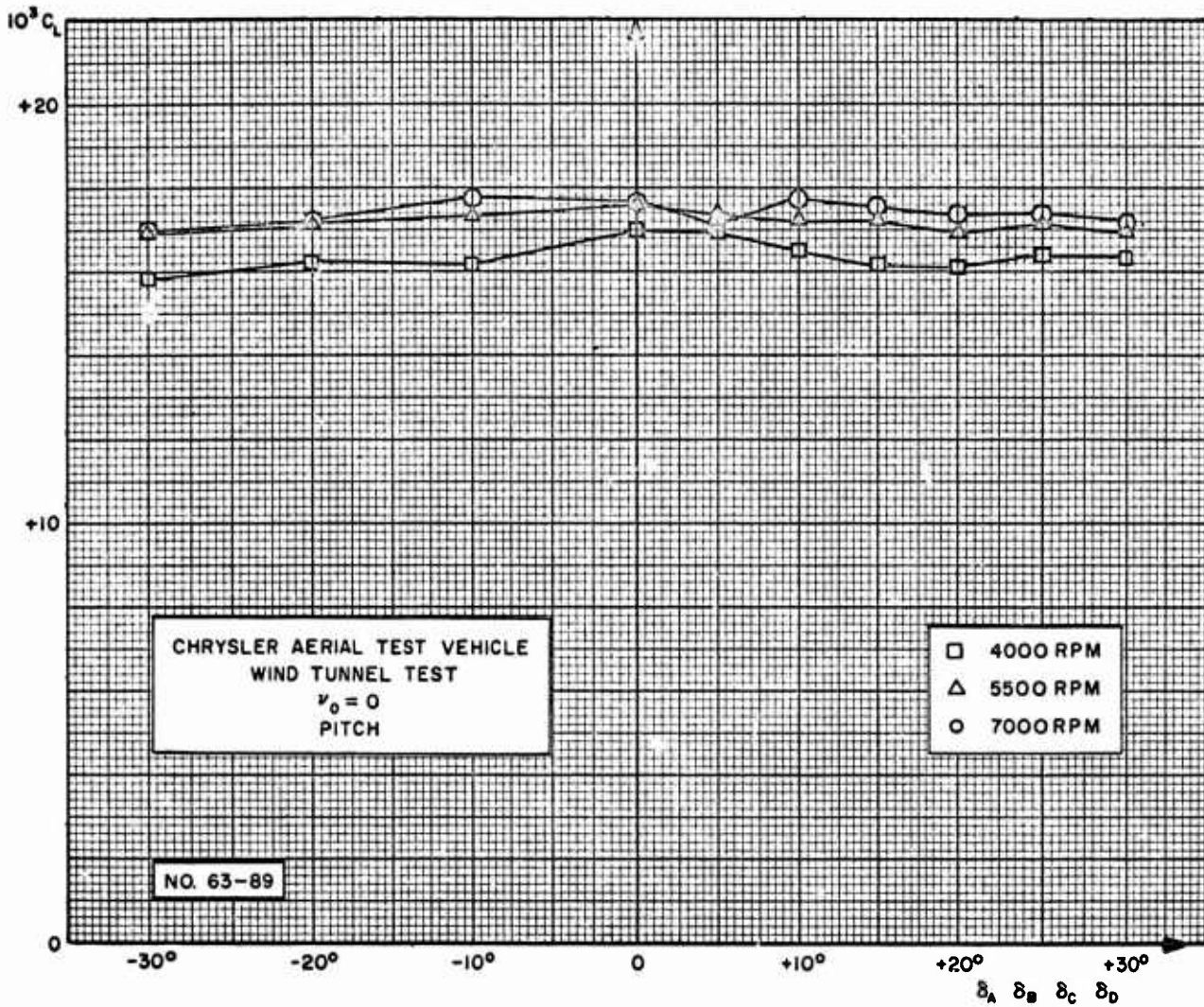


Figure 22.  $C_L$  vs Vane Deflection for Pitch in Hovering

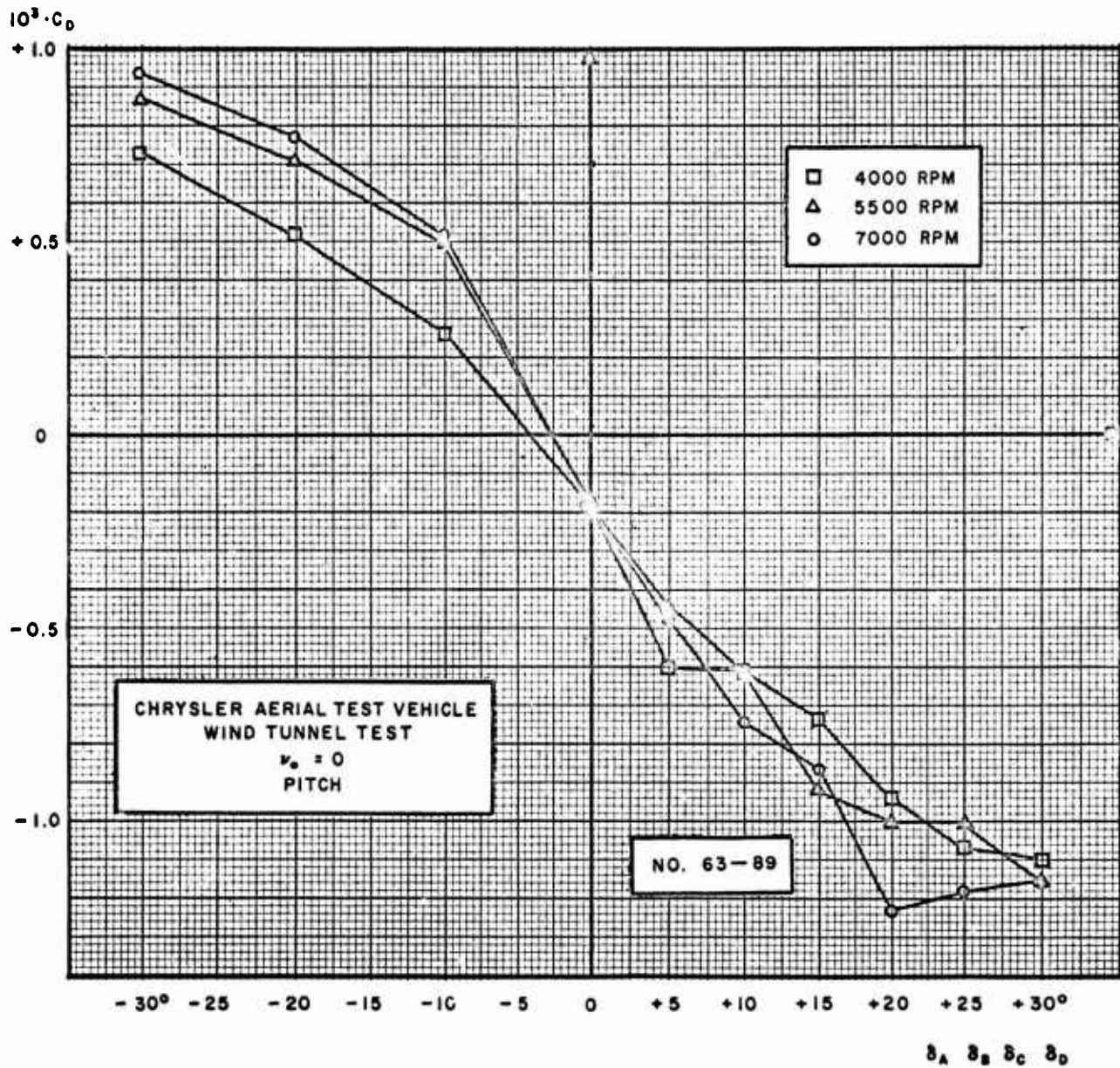


Figure 23.  $C_D$  vs Vane Deflection for Pitch in Hovering

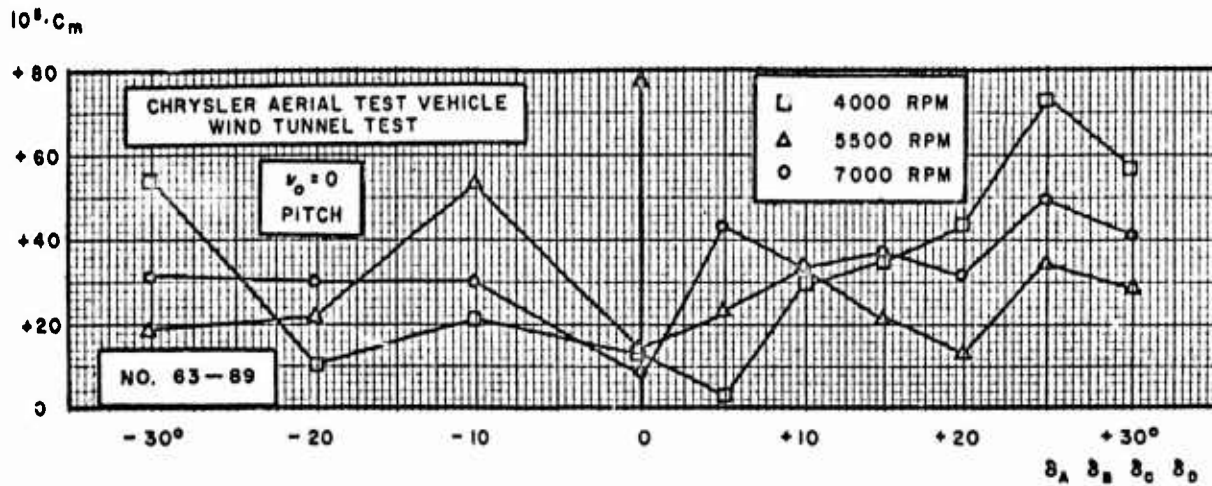


Figure 24.  $C_m$  vs Vane Deflection for Pitch in Hovering

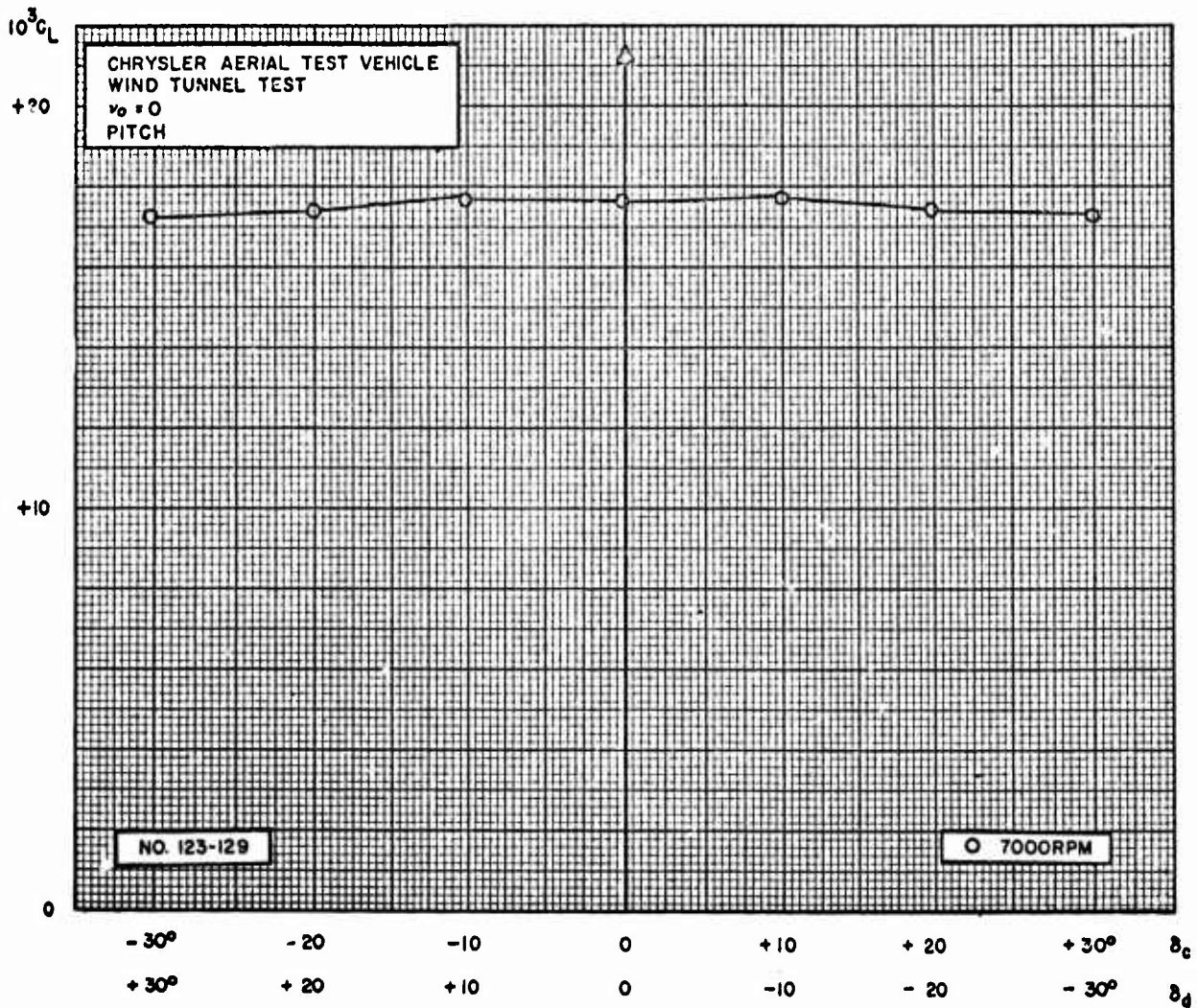


Figure 25.  $C_L$  vs Vane Deflection with Rear Shroud Pitch Vanes Deflected in Opposite Directions



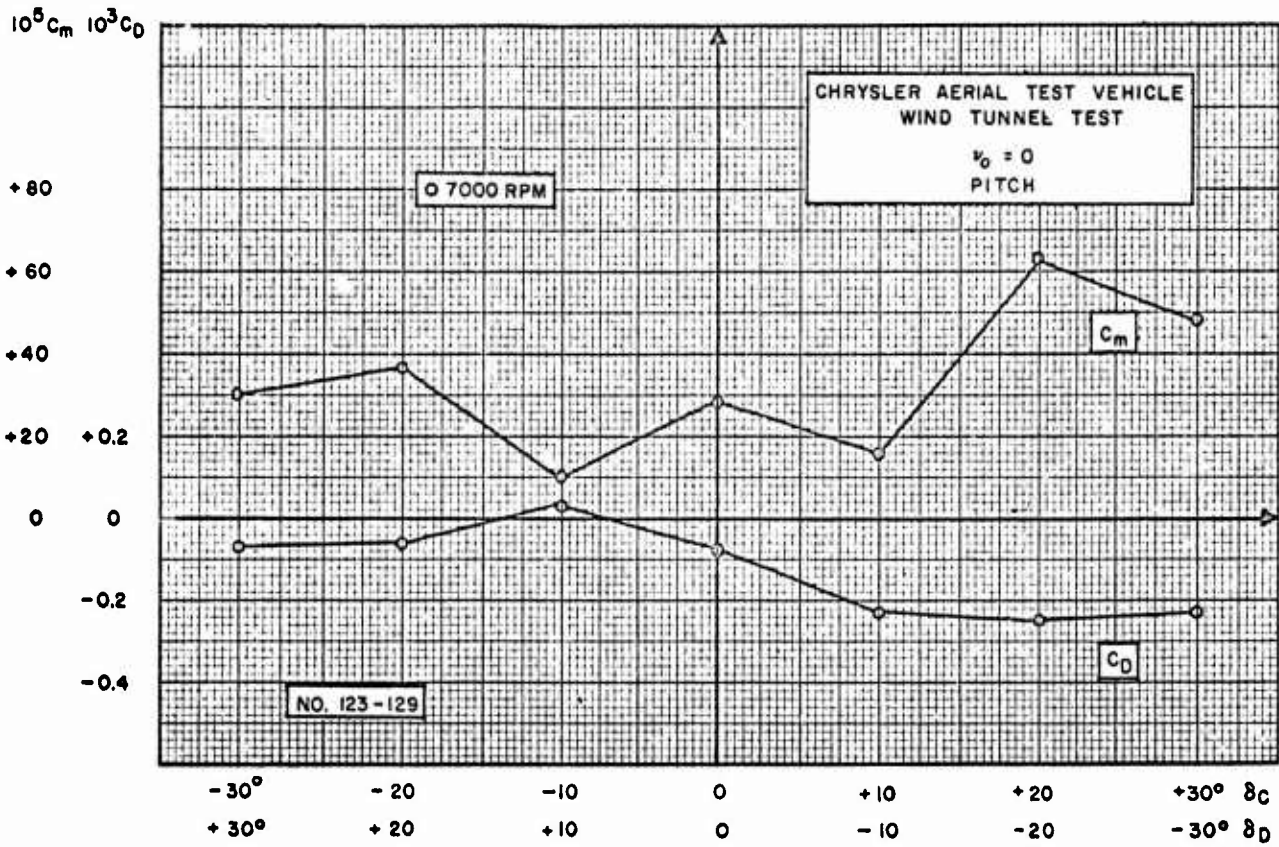


Figure 26.  $C_D$  and  $C_m$  vs Vane Deflection with Rear Shroud Pitch  
Vaness Deflected in Opposite Directions

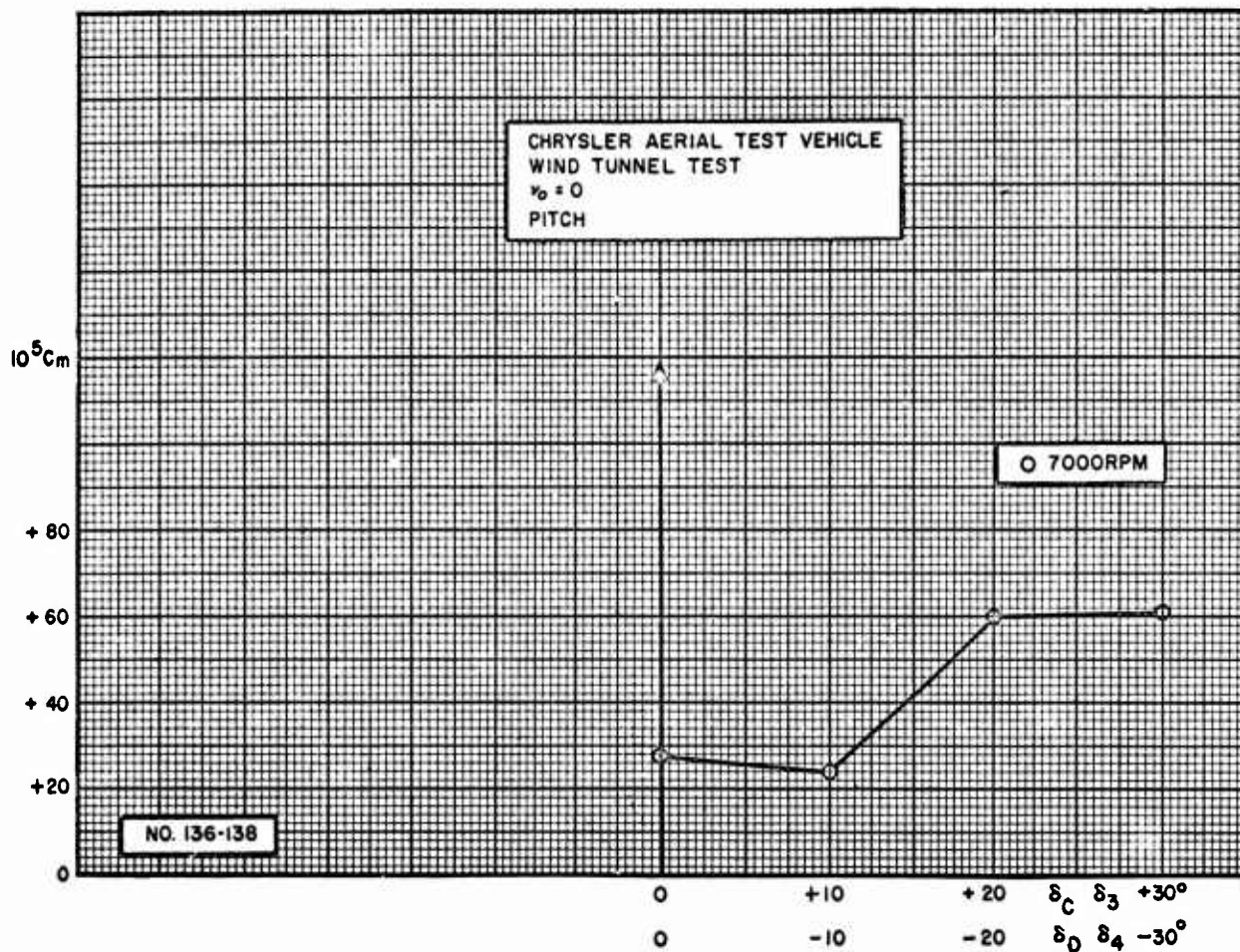


Figure 27.  $C_m$  vs Vane Deflection with Vanes in Rear Shroud Deflected Inward

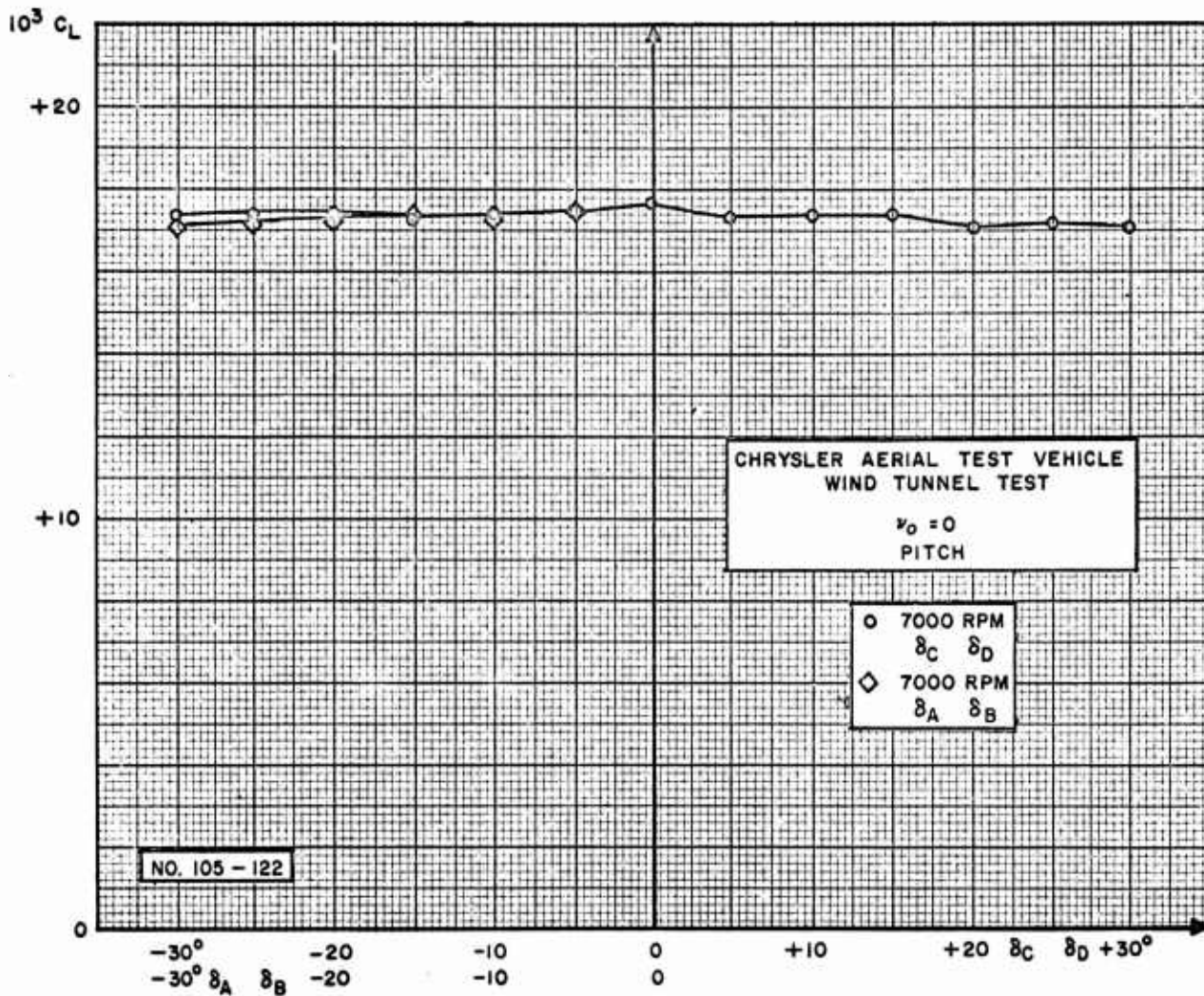


Figure 28.  $C_L$  vs Vane Deflection with Pitch Vanes Deflected in Rear or Front Shroud Only

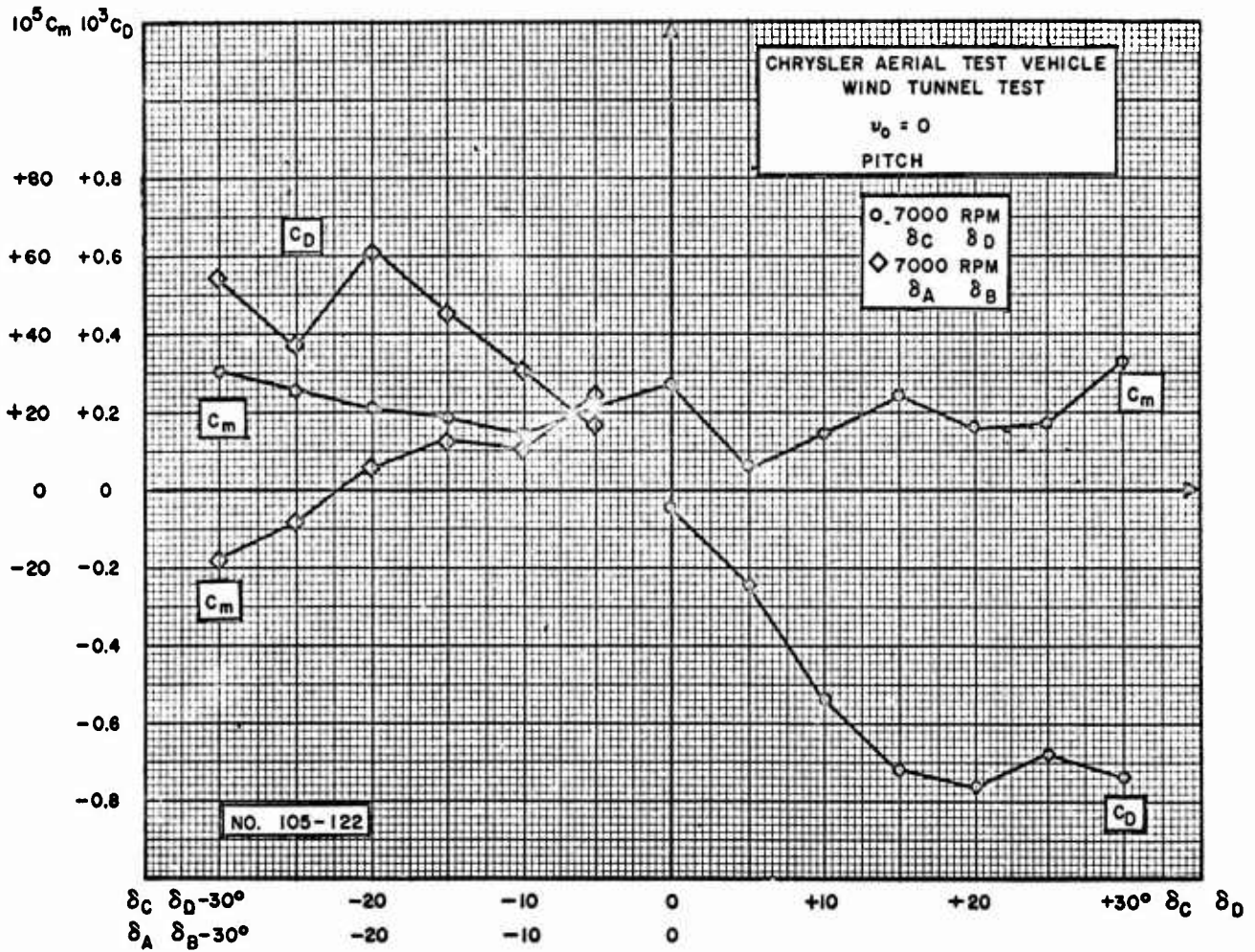


Figure 29.  $C_D$  and  $C_m$  vs Vane Deflection with Pitch Vanes Deflected in Front or Rear Shroud Only

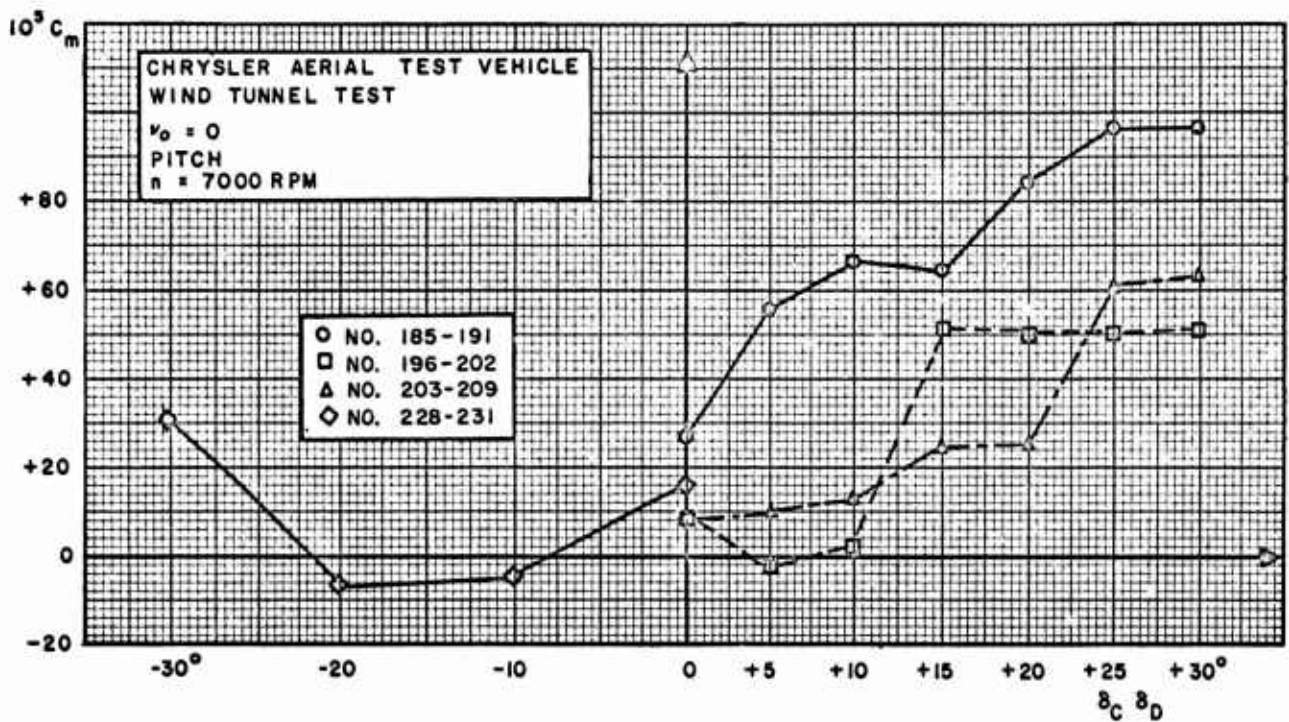
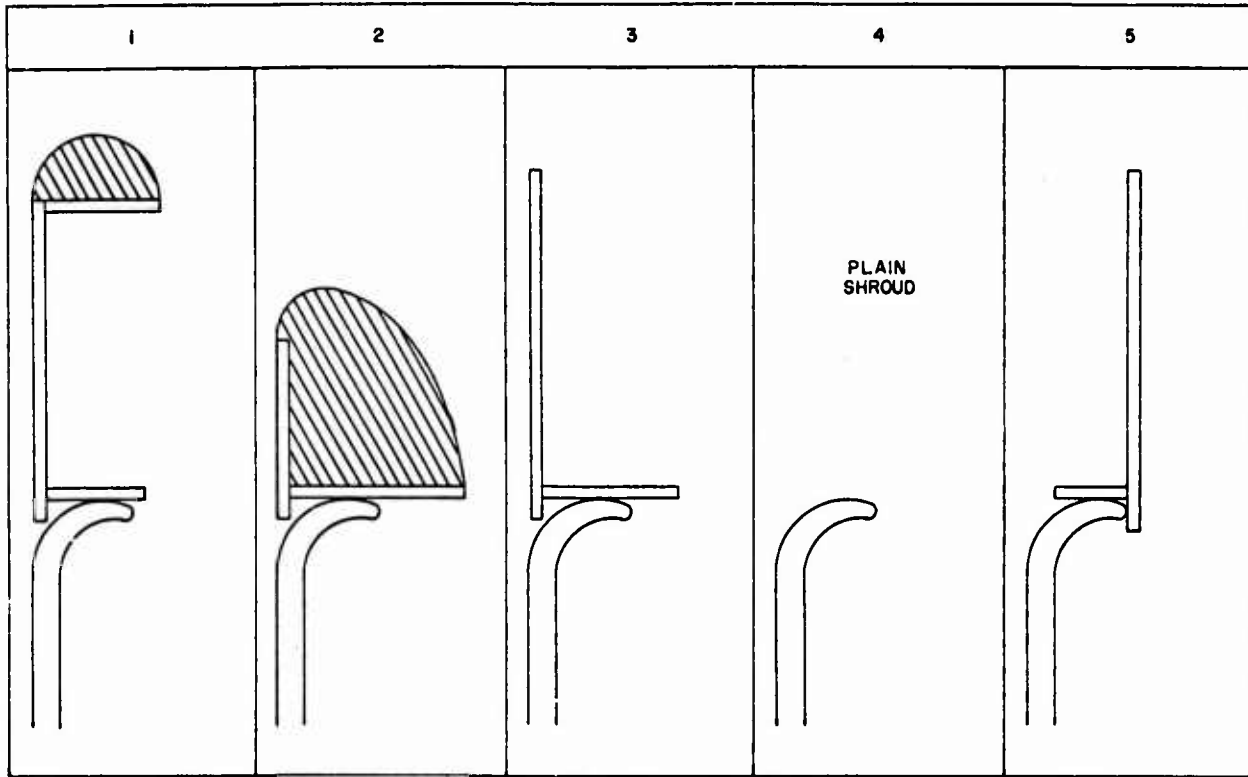


Figure 30.  $C_m$  vs Vane Deflection with Vanes in Rear Shroud at Position 3 and Double Pitch Vanes Installed

TESTS 1-5



TESTS 6-10

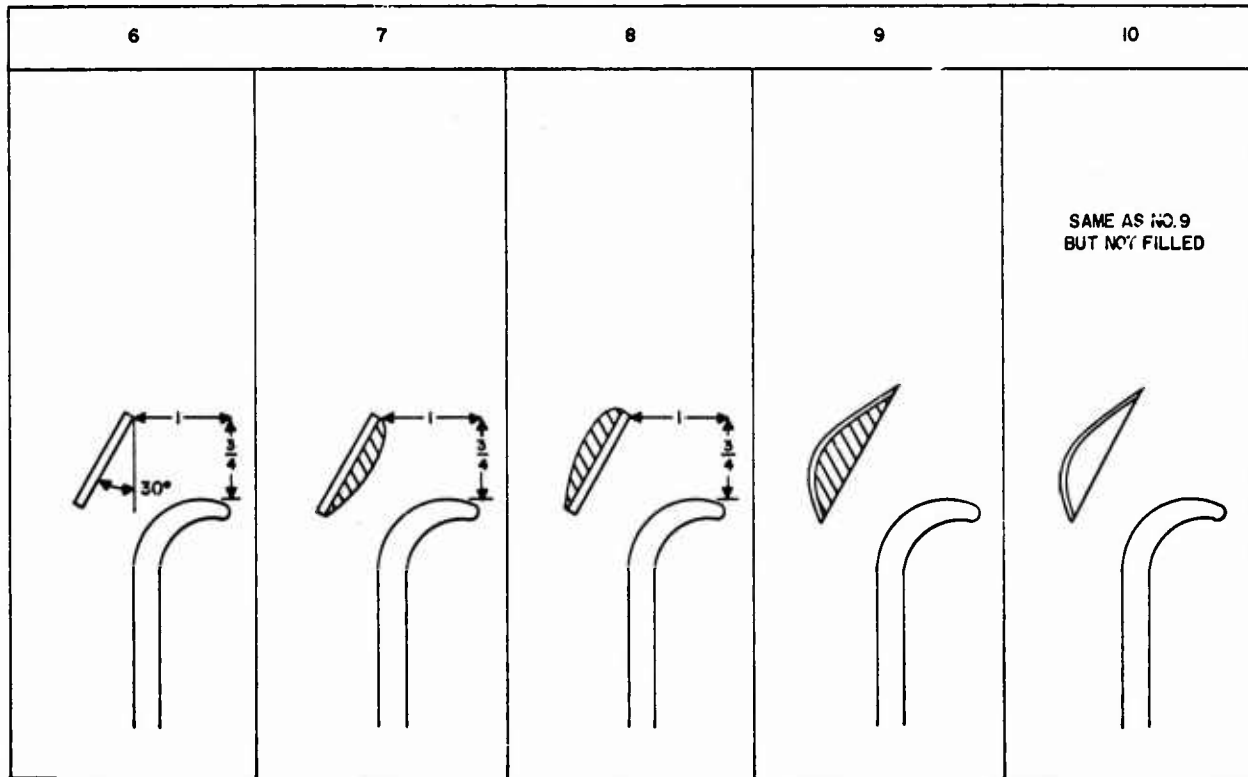


Figure 31. Shroud Inlet Modification

TEST NO. 11-16

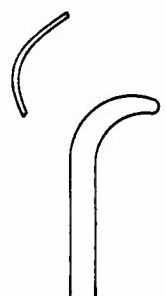
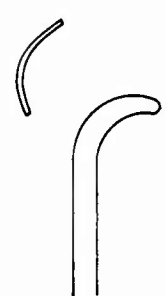
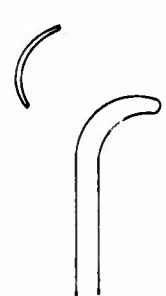
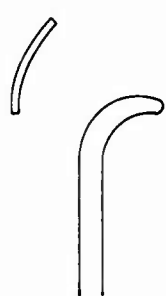
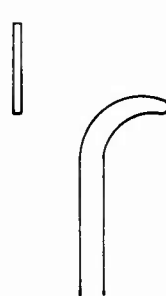
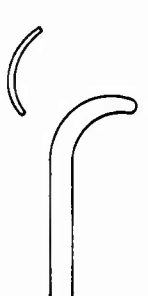
11	12	13	14	15	16
SAME AS NO.10 BUT $\frac{1}{2}$ IN. CUT FROM TOP OF RING	SAME AS NO.11 BUT $\frac{1}{4}$ IN. ADDITIONAL CUT FROM TOP OF RING	SAME AS NO.12 BUT SMALLER RADIUS OF CURVATURE	SAME AS NO.12 BUT LARGER RADIUS OF CURVATURE		FINAL FORM OF RING FOR BEST RESULTS
					

Figure 32. Shroud Inlet Modification (Cont)

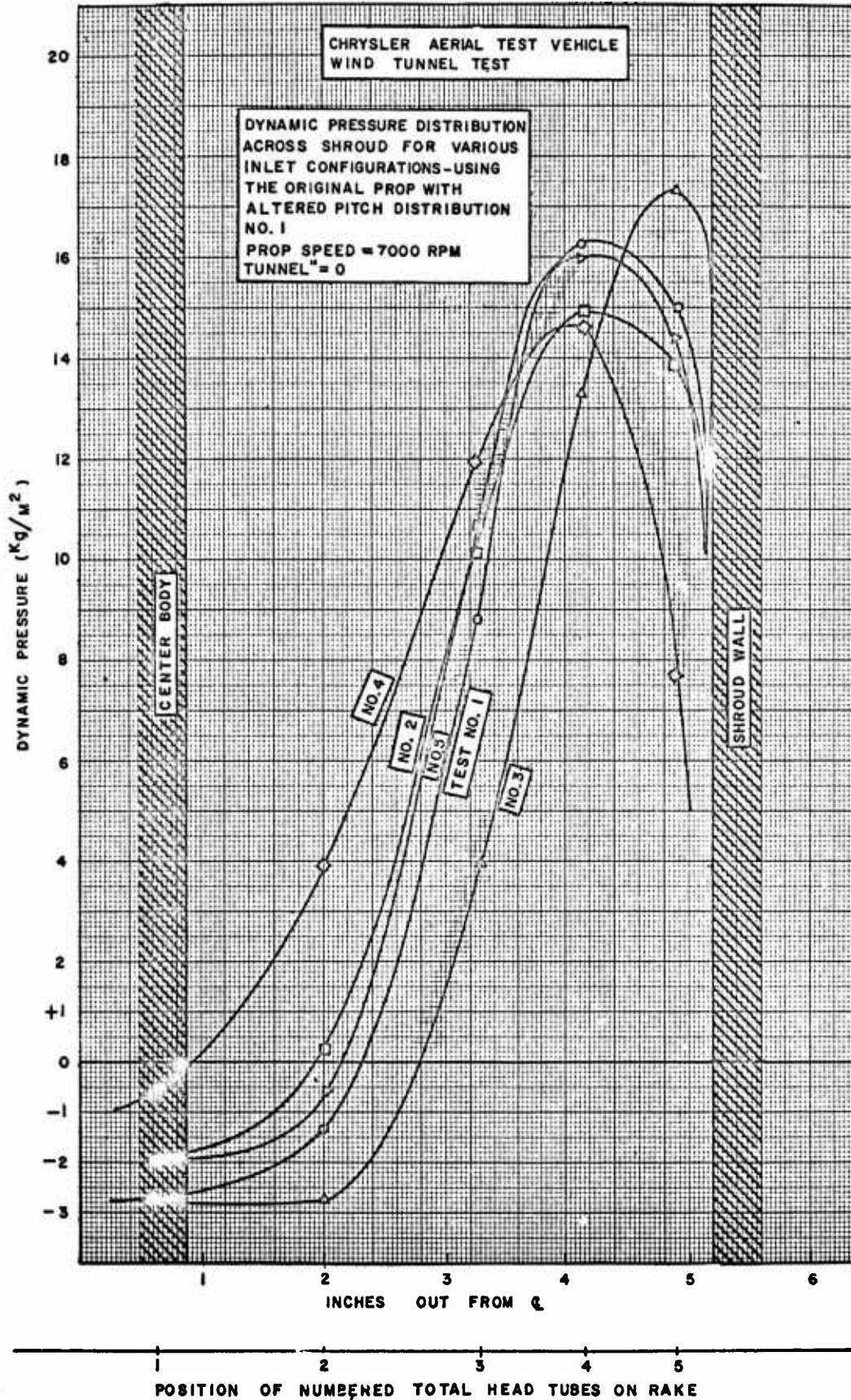


Figure 33. Dynamic Pressure Distribution Curves Obtained from Configurations in Figure 31 with Prop Pitch Distribution #1



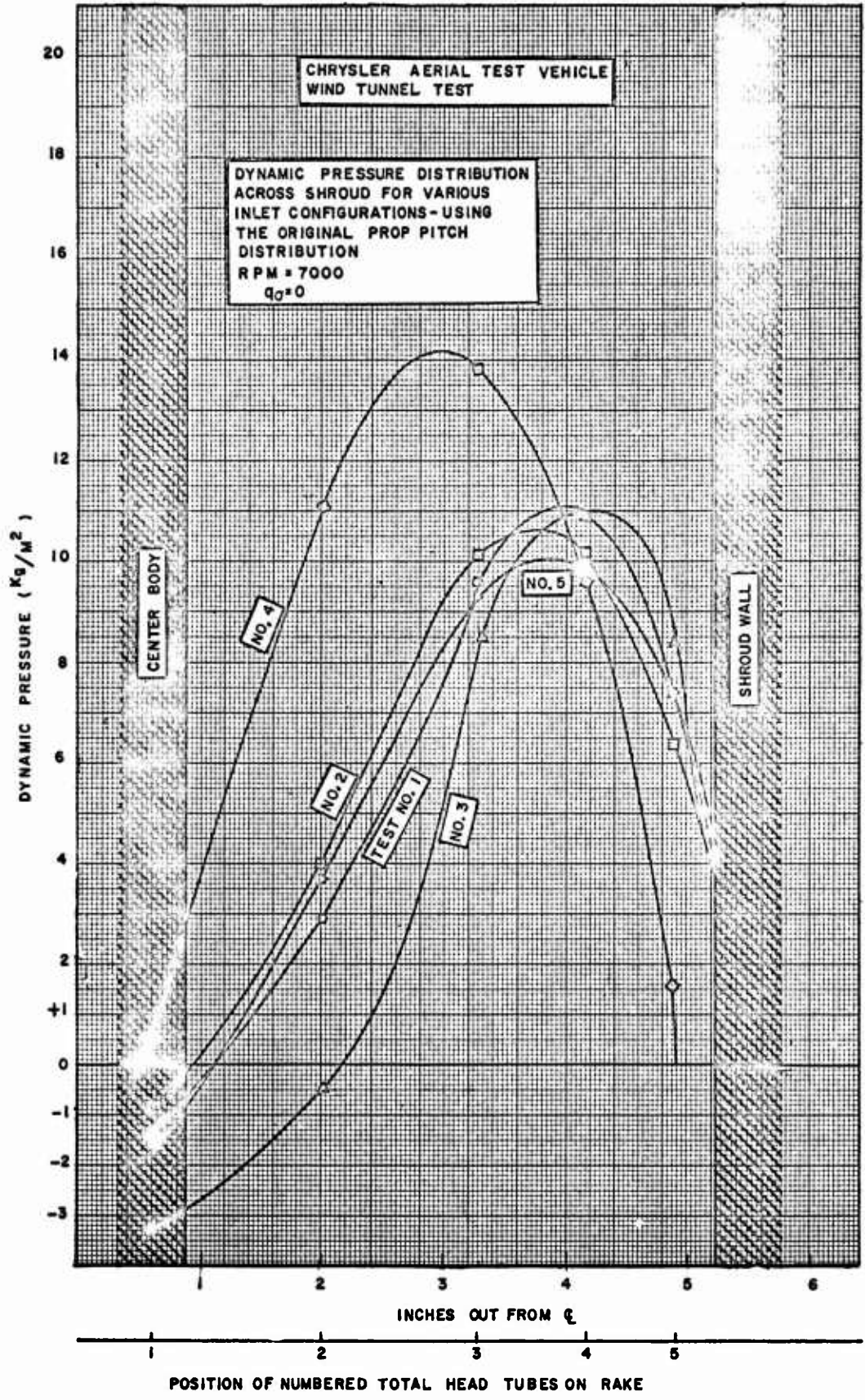


Figure 34. Dynamic Pressure Distribution Curves Obtained from Configurations in Figure 31 with Original Prop Pitch Distributions

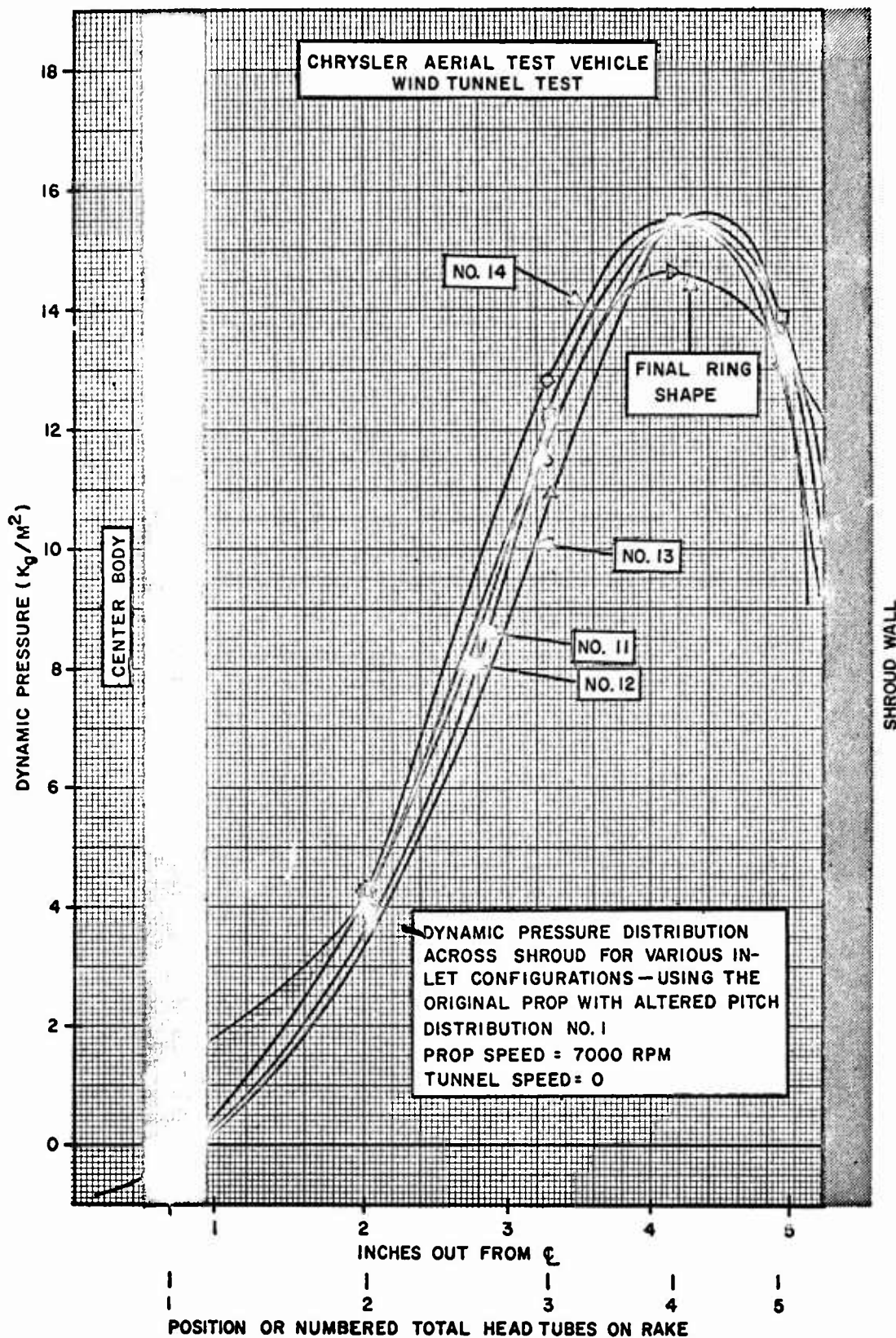


Figure 35. Dynamic Pressure Distribution Curves Obtained from Configurations in Figure 32 with Prop Pitch Distribution #1

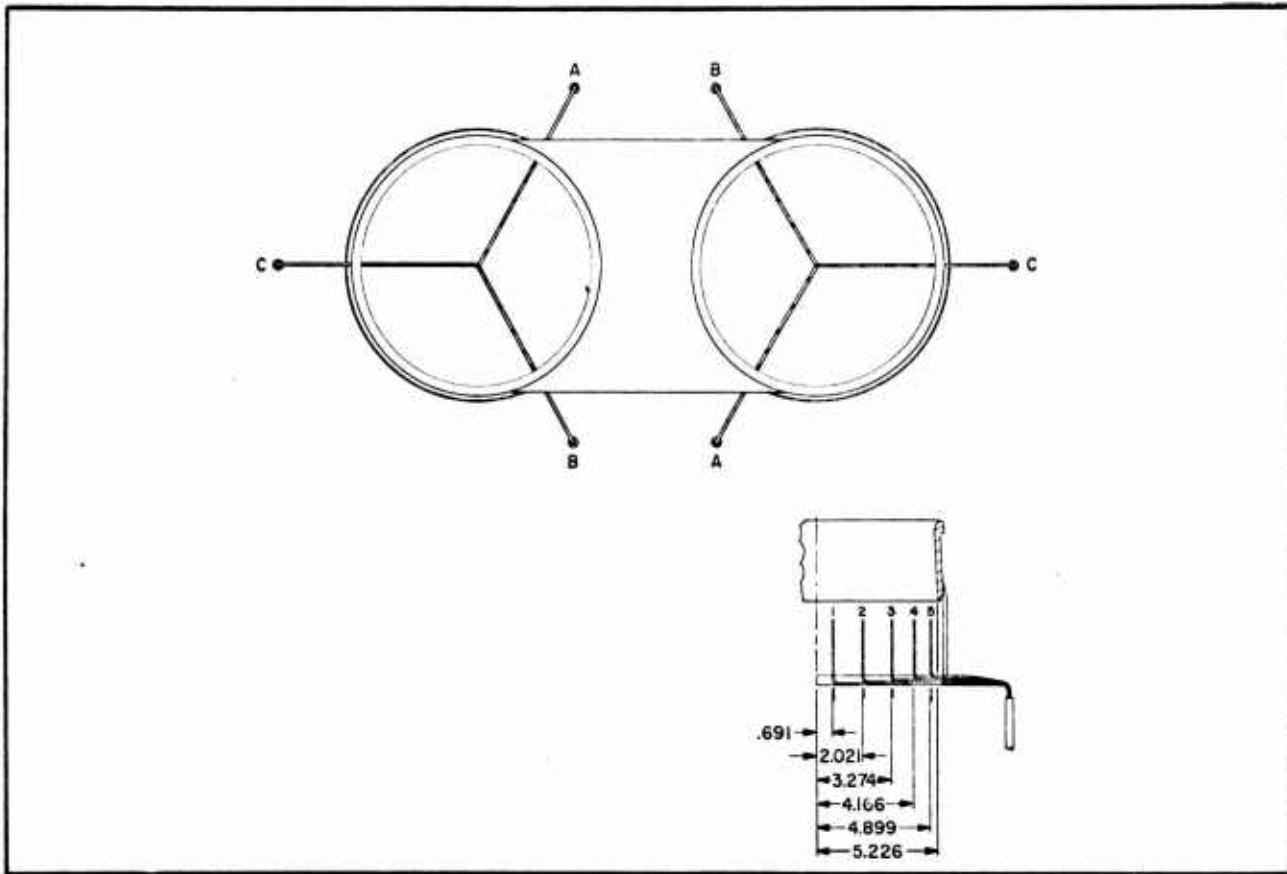


Figure 35A. Detail of Total Head Rake

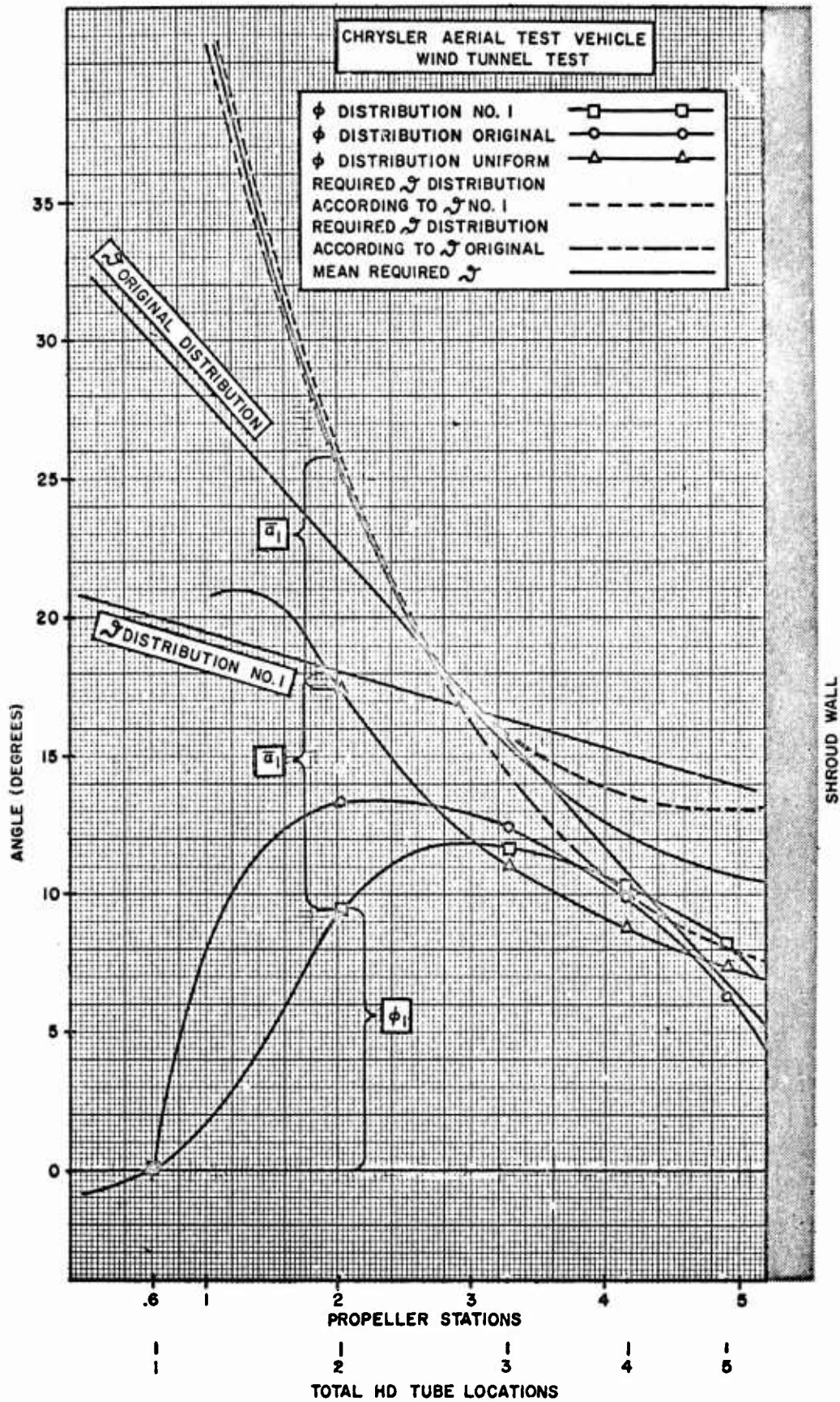


Figure 36. First Propeller Pitch Modification Curves

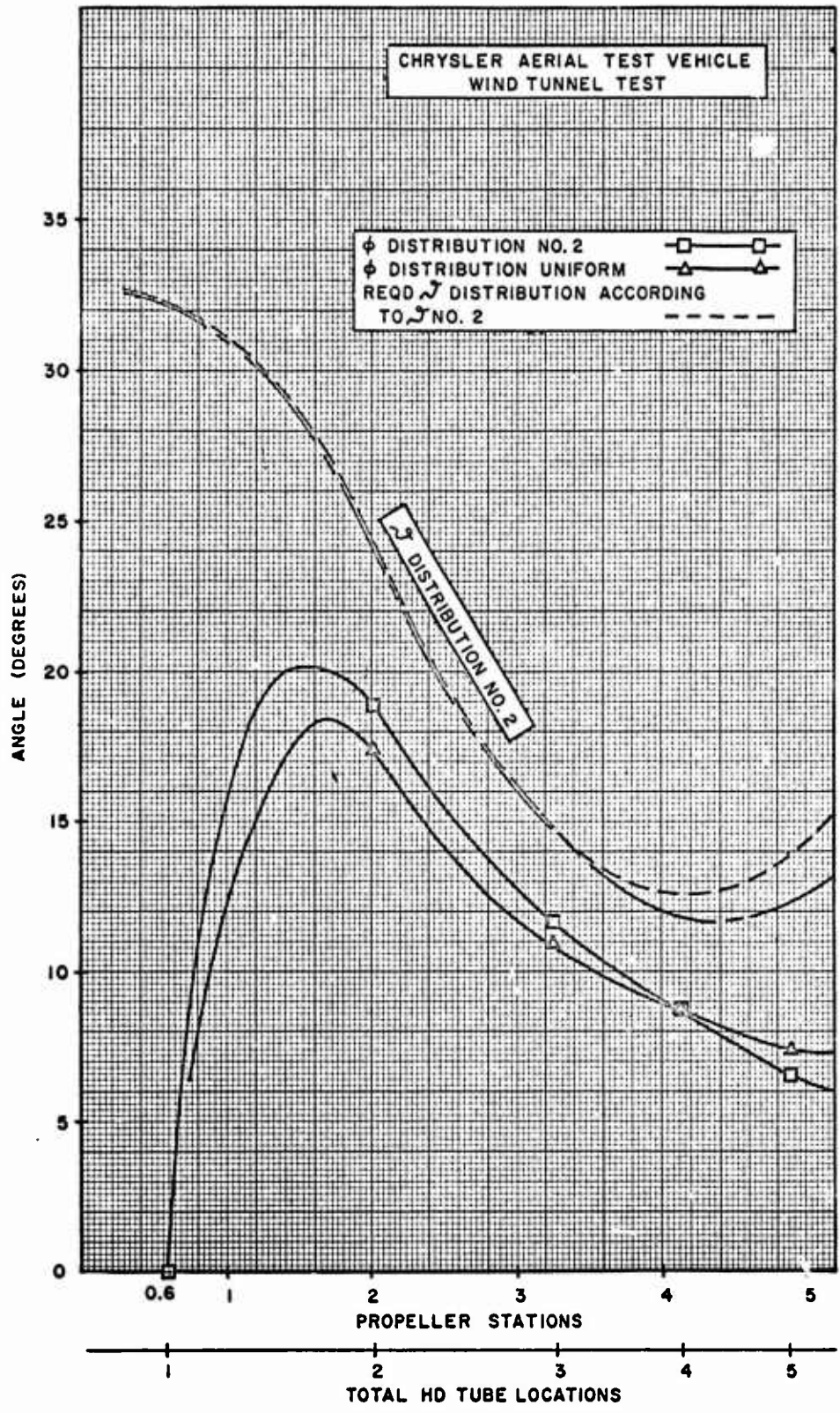


Figure 37. Second Propeller Pitch Modification Curves

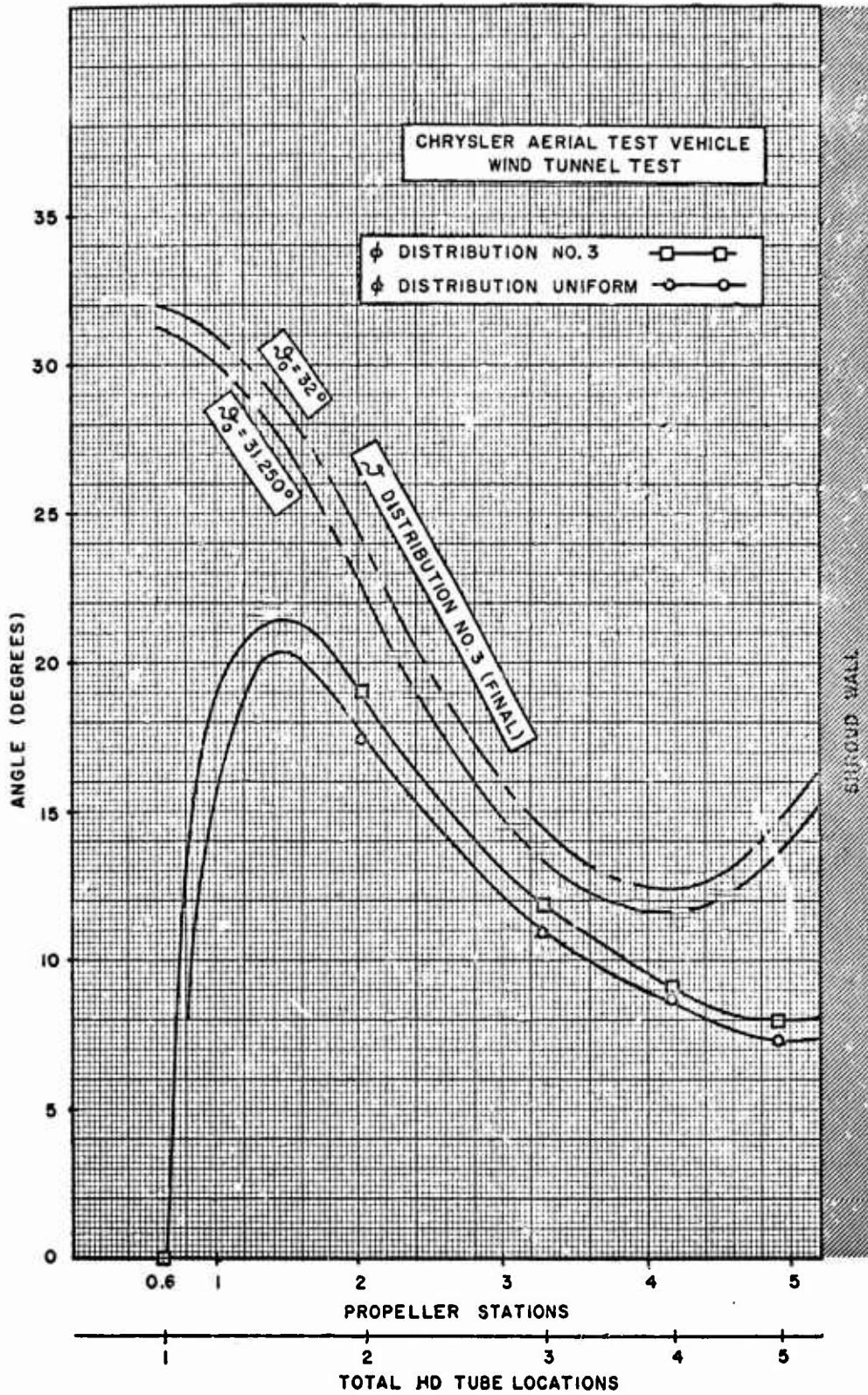


Figure 38. Final Propeller Pitch Modification Curves

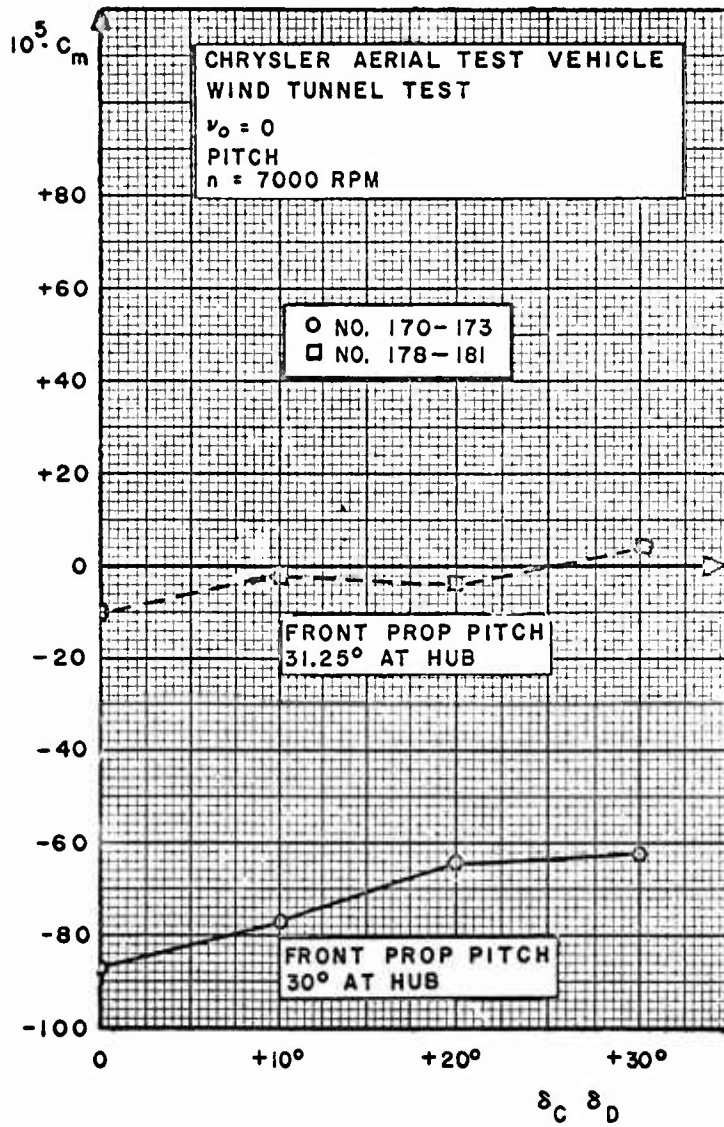


Figure 39. Variation of  $C_m$  with  $\delta$  for Deflection of Pitch Vanes in Rear Shroud Only

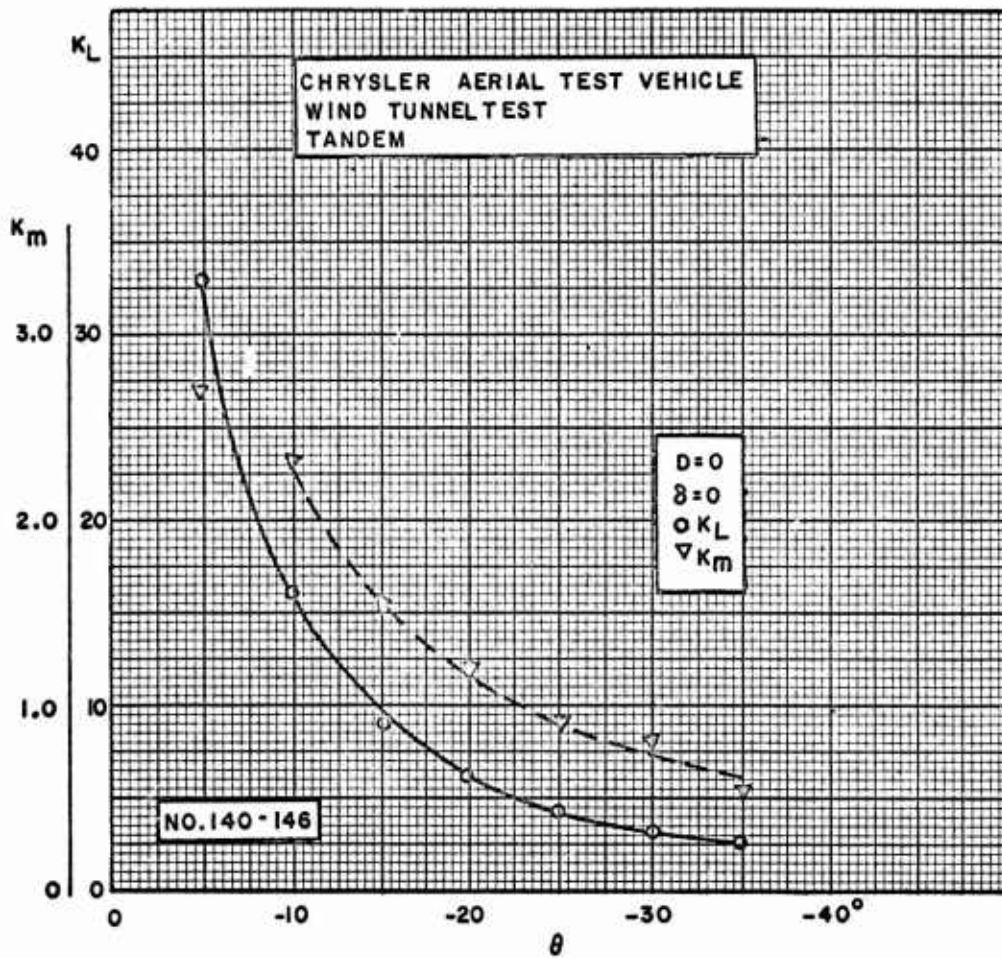


Figure 40.  $K_L$  and  $K_m$  vs  $\theta$  for Forward Flight in Tandem Configuration and Zero Drag



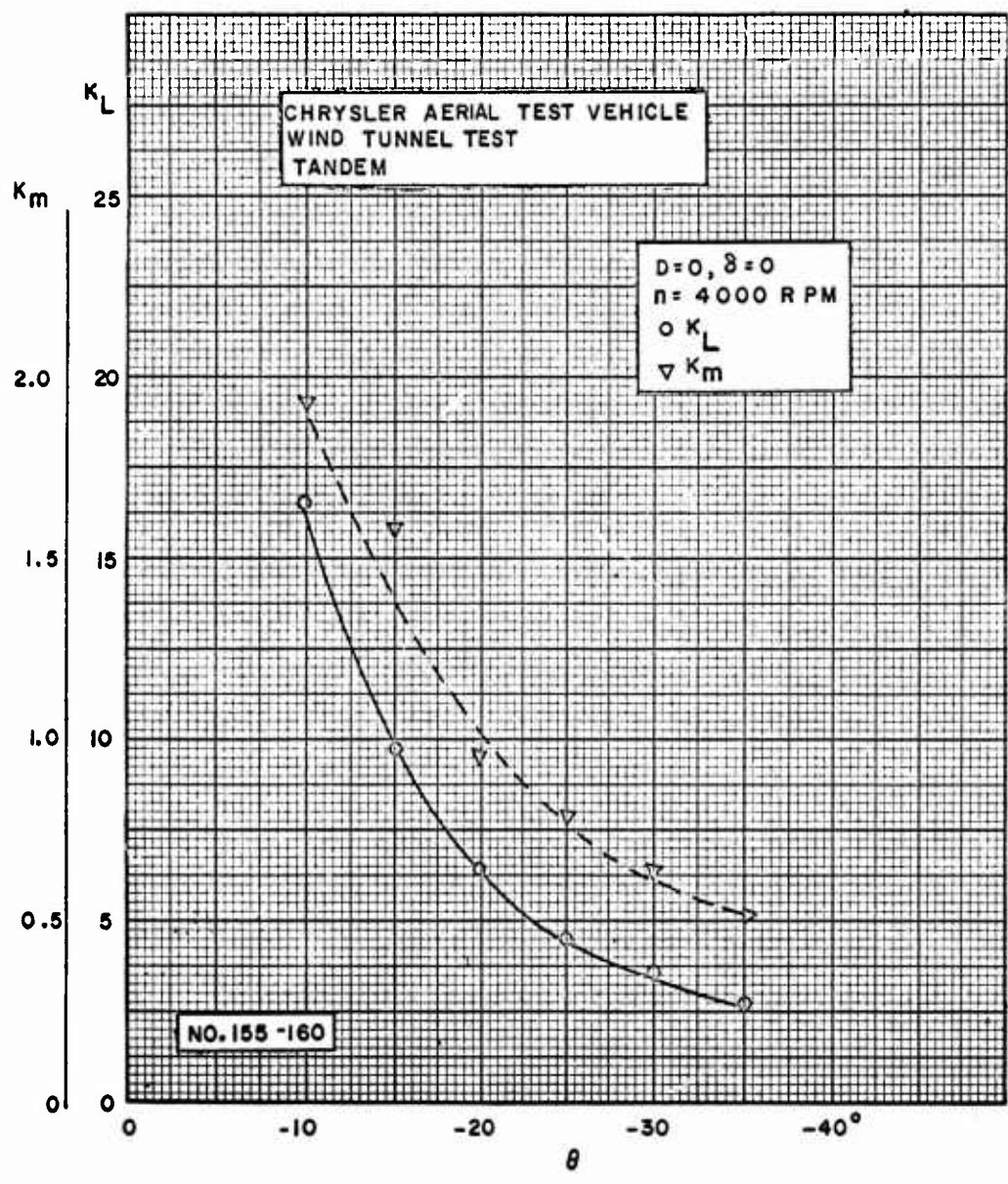


Figure 41.  $K_L$  and  $K_m$  vs  $\theta$  for Forward Flight in Tandem Configuration, Zero Drag and Constant RPM ( $n = 4000$ )

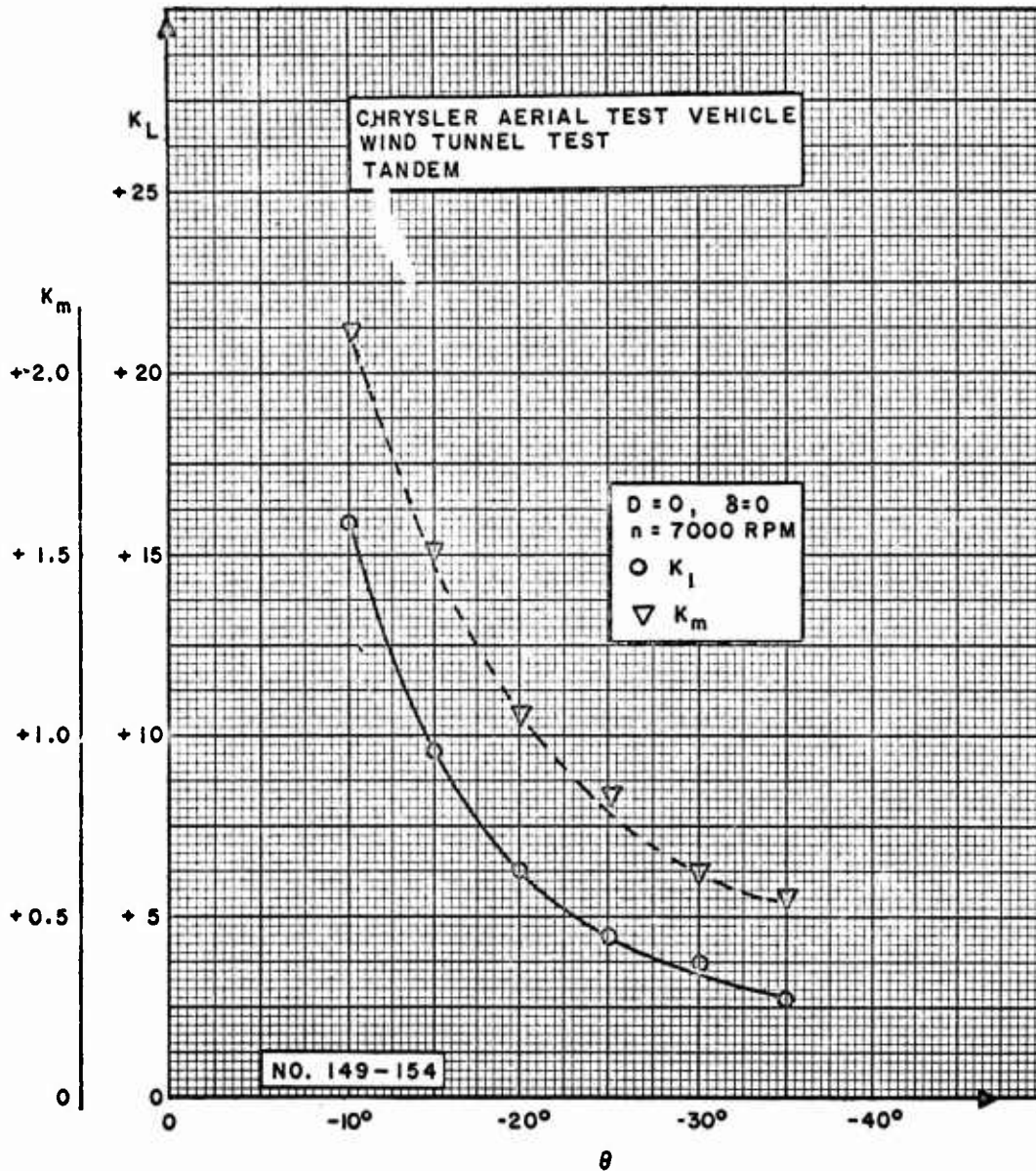


Figure 42.  $K_L$  and  $K_m$  vs  $\theta$  for Forward Flight in Tandem Configuration, Zero Drag and Constant RPM ( $n = 7000$ )

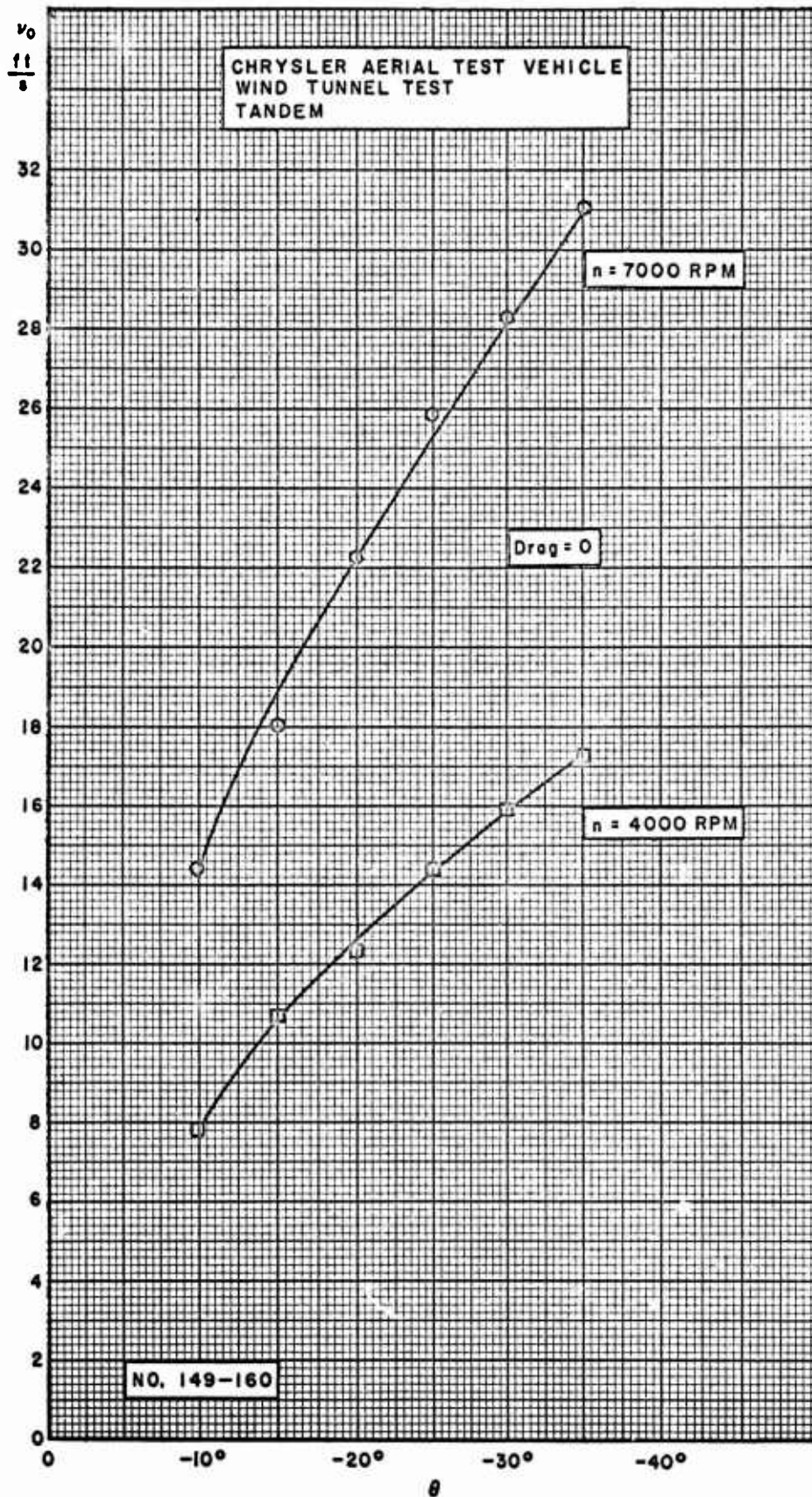


Figure 43.  $v_0$  vs  $\theta$  for Forward Flight in Tandem Configuration, Zero Drag and Constant RPM ( $n = 4000$  and  $7000$ )

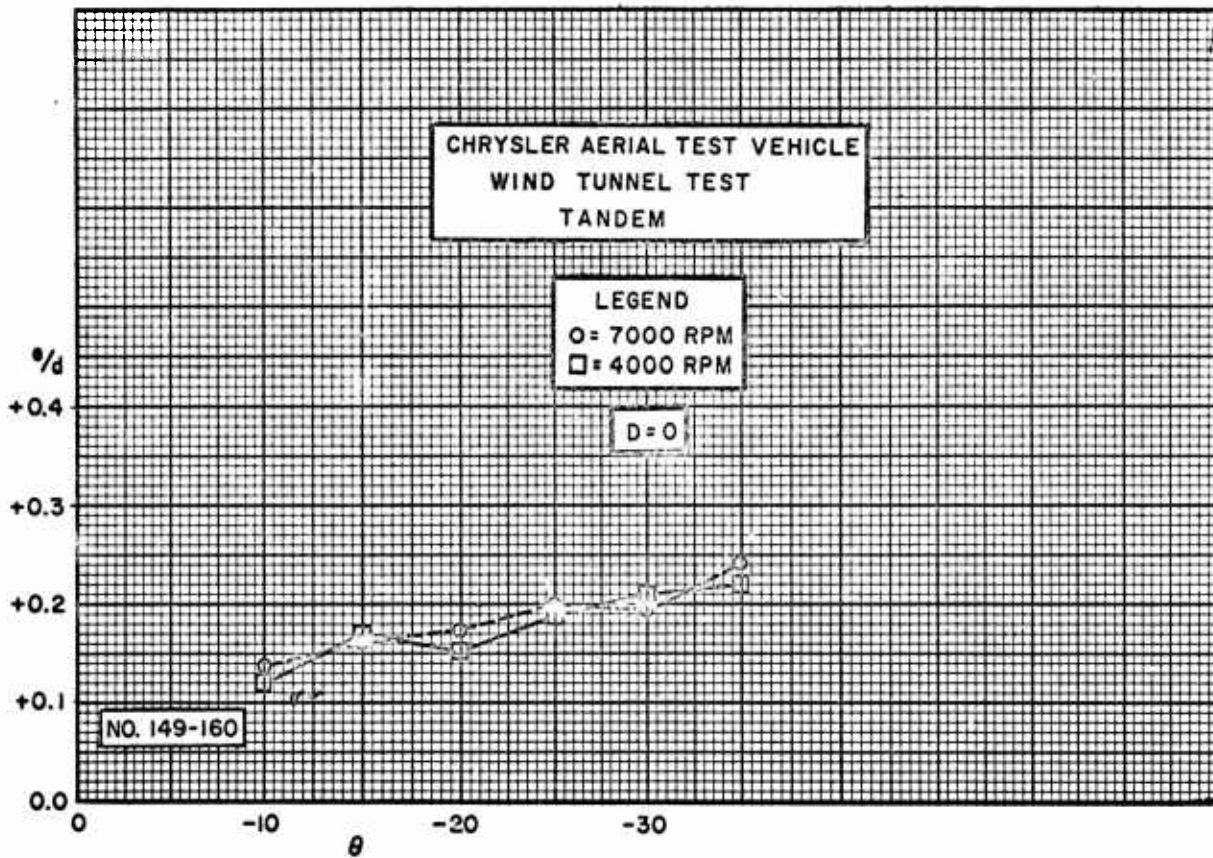


Figure 44.  $e/d$  vs  $\theta$  for Forward Flight in Tandem Configuration,  
Zero Drag and Constant RPM  
( $n = 4000$  and  $7000$ )

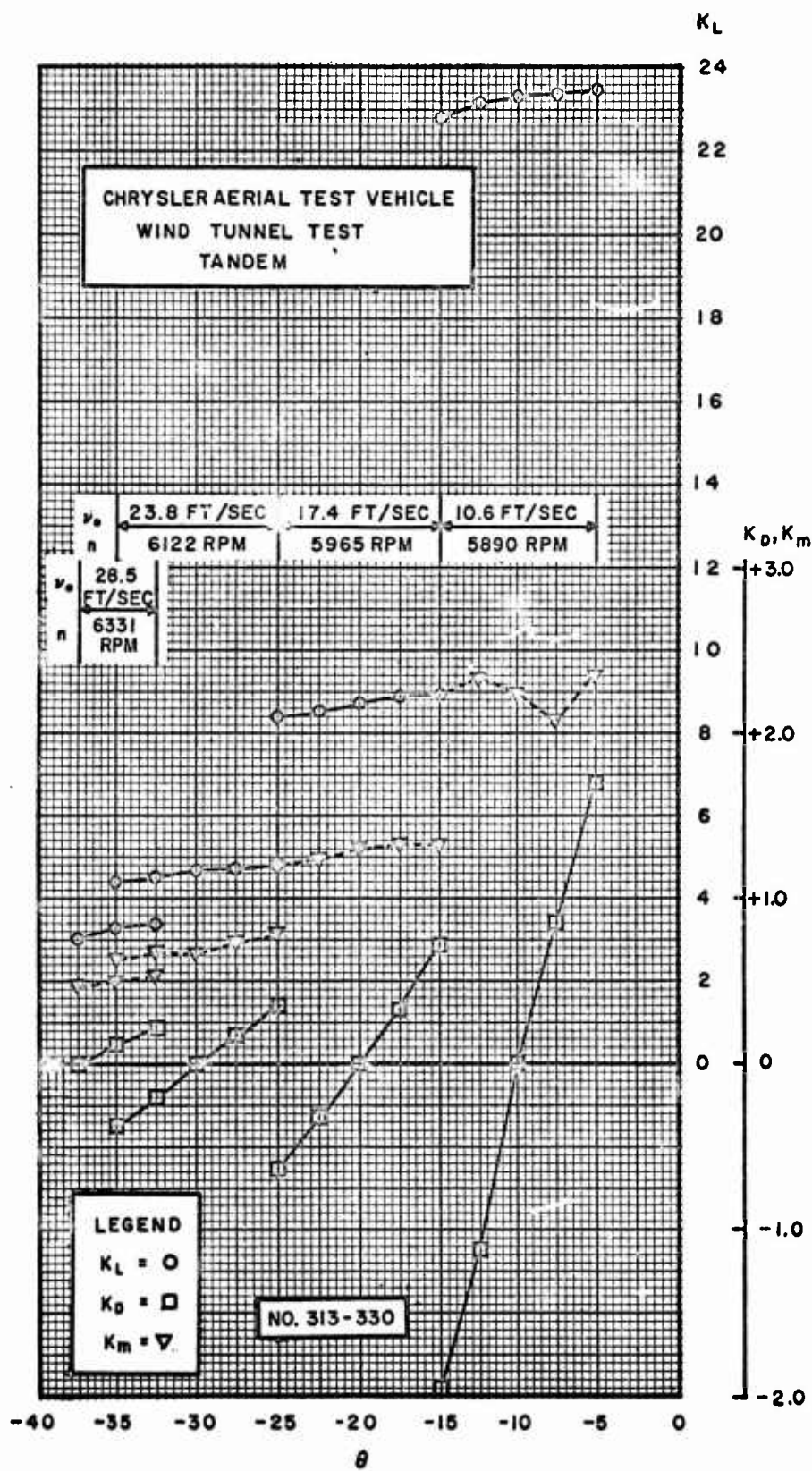


Figure 45. Change of  $K_L$ ,  $K_D$  and  $K_m$  Due to Variation of  $\theta_0$  for Forward Flight in Tandem Configuration

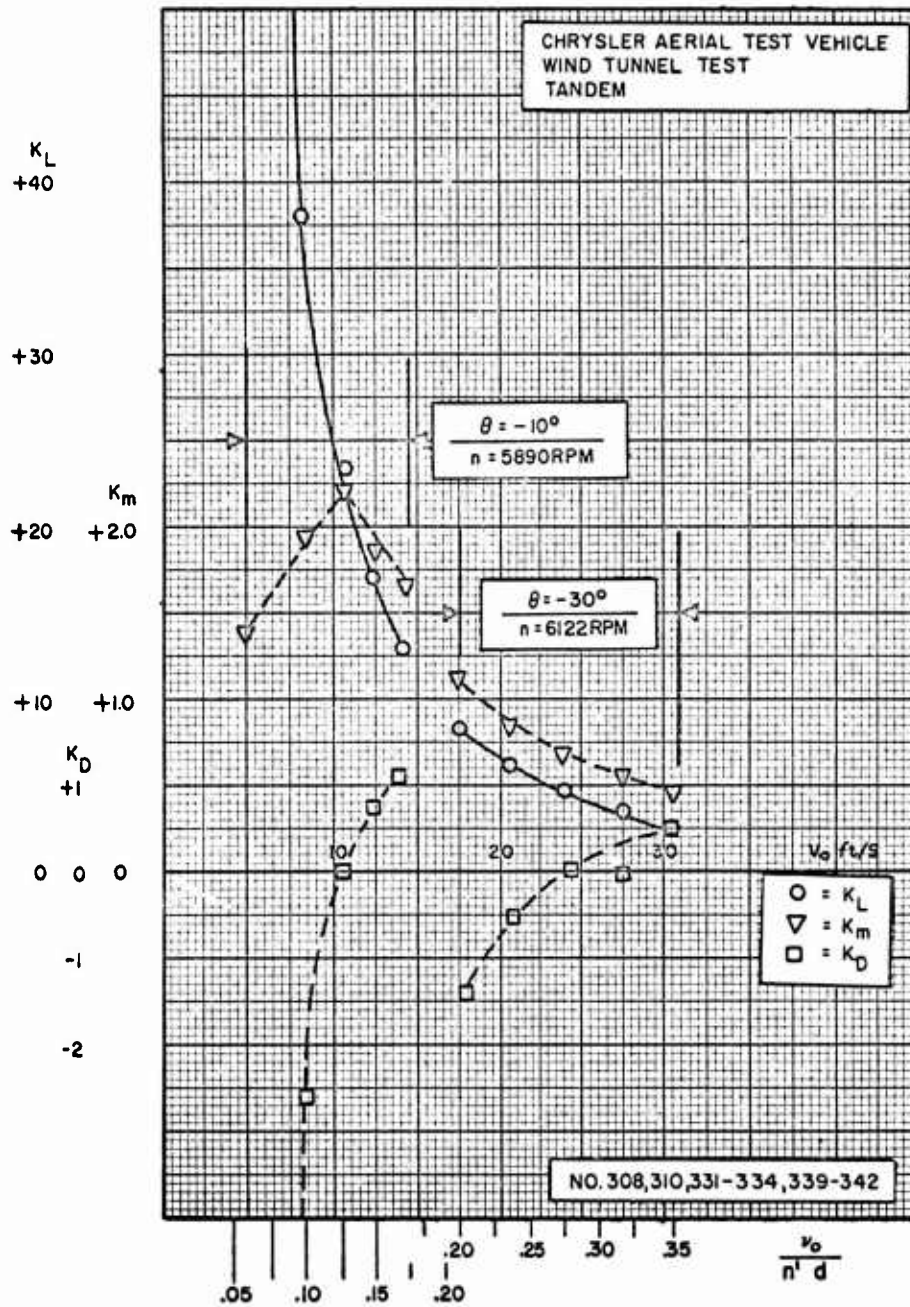


Figure 46. Change of  $K_L$ ,  $K_D$  and  $K_m$  Due to Variation of  $v_0$  for Forward Flight in Tandem Configuration

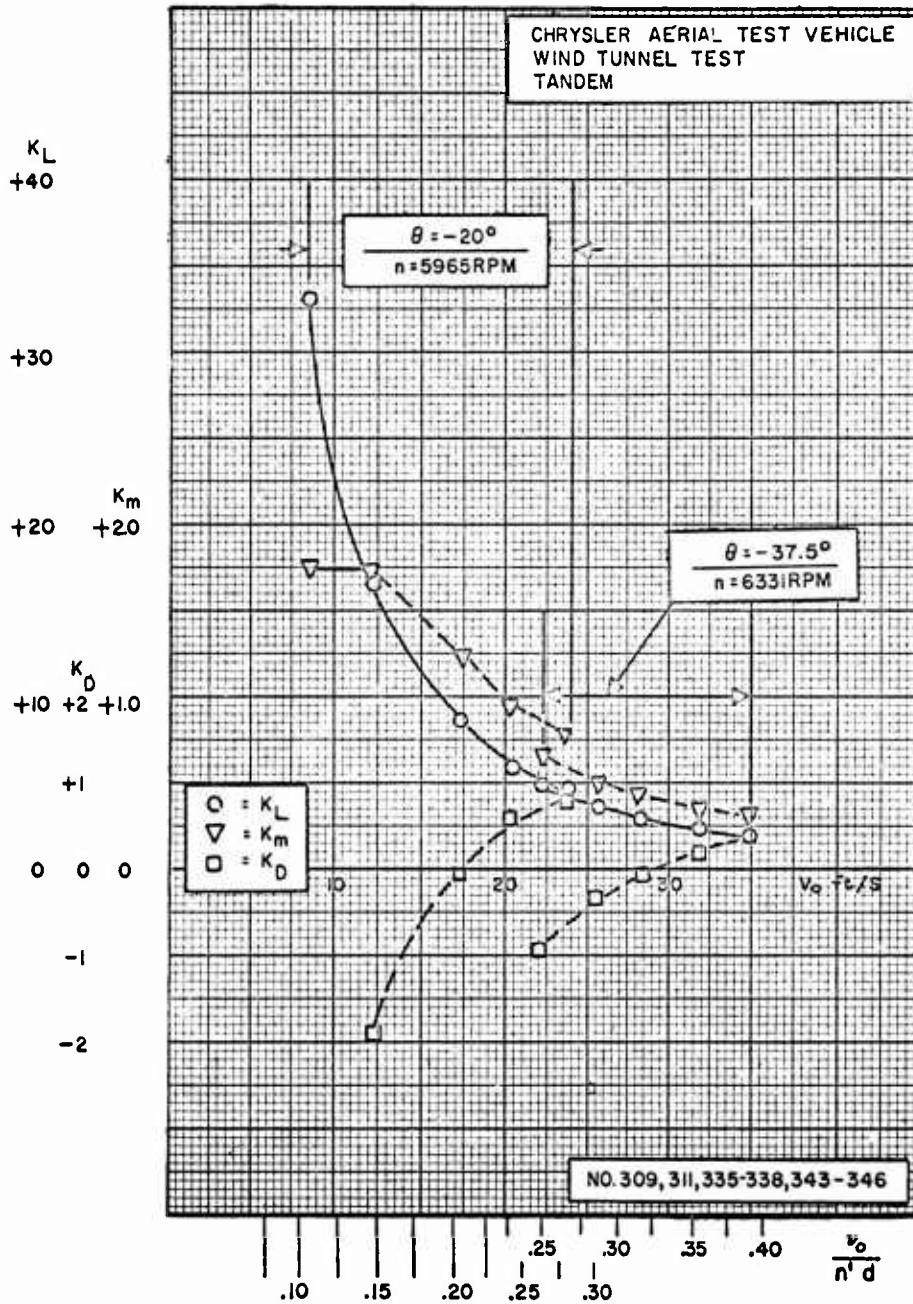


Figure 47. Change of  $K_L$ ,  $K_D$  and  $K_m$  due to Variation of  $v_0$  for Forward Flight in Tandem Configuration

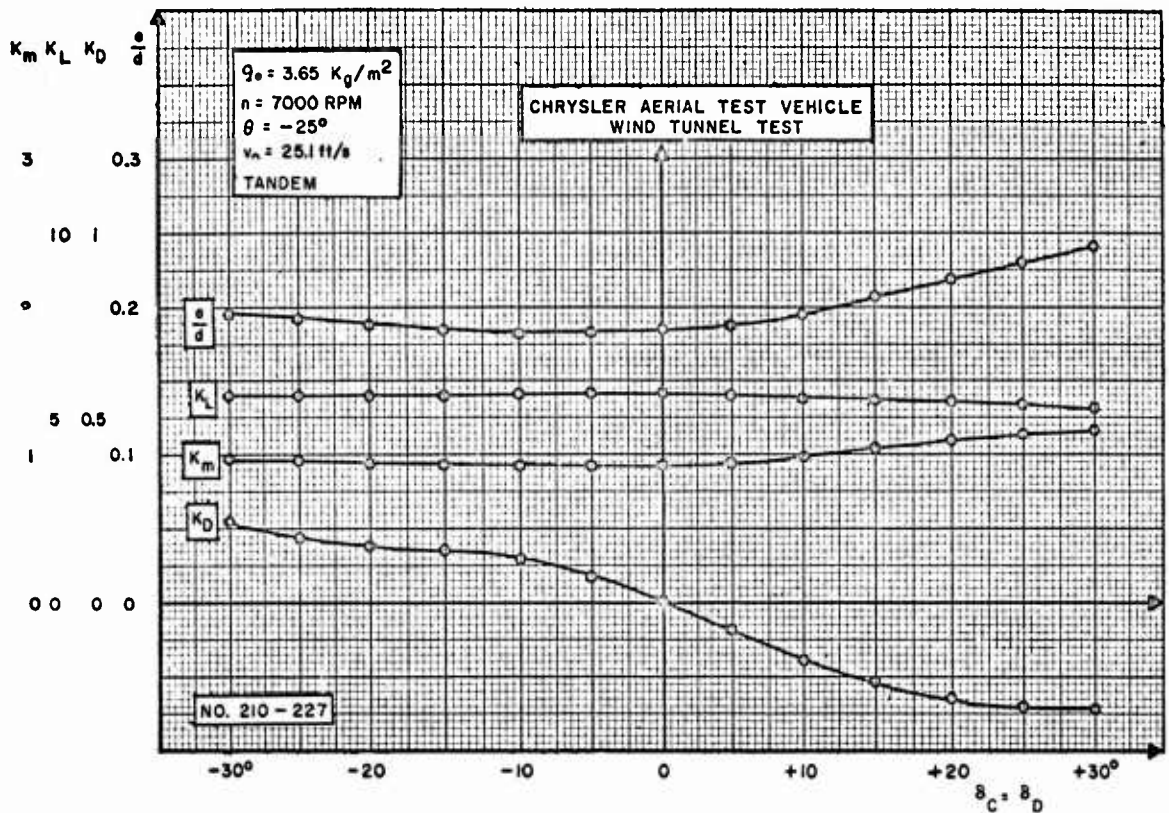


Figure 48.  $K_L$ ,  $K_D$ ,  $K_m$  and  $e/d$  vs Vane Deflection for Forward Flight in Tandem Configuration. Double Pitch Vanes in Position 3 in Rear Shroud Deflected

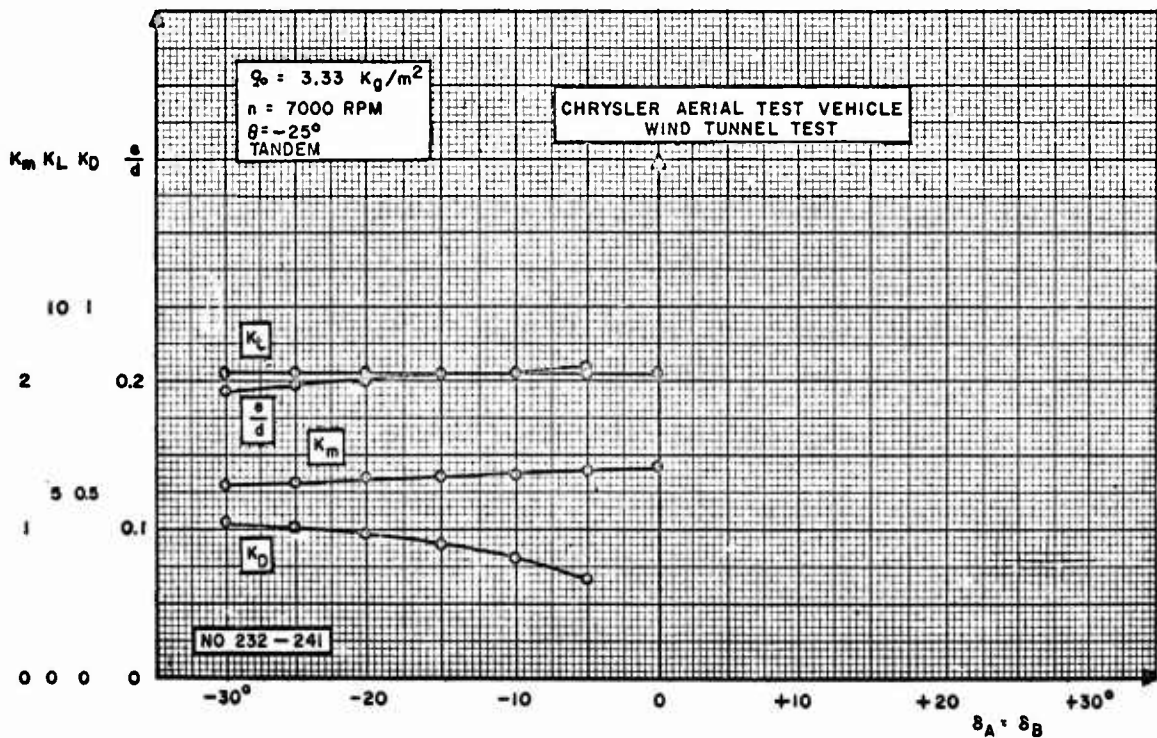


Figure 49.  $K_L$ ,  $K_D$ ,  $K_m$  and  $e/d$  vs Vane Deflection for Forward Flight in Tandem Configuration. Double Pitch Vanes in Position 3 in Front Shroud Deflected



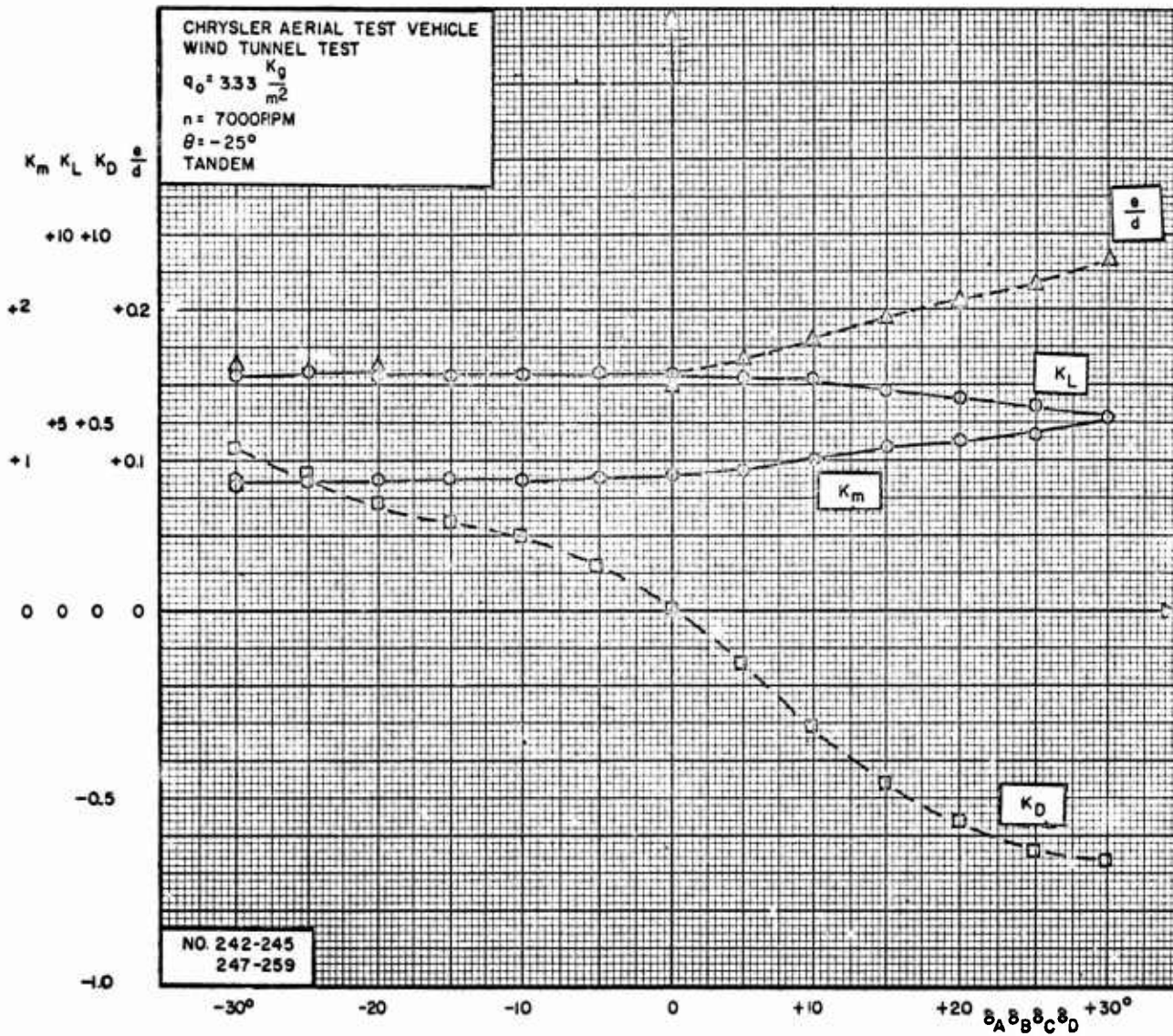


Figure 50.  $K_L$ ,  $K_D$ ,  $K_m$  and  $e/d$  vs Vane Deflection for Forward Flight in Tandem Configuration. Double Pitch Vanes in Position 3 Deflected in Both Shrouds

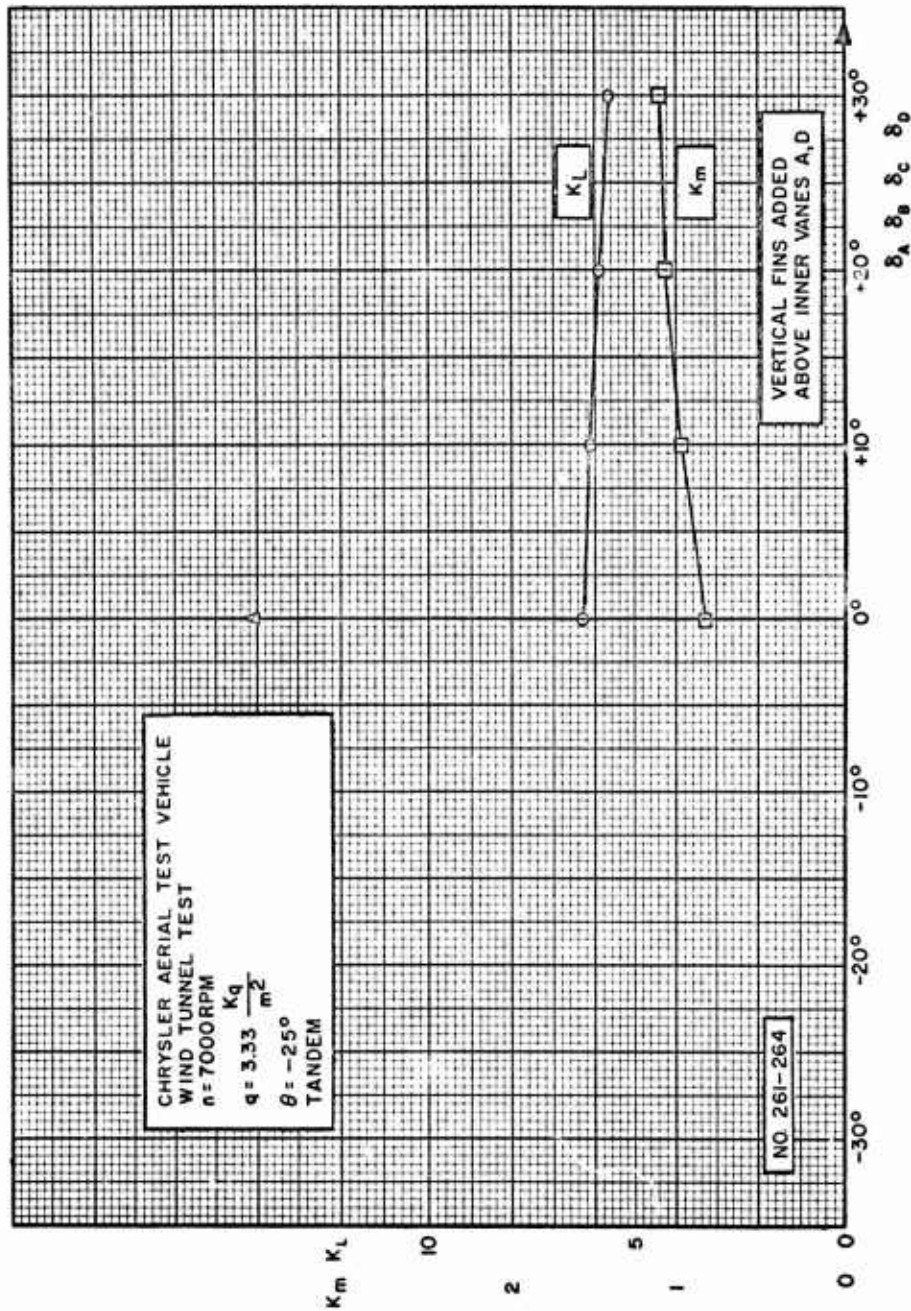


Figure 51.  $K_L$  and  $K_m$  vs Vane Deflection for Forward Flight in Tandem Configuration. Double Pitch Vanes Deflected in Both Shrouds. Fins Added.

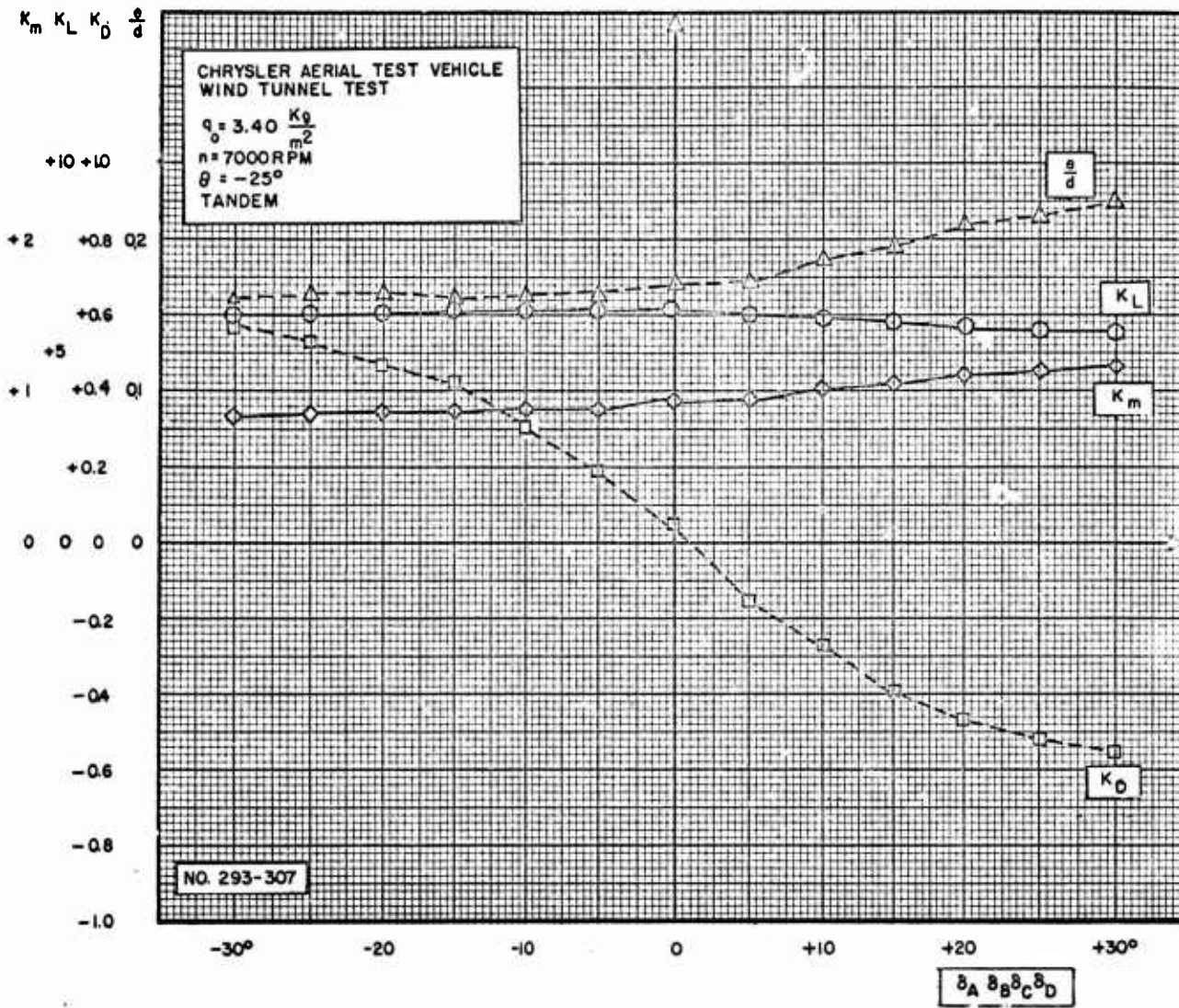


Figure 52.  $K_L$ ,  $K_D$ ,  $K_m$  and  $e/d$  vs Vane Deflection for Forward Flight in Tandem Configuration. All Vanes in Position 2 Deflected in Both Shrouds

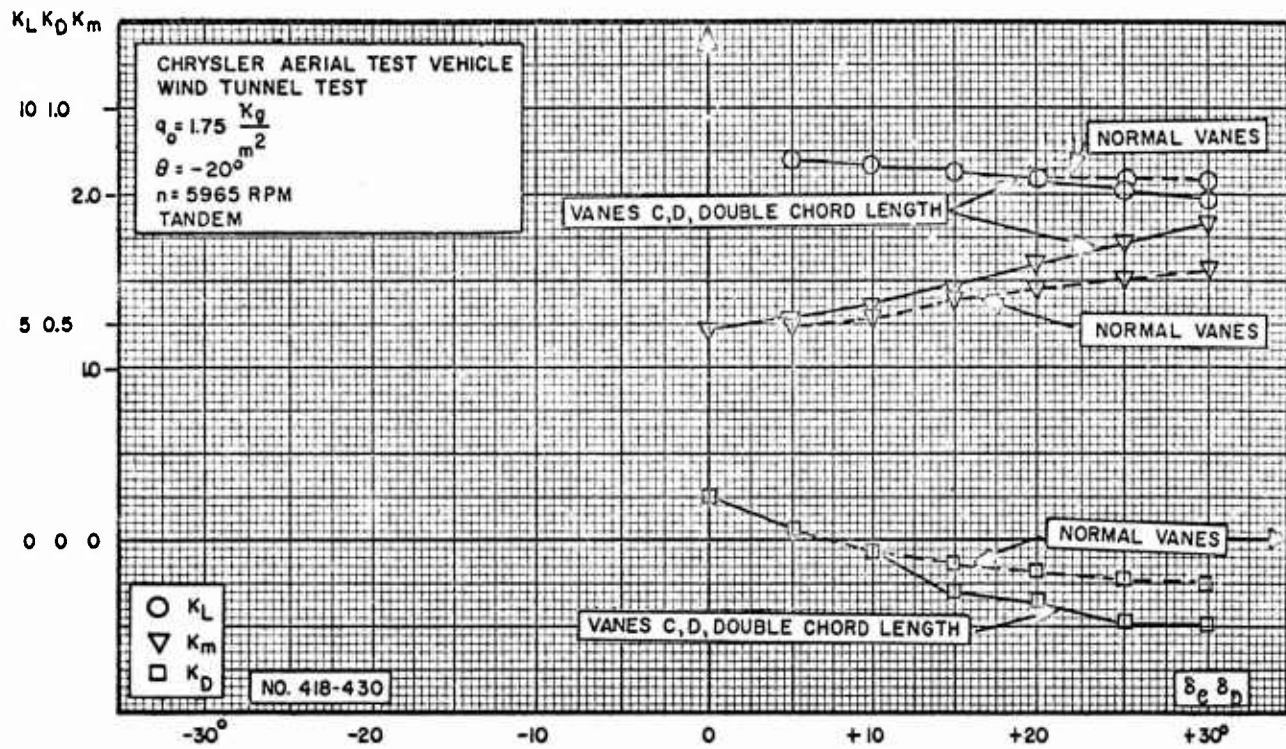


Figure 53.  $K_L$ ,  $K_D$ , and  $K_m$  vs Vane Deflection for Forward Flight in Tandem Configuration. Comparison Between Normal and Double Chord Length Vanes Deflected in Rear Shroud

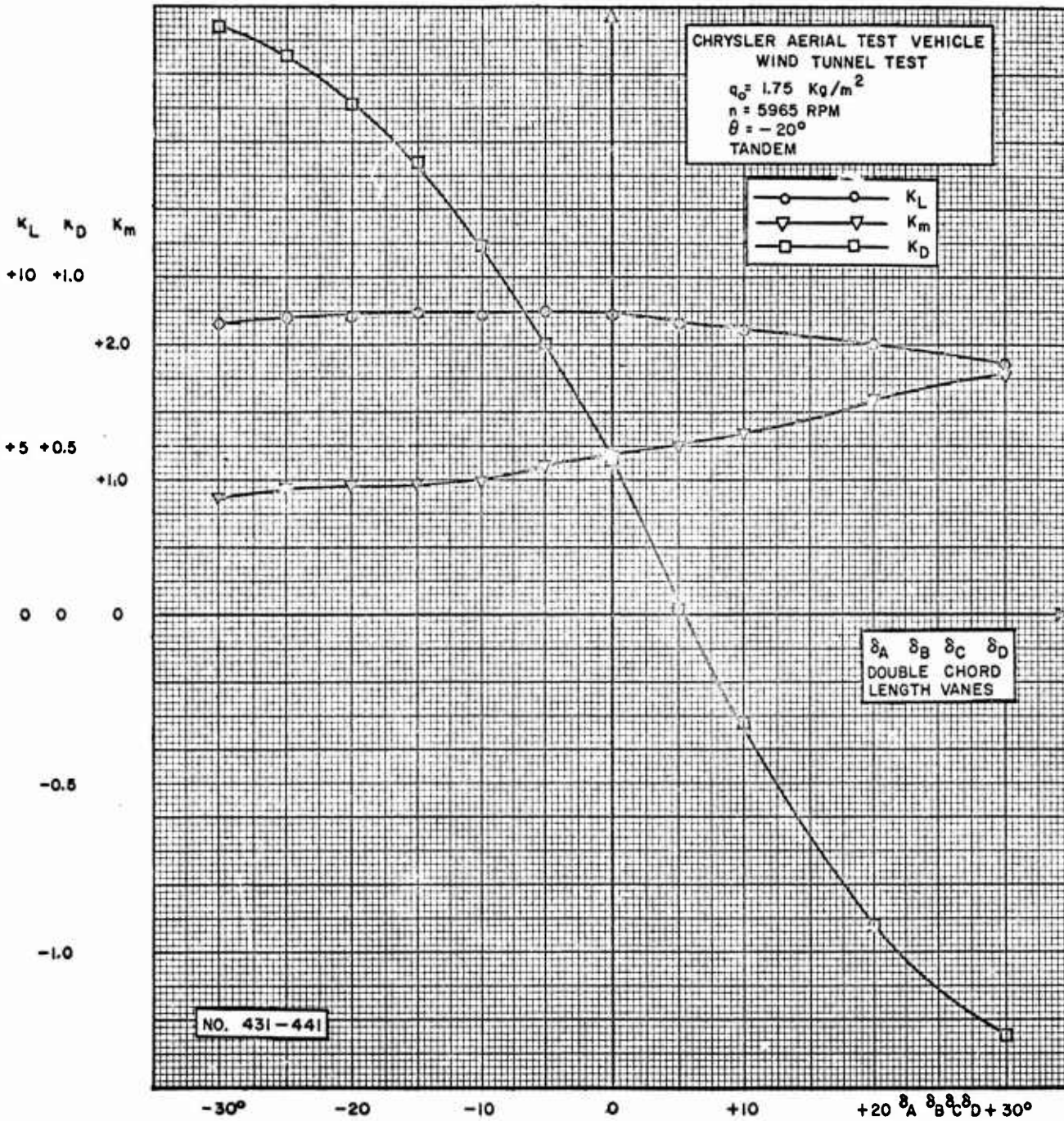


Figure 54.  $K_L$ ,  $K_D$ ,  $K_m$  vs Vane Deflection for Forward Flight in Tandem Configuration. Double Chord Length Vanes Deflected in Both Shrouds.

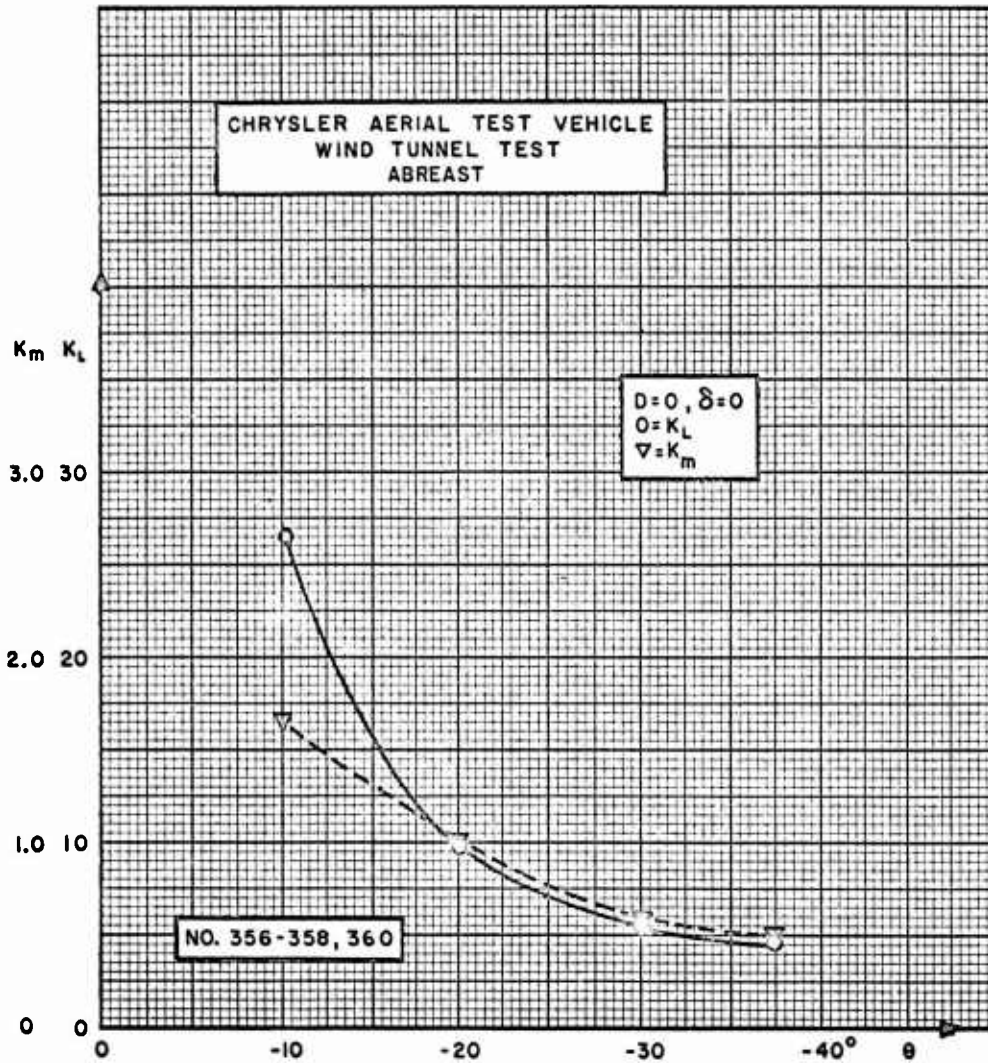


Figure 55.  $K_L$  and  $K_m$  vs  $\theta$  for Forward Flight in Abreast Configuration at Zero Drag

UNCLASSIFIED

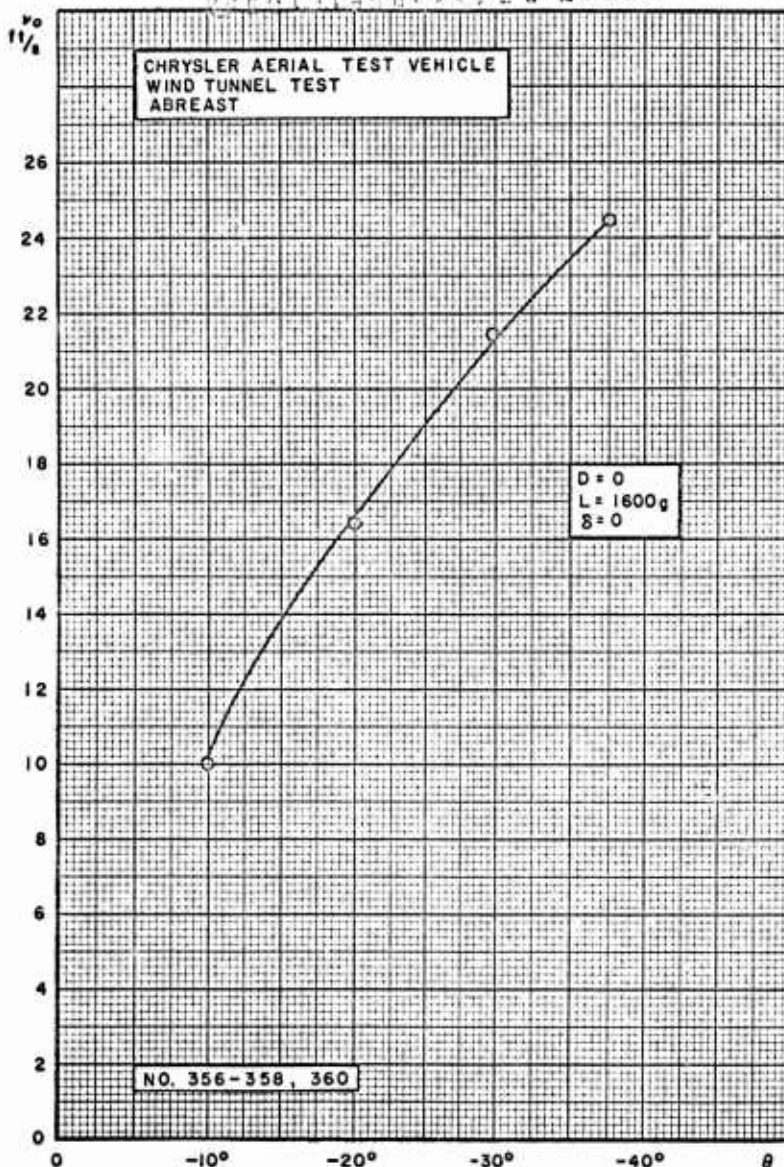


Figure 56.  $v_0$  vs  $\theta$  for Forward Flight in Abreast Configuration at Zero Drag and Constant Lift

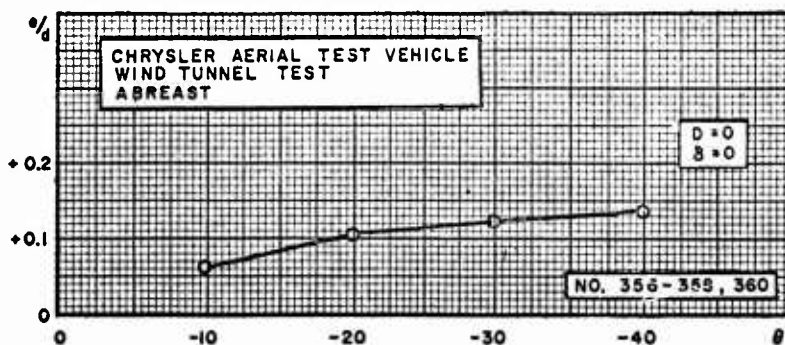


Figure 57.  $e/d$  vs  $\theta$  for Forward Flight in Abreast Configuration at Zero Drag

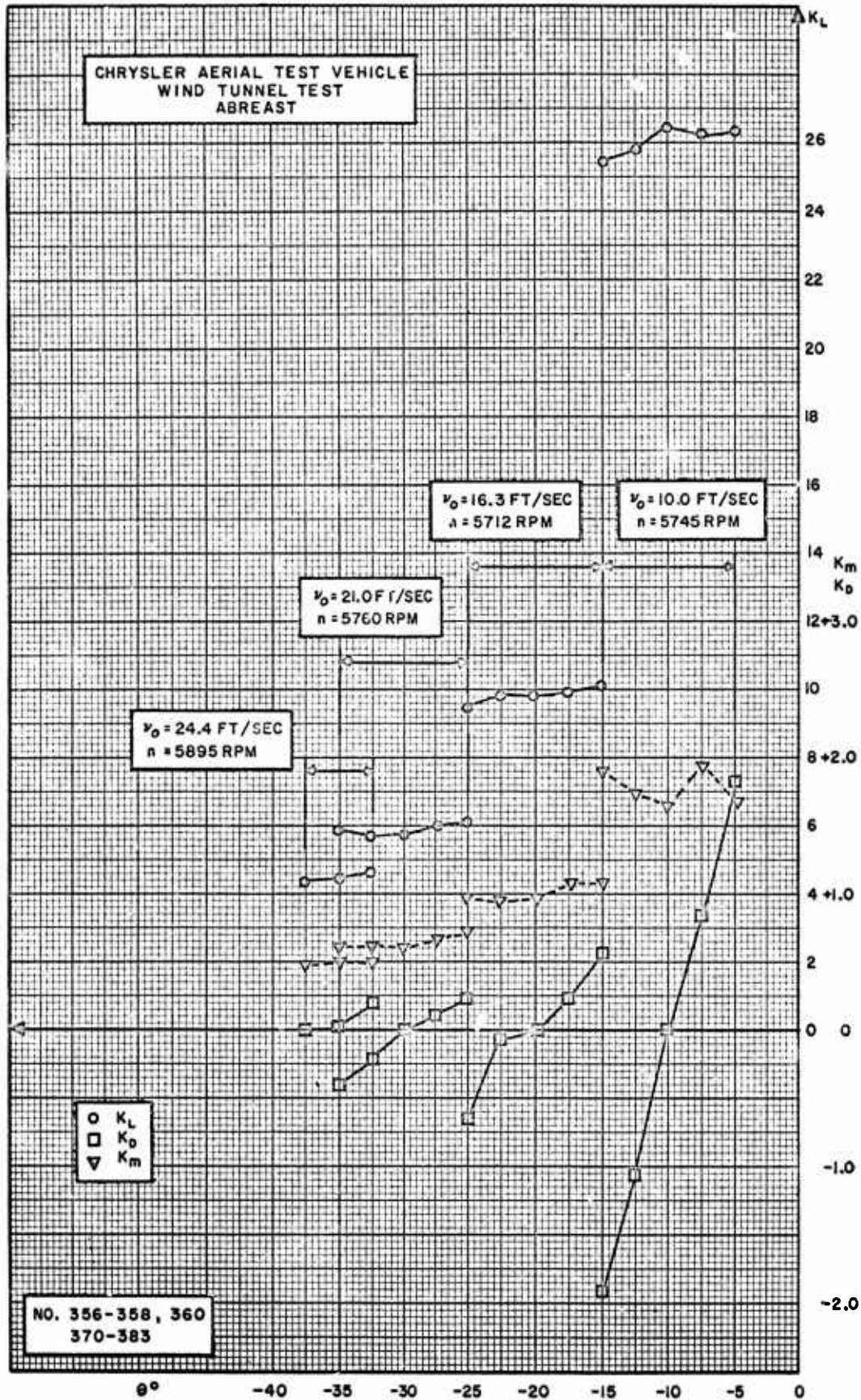


Figure 58. Change of  $K_L$ ,  $K_D$  and  $K_m$  Due to Variation of  $\theta$  for Forward Flight in Abreast Configuration



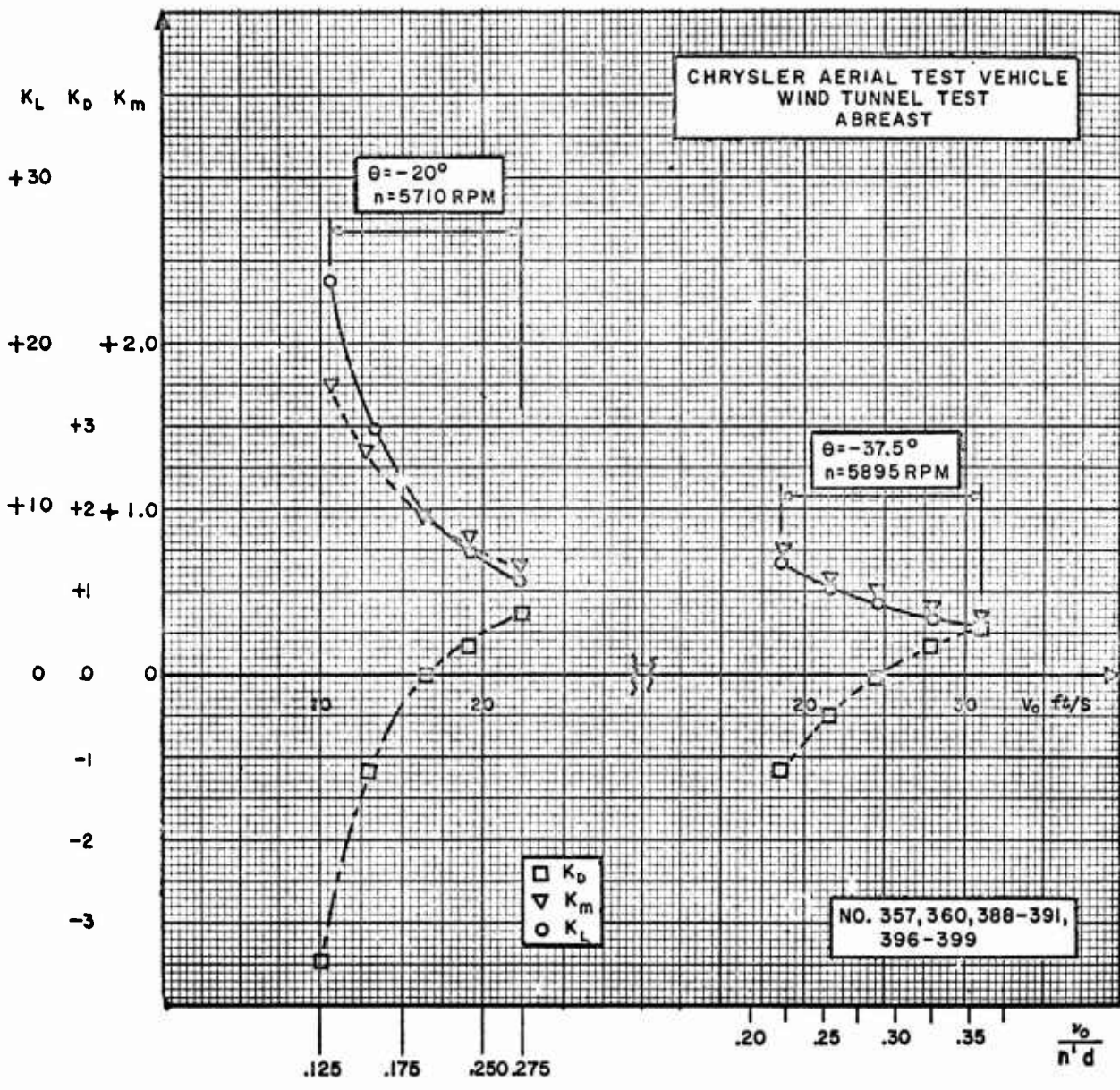


Figure 59. Change of  $K_L$ ,  $K_D$  and  $K_m$  Due to Variation of  $v_o$  for Forward Flight in Abreast Configuration

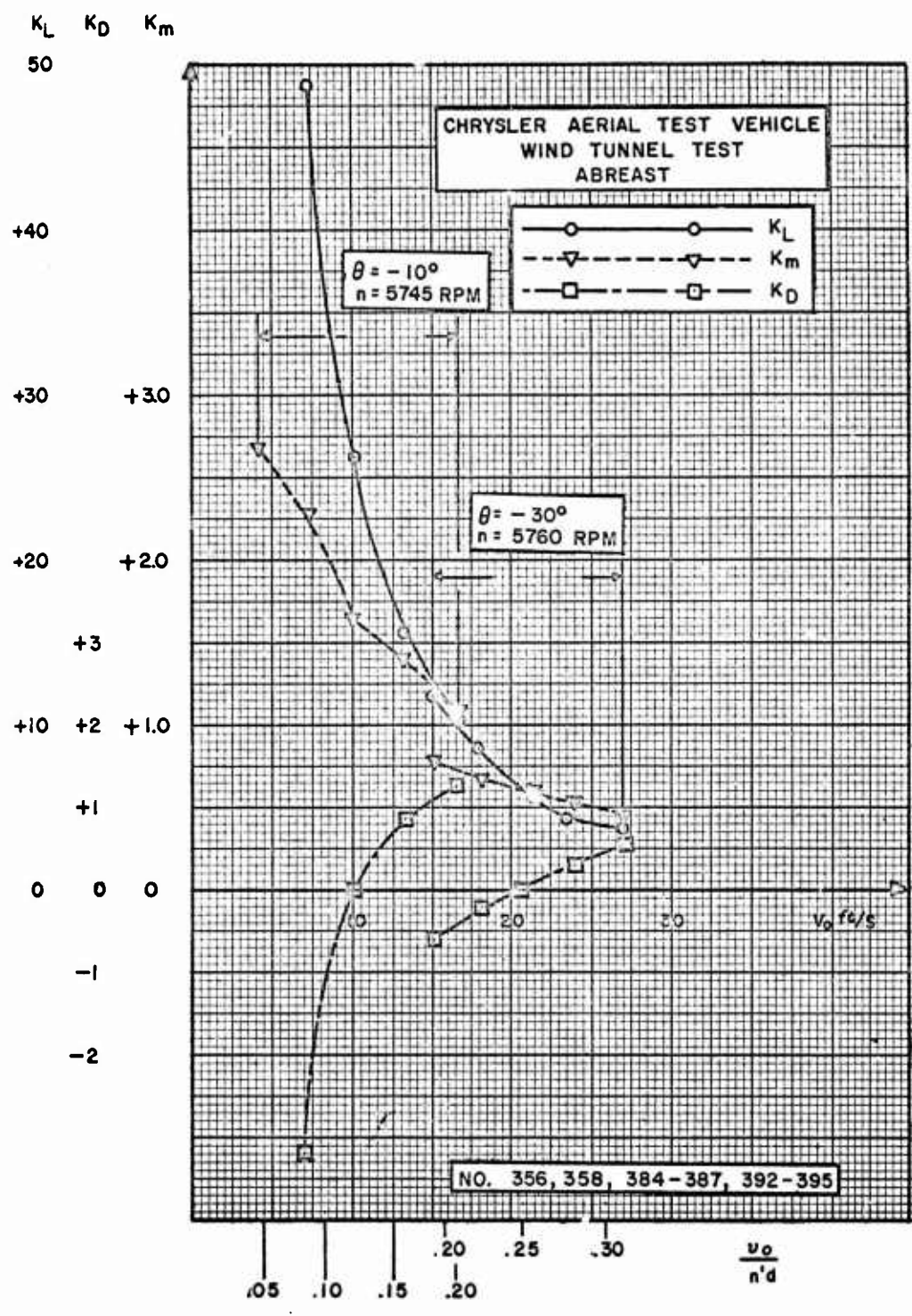


Figure 60. Change of  $K_L$ ,  $K_D$  and  $K_m$  Due to Variation of  $v_0$  for Forward Flight in Abreast Configuration

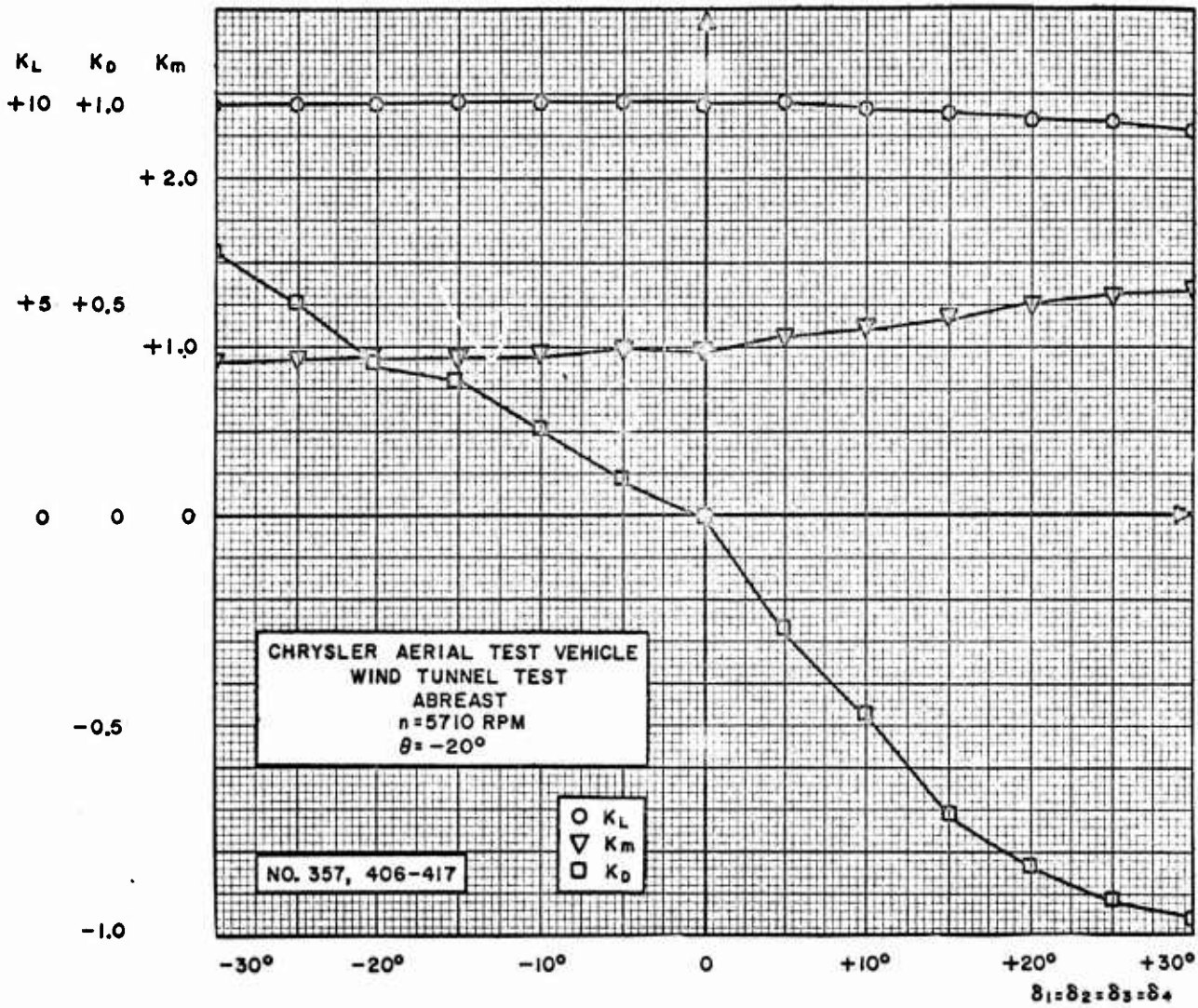


Figure 61.  $K_L$ ,  $K_D$  and  $K_m$  vs Vane Deflection for Forward Flight in Abreast Configuration.  
Pitch Vanes Deflected in Both Shrouds

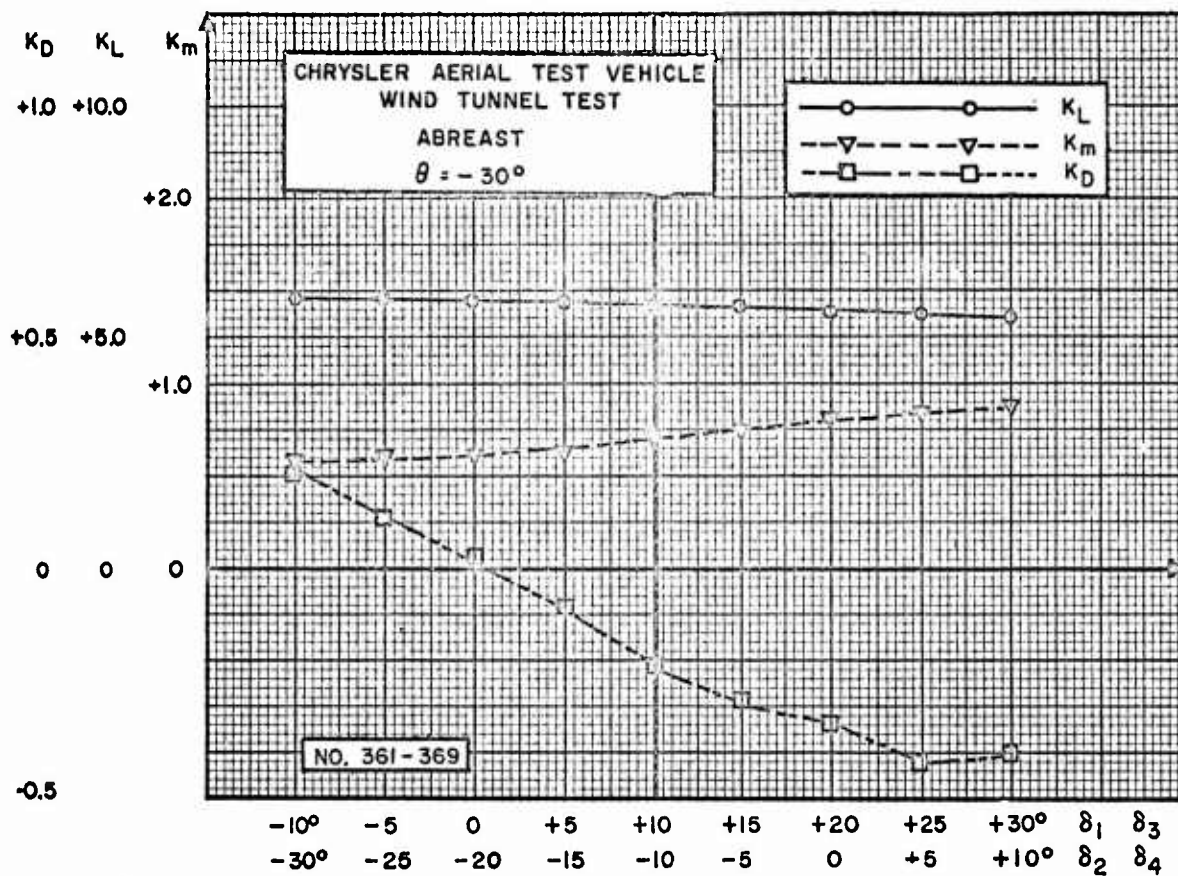


Figure 62.  $K_L$ ,  $K_D$  and  $K_m$  vs Vane Deflection for Forward Flight in Abreast Configuration. Pitch Vanes in Both Shrouds Deflected Outward by  $10^\circ$

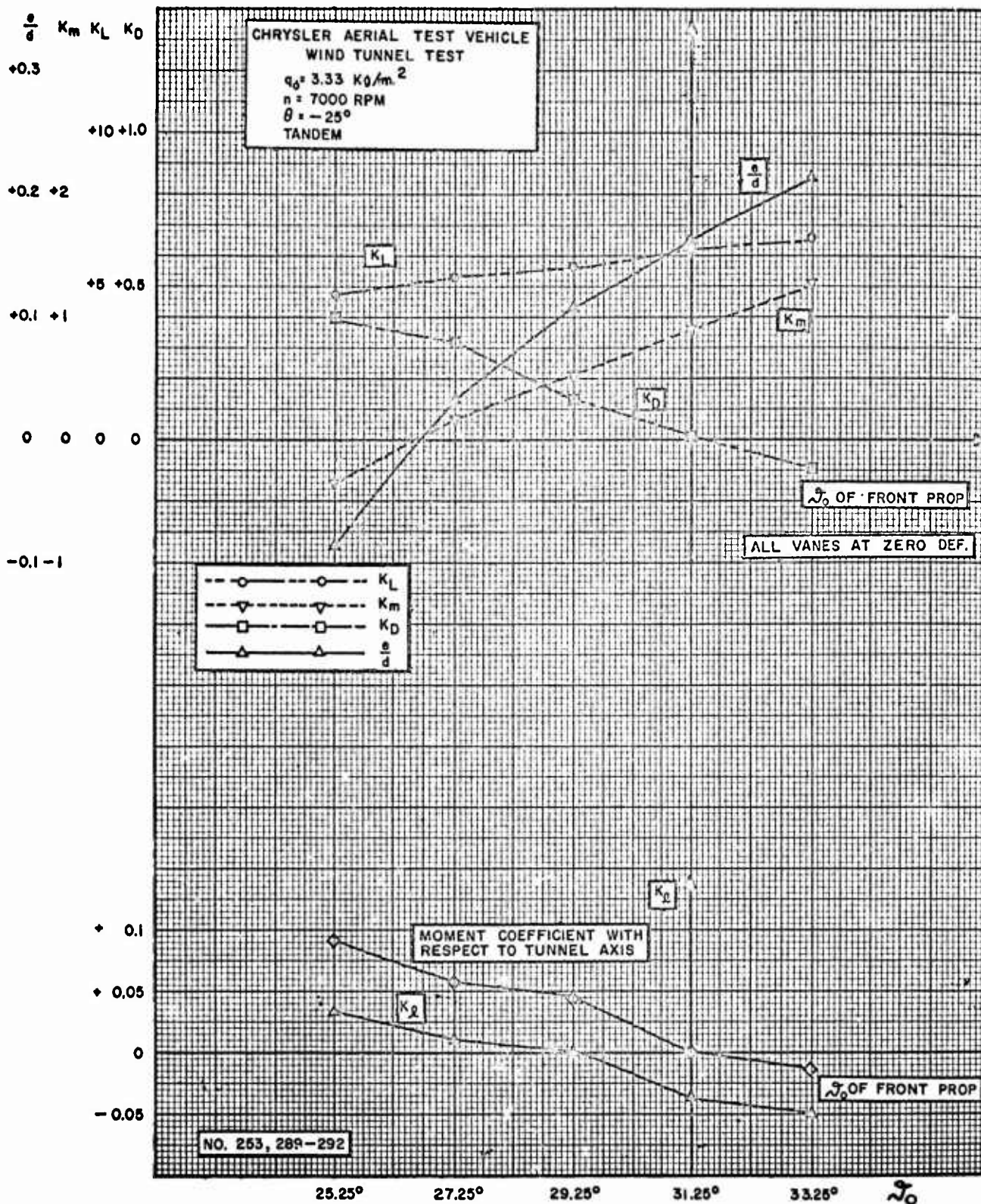


Figure 63.  $K_L$ ,  $K_D$ ,  $K_m$ ,  $e/d$  and  $K_1$  vs  $\alpha_0$  for Forward Flight in Tandem Configuration with all Vanes in Neutral Positions

N.O.	SKETCH OF CONFIGURATION	COMMENTS ON CONFIGURATION	NO.	SKETCH OF CONFIGURATION	COMMENTS ON CONFIGURATION
1		PLAIN SHROUD WITH RINGS PATTERN AFTER THE FINISH IN PART NO.1 NO. REDUCERS.	8		PLAIN SHROUD WITH FLAT BAFFLES ARRANGED AS SHOWN
2		SAME AS NO.1 WITH FLAT SHEET LAYING ON TOP OF STRUTS IN SHROUD.	9		FILLED IN SPACE BELOW FRONT LIP, COVERING FRONT HALF OF SHROUD
3		SAME AS NO.2 WITHOUT RINGS ABOVE INLET	10		ATTEMPT TO STREAM-LINE REAR OF MODEL
4		PLAIN SHROUD WITHOUT RINGS INLET AND WITHOUT BAFFLE	11		FILLED IN SPACE BELOW REAR 1/2 OF REAR SHROUD LIP
5		PLAIN SHROUD WITHOUT RINGS BUT WITH THRUST REVERSER - OPERATION VERY ROUGH	12		CONTOURED SPACE BELOW REAR 1/2 OF REAR SHROUD LIP
6		PLAIN SHROUD WITH 1/2" CYLINDER PROJECTING ABOVE FRONT 1/4 OF SHROUD FLUSH WITH INSIDE WALL.	13		PLAIN SHROUD WITH 1" CYLINDER PROJECTING ABOVE FRONT 1/2 OF SHROUD FLUSH WITH INSIDE WALL
7		SAME AS NO.3 WITH BAFFLE PERFORATED WITH 1/4" HOLES 1/2" APART	14		SHROUDS ABREAST, LARGE VANE ADDED ACROSS REAR AS SHOWN a. $\alpha = 35^\circ$ b. $\alpha = 45^\circ$ c. $\alpha = 55^\circ$ d. $\alpha = 20^\circ$

Figure 64. Pitching Moment Reducing Devices

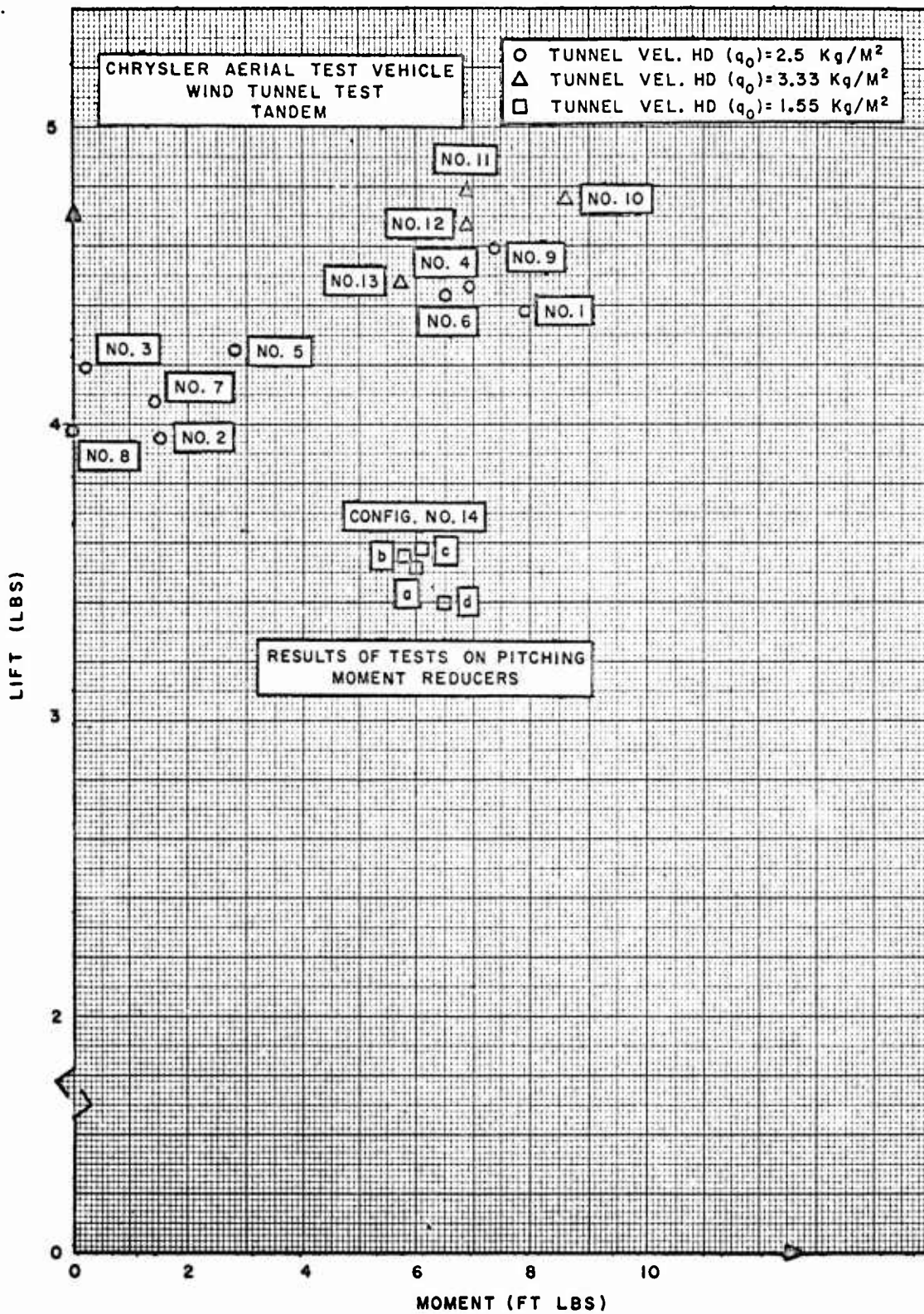


Figure 65. Results of Pitching Moment Reducer Tests

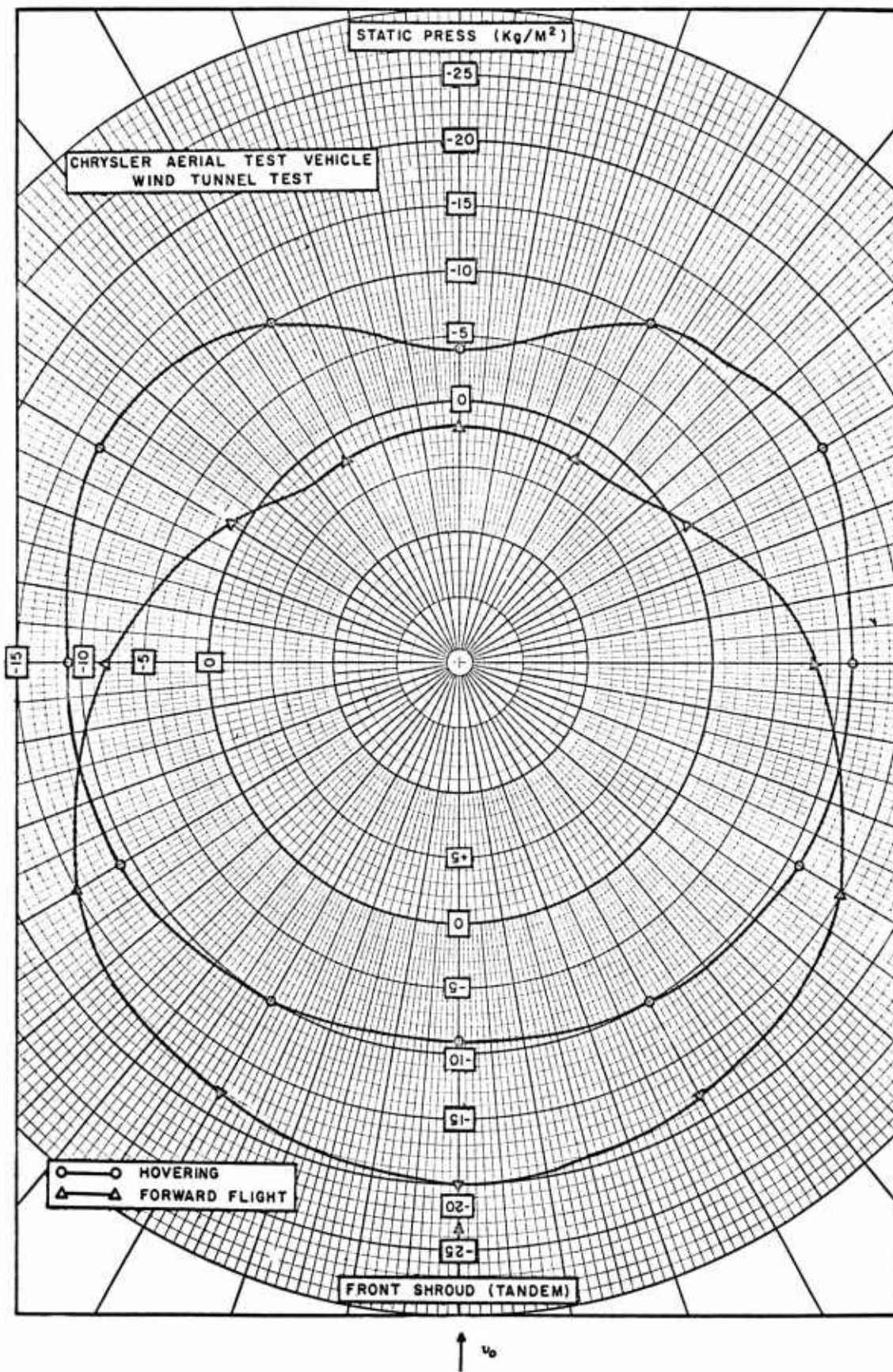


Figure 66. Inlet Pressure Distribution on Front Shroud in Tandem



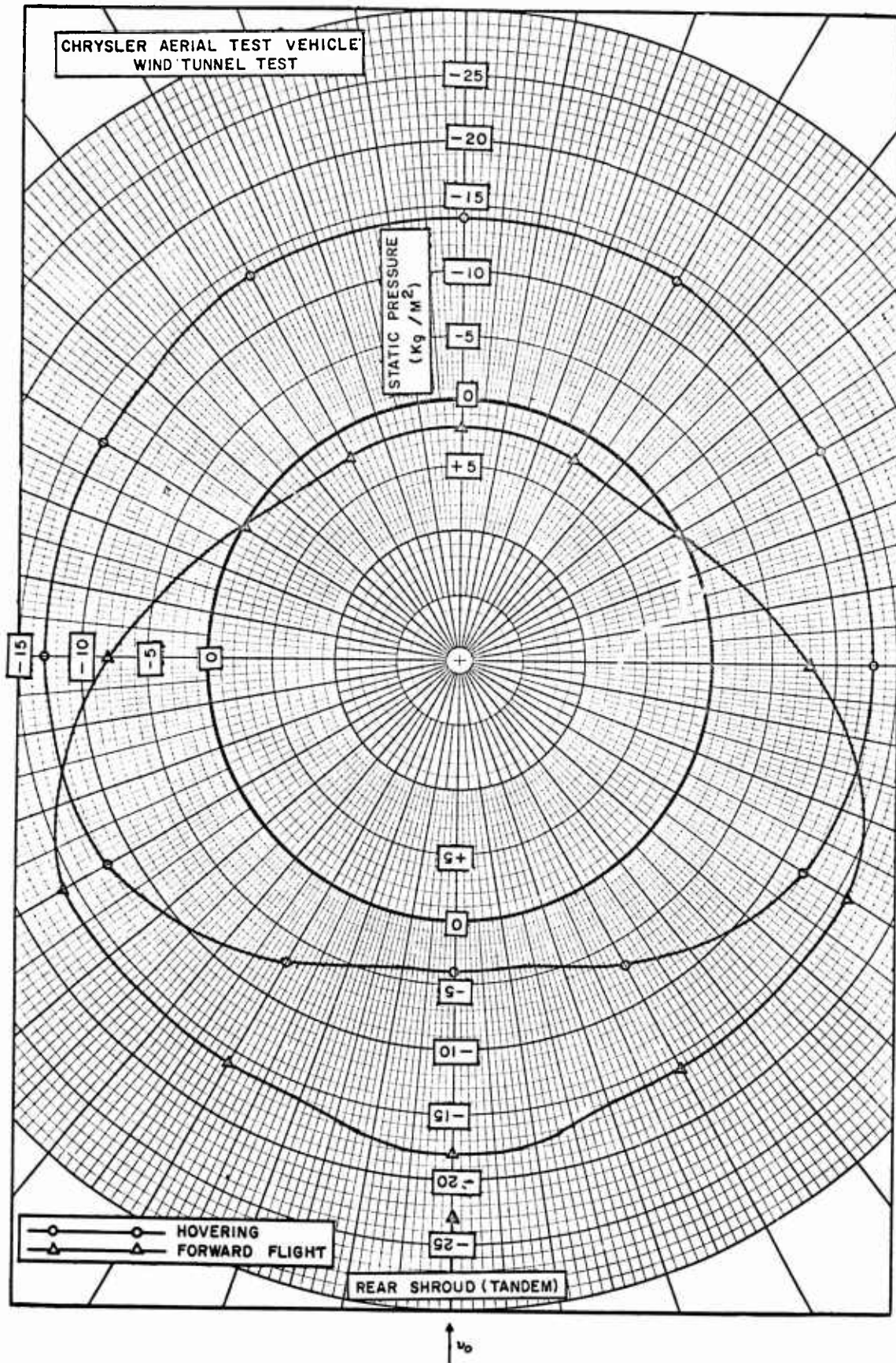


Figure 67. Inlet Pressure Distribution on Rear Shroud in Tandem

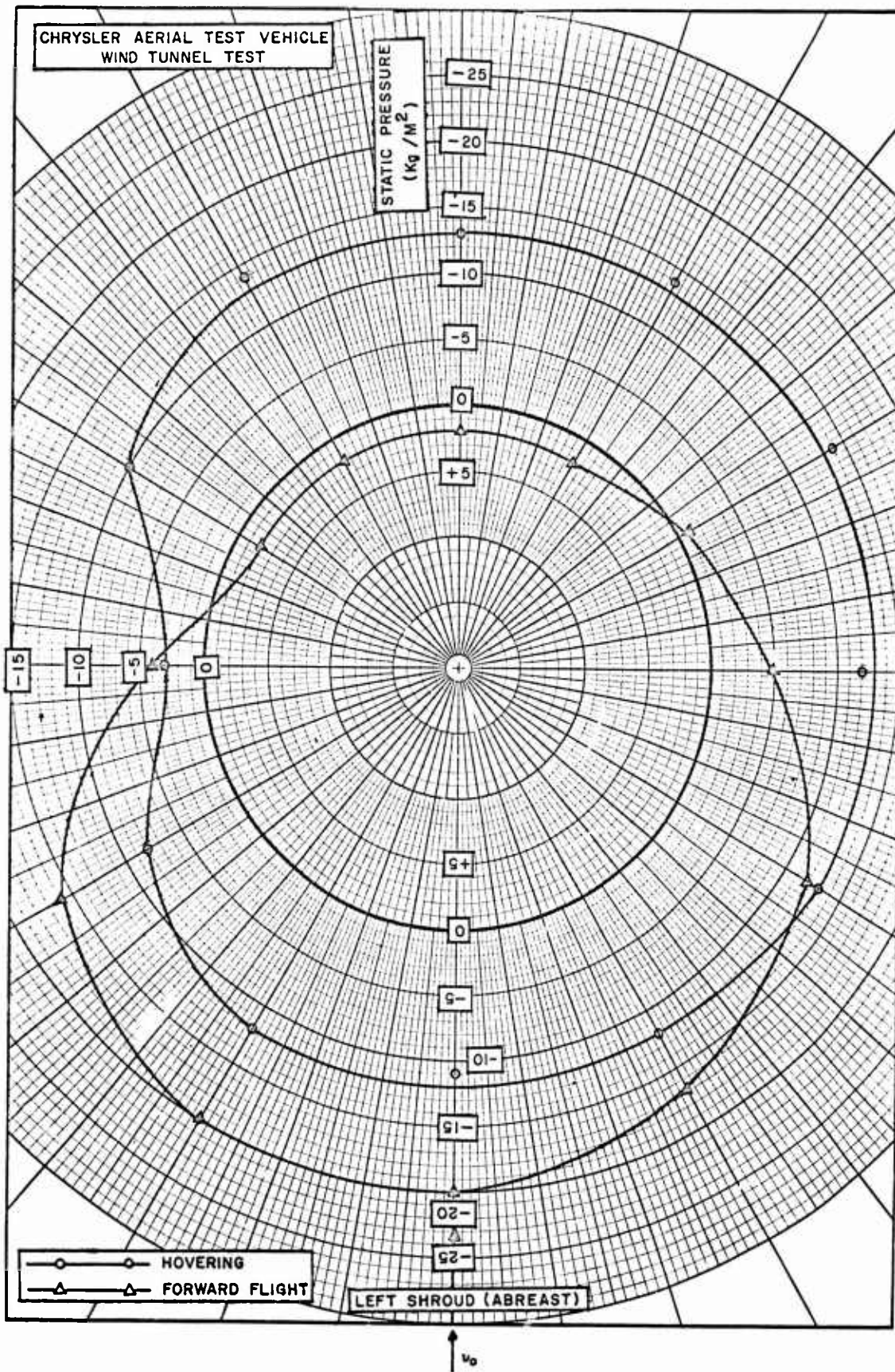


Figure 68. Inlet Pressure Distribution on Left Shroud in Abreast

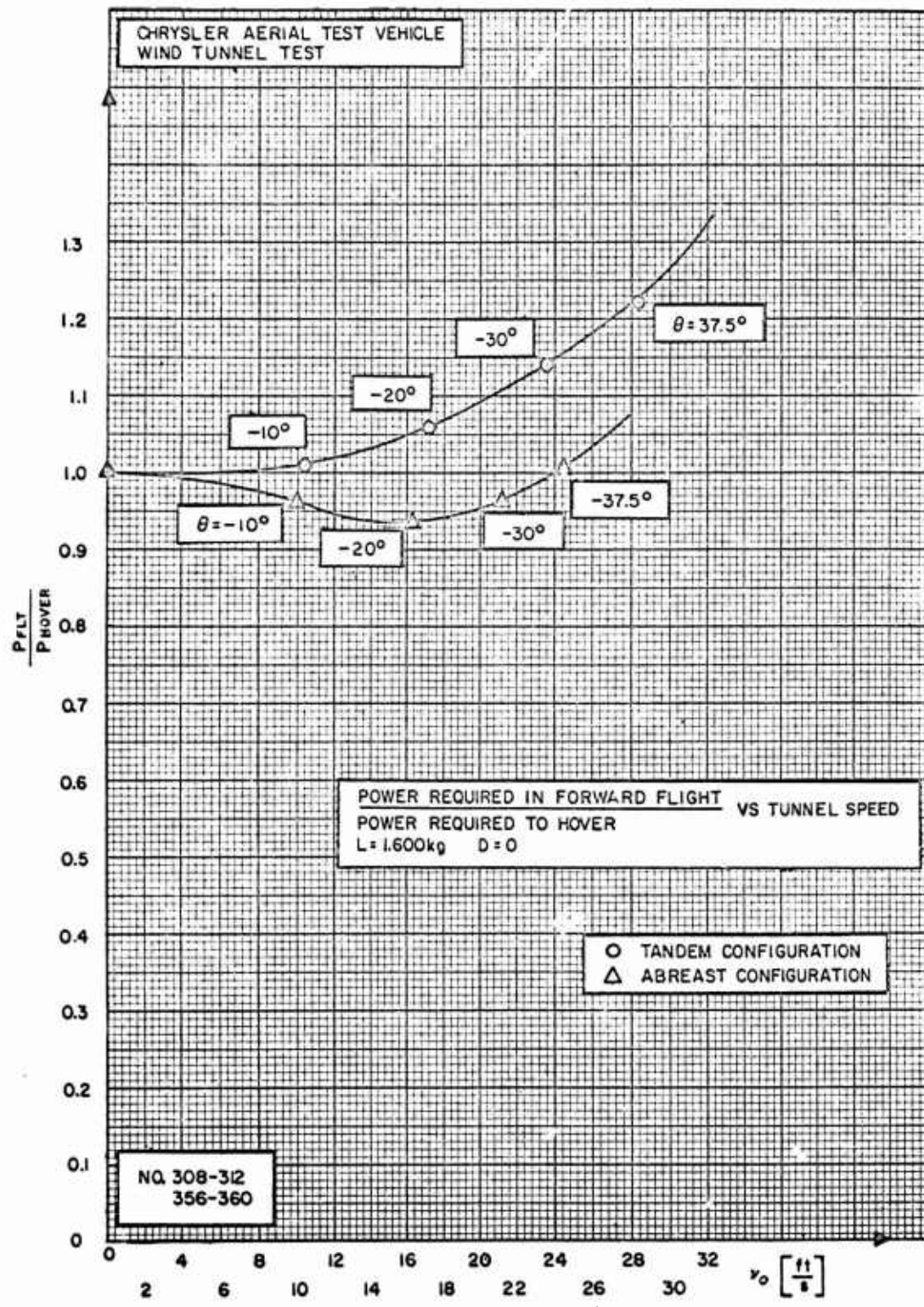


Figure 69. Power Ratio for Forward Flight in Tandem and in Abreast

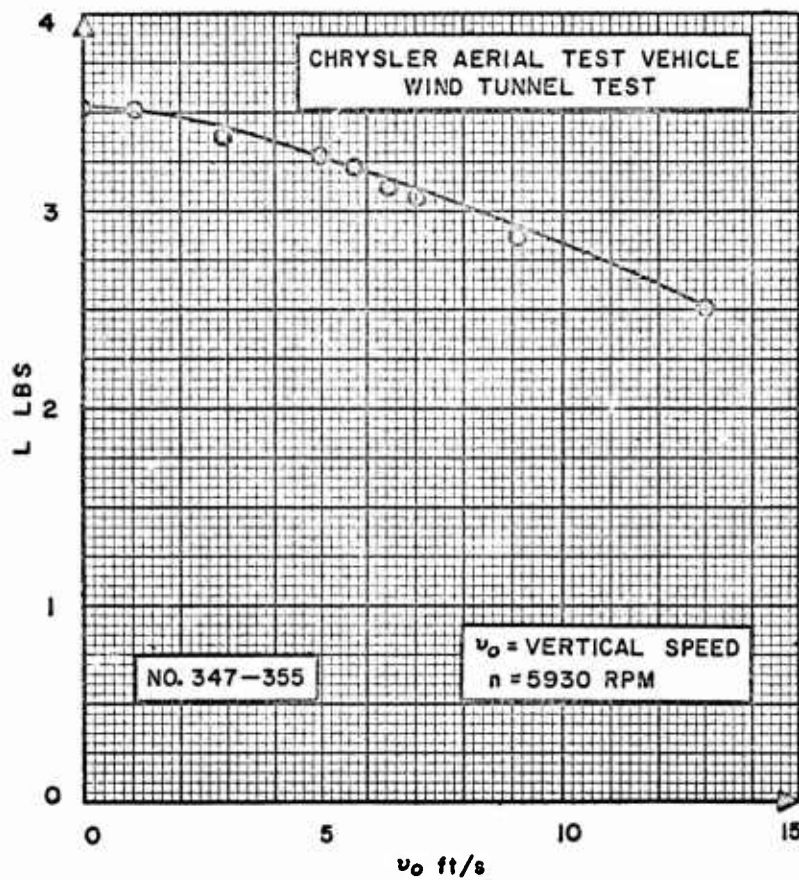


Figure 70. Lift as a Function of Upward Speed at Constant RPM

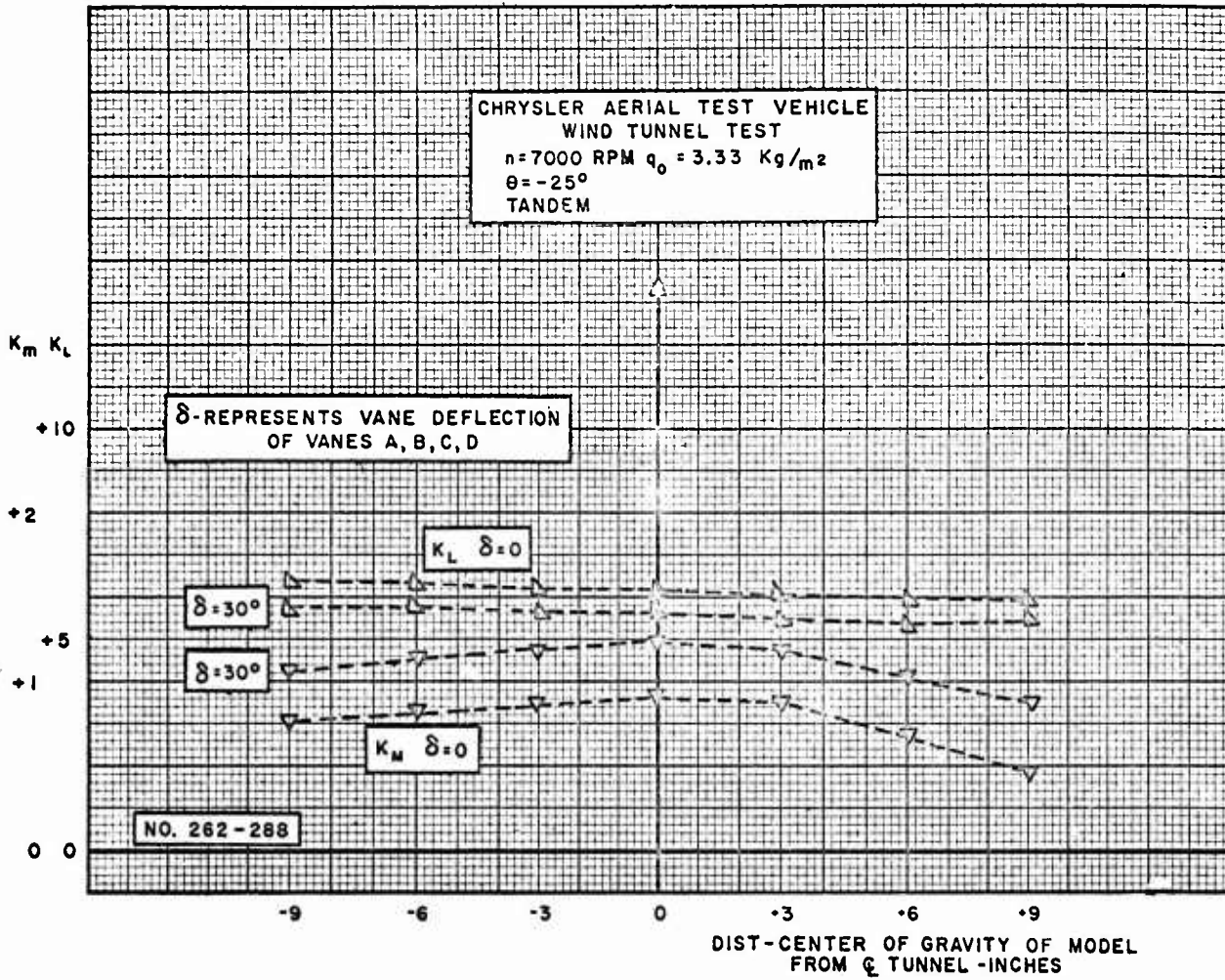


Figure 71.  $K_L$ ,  $K_m$  vs Distance of C.G. of Model from Center Line of Tunnel